BioMed Research International

Gliomas

Guest Editors: Giuseppe Lombardi, Alessandro Della Puppa,
Anna Luisa Di Stefano, Andrea Pace, Roberta Rudà, and Emeline Tabouret

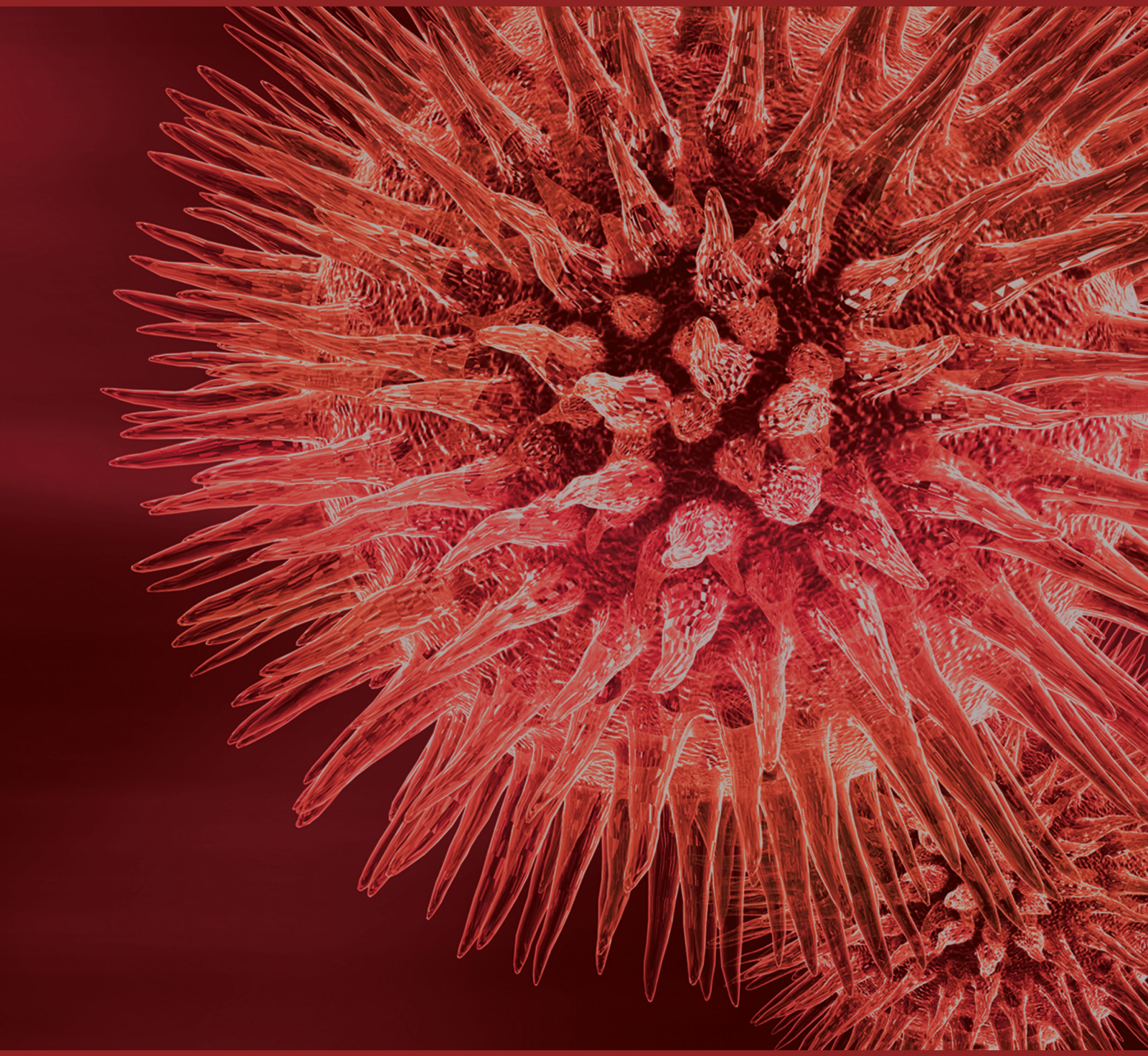

Gliomas

BioMed Research International

Gliomas

Guest Editors: Giuseppe Lombardi, Alessandro Della Puppa, Anna Luisa Di Stefano, Andrea Pace, Roberta Rudà, and Emeline Tabouret

Contents

Hindawi Publishing Corporation
BioMed Research International
Volume 2014, Article ID 470523, 2 pages
http://dx.doi.org/10.1155/2014/470523

Editorial

Gliomas

Giuseppe Lombardi,[1] Alessandro Della Puppa,[2] Anna Luisa Di Stefano,[3,4] Andrea Pace,[5] Roberta Rudà,[6] Emeline Tabouret,[7] and Vittorina Zagonel[1]

[1] *Medical Oncology 1, Veneto Institute of Oncology-IRCCS, Via Gattamelata 64, 35128 Padua, Italy*
[2] *Neurosurgery Department, Padua Hospital, 35128 Padua, Italy*
[3] *Department of Neuro-Oncology, UPMC, GH Pitié-Salpétrière, 75005 Paris, France*
[4] *DBBS, National Neurological Institute C. Mondino, University of Pavia, 27100 Pavia, Italy*
[5] *Neurology Unit, National Cancer Unit, Regina Elena, 00144 Rome, Italy*
[6] *Department of Neuro-Oncology, Città della Salute e della Scienza, University of Turin, 10126 Turin, Italy*
[7] *Department of Neuro-Oncology, Hopitaux de Marseille, Marseille, France*

Correspondence should be addressed to Giuseppe Lombardi; giuseppe.lombardi@ioveneto.it

Received 25 June 2014; Accepted 25 June 2014; Published 26 August 2014

Gliomas are a heterogeneous group of tumors developing from glial cells in the central nervous system. Gliomas are divided into two histopathological subgroups: low and high grade gliomas. High-grade gliomas, such as glioblastoma and anaplastic astrocytoma, are extremely aggressive lesions and represent the most common primary malignant brain tumors.

In the last years, there have been important developments about their biologic mechanism, their surgical and drug treatment, and their diagnosis and genetic mutations; indeed, the recent IDH gene mutation identification in gliomas has been an important contribution to the knowledge improvement of biological mechanism and prognosis of these tumors. Through the analysis of IDH gene mutation it is possible to add molecular characteristics to refine the WHO classification in order to define more homogeneous gliomas subgroups. X.-W. Wang et al. showed that IDH mutation is almost constant in 1p19q codeleted tumors and they stratified low- and high-grade gliomas according to the codeletion of 1p19q and IDH mutation to define three prognostic subgroups: 1p19q and IDH mutated, IDH mutated alone, and none of these alterations; they demonstrated that the presence of IDH mutation combined with other genomic markers can be used to refine the prognostic classification of gliomas, independently of tumor grade. Noteworthy, X.-W. Wang et al., in another work, showed that IDH1-R132H mutation could be predictive of response to radiation therapy; indeed, they suggested that IDH mutation could increase radiosensitivity in hypoxic conditions, underlining the primordial IDH mutation determination whatever the diagnostic approach. Indeed, in a recent work, G. Lombardi et al. [1] reported the possibility to discriminate IDH mutation analyzing the concentration of 2-hydroxyglutarate in urinary and plasma samples.

As described by P. Gonzalez-Gomez et al., another signaling pathway such as bone morphogenetic proteins (BMPs) could present with both prognostic value and promising therapeutic tools for gliomas.

A very interesting study about the use of 5-aminolevulinic acid (5-ALA) fluorescence in high-grade gliomas surgery was reported by A. Della Puppa et al.; they analyzed 94 patients who underwent surgery guided by 5-ALA fluorescence and stratified data for recurrent surgery, tumor location, tumor size, and tumor grade; they concluded that this surgical approach enables a gross total resection in 100% of cases and recurrent surgery, location, size, and tumor grade can be predictor of surgical outcome. The role of salvage radiosurgery in patients with recurrent malignant gliomas was studied by M. Martínez-Carrillo et al.; retrospectively, they analyzed 87 patients with recurrent anaplastic astrocytoma

and glioblastoma who underwent stereotactic radiosurgery; although the population was very heterogeneous and various prior studies showed conflicting results about the efficacy of reirradiation, they concluded that this treatment was safe and may be a potential treatment option in selected patients.

New technological instruments such as brain magnetic resonance imaging (MRI) with spectroscopy and perfusion can help in the right diagnosis for these tumors; in fact, A. L. Di Stefano et al., evaluating perfusion MRI in grades III and IV gliomas, showed that any significant difference in rCBV between grade III and grade IV is detectable in the contrast-enhancement area while areas of high perfusion on CBV map appear capable of best characterizing the degree of neovascularization and should be considered as the reference areas to be targeted for gliomas grading. The role of diffusion tensor histogram analysis was studied in pediatric diffuse intrinsic pontine gliomas by E. A. Steffen-Smith et al. from National Institutes of Health in Bethesda; they evaluated tumor structure in children using histogram analyses of mean diffusivity, concluding that this method can show significant interpatient and intratumoral differences and quantifiable changes in tumor structure.

Finally, an Italian study by V. Vaccaro et al. analyzed the efficacy of bevacizumab in association with fotemustine in patients with recurrent malignant gliomas. Antiangiogenic treatments for glioma patients have been tested in numerous clinical trials, both retrospective and prospective studies, with conflicting results; indeed, recently, two randomized prospective phase III studies failed to demonstrate the bevacizumab efficacy when added to temozolomide and radiation therapy for new glioblastoma patients [2, 3]. The combination treatment with bevacizumab and fotemustine was previously studied by R. Soffietti et al. [4] in recurrent glioblastoma patients, although with a different dosage and schedule. In both studies, this regimen showed interesting results with good safety in these patients.

In conclusion, gliomas represent an important subject of study and in this special issue very interesting works on recent developments about diagnosis, molecular biology, surgical treatment, and new targeted therapies for gliomas were selected.

Giuseppe Lombardi
Alessandro Della Puppa
Anna Luisa Di Stefano
Andrea Pace
Roberta Rudà
Emeline Tabouret
Vittorina Zagonel

References

[1] G. Lombardi, G. Corona, P. Farina et al., "Diagnostic value of plasma and urinary 2-hydroxyglutarate to identify patients with IDH-mutated glioma," *Journal of Clinical Oncology*, vol. 32, article 5s, 2014.

[2] O. L. Chinot, W. Wick, and T. Cloughesy, "Bevacizumab for newly diagnosed glioblastoma," *The New England Journal of Medicine*, vol. 370, article 2049, 2014.

[3] M. R. Gilbert, E. P. Sulman, and M. P. Mehta, "Bevacizumab for newly diagnosed glioblastoma," *The New England Journal of Medicine*, vol. 370, pp. 2048–2049, 2014.

[4] R. Soffietti, E. Trevisan, L. Bertero et al., "Bevacizumab and fotemustine for recurrent glioblastoma: a phase II study of AINO (Italian Association of Neuro-Oncology)," *Journal of Neuro-Oncology*, vol. 116, pp. 533–541, 2014.

Hindawi Publishing Corporation
BioMed Research International
Volume 2014, Article ID 647356, 9 pages
http://dx.doi.org/10.1155/2014/647356

Clinical Study

Diffusion Tensor Histogram Analysis of Pediatric Diffuse Intrinsic Pontine Glioma

Emilie A. Steffen-Smith,[1] Joelle E. Sarlls,[2] Carlo Pierpaoli,[3] Joanna H. Shih,[4] Robyn S. Bent,[1] Lindsay Walker,[3,5] and Katherine E. Warren[1]

[1] *Pediatric Oncology Branch, National Cancer Institute, Center for Cancer Research, National Institutes of Health, Building 10, Room 1-5750, 9000 Rockville Pike, Bethesda, MD 20892, USA*
[2] *In Vivo NMR Center, National Institute of Neurological Disorders and Stroke, National Institutes of the Health, Bethesda, MD 20892, USA*
[3] *Program on Pediatric Imaging and Tissue Sciences, National Institute of Child Health and Human Development, National Institutes of Health, Bethesda, MD 20892, USA*
[4] *Biostatistics and Data Management Section, National Cancer Institute, Center for Cancer Research, National Institutes of the Health, Bethesda, MD 20892, USA*
[5] *Center for Biomedical Engineering, School of Engineering, Brown University, Providence, RI 02912, USA*

Correspondence should be addressed to Katherine E. Warren; warrenk@mail.nih.gov

Received 12 February 2014; Accepted 24 May 2014; Published 11 June 2014

Academic Editor: Roberta Rudà

Purpose. To evaluate tumor structure in children with diffuse intrinsic pontine glioma (DIPG) using histogram analyses of mean diffusivity (MD), determine potential treatment and corticosteroid-related effects on MD, and monitor changes in MD distributions over time. *Materials and Methods*. DTI was performed on a 1.5T GE scanner. Regions of interest included the entire FLAIR-defined tumor. MD data were used to calculate histograms. Patterns in MD distributions were evaluated and fitted using a two-normal mixture model. Treatment-related effects were evaluated using the R^2 statistic for linear mixed models and Cox proportional hazards models. *Results*. 12 patients with DIPG underwent one or more DTI exams. MD histogram distributions varied among patients. Over time, histogram peaks became shorter and broader ($P = 0.0443$). Two-normal mixture fitting revealed large lower curve proportions that were not associated with treatment response or outcome. Corticosteroid use affected MD histograms and was strongly associated with larger, sharper peaks ($R^2 = 0.51$, $P = 0.0028$). *Conclusions*. MD histograms of pediatric DIPG show significant interpatient and intratumoral differences and quantifiable changes in tumor structure over time. Corticosteroids greatly affected MD and must be considered a confounding factor when interpreting MD results in the context of treatment response.

1. Introduction

Pediatric diffuse intrinsic pontine gliomas (DIPGs) are highly invasive, aggressive lesions that infiltrate the pons. The location and infiltrative nature of DIPG precludes surgical intervention. Diagnostic biopsy is controversial and not routinely performed at most institutions for patients with a typical presentation, resulting in a paucity of histological data and limited understanding of DIPG biology at diagnosis [1, 2]. Studies at autopsy indicate that the majority of DIPGs are high-grade with substantial interpatient variation in gene expression and molecular genetic aberrations [3–5]. Imaging remains the primary modality for diagnosis, assessment of therapeutic response, and management. However, standard MRI findings, including enhancement and tumor size measurements, are difficult to interpret, obtain consistently, and provide little insight into underlying tumor structure and biology. Changes on standard MRI are not specific to response or outcome [6–11]. Given the limited utility of standard MRI and the heterogeneous nature of DIPG, advanced imaging techniques, including diffusion tensor imaging (DTI), are currently under investigation to interrogate the structure and behavior of DIPG [12, 13]. Most studies using DTI to evaluate brain tumors have used measurements

of the average value of mean diffusion (MD) from a specific region to represent the entire tumor. MD is more sensitive to changes in cellularity and edema compared to fractional anisotropy (FA), which may increase or decrease depending upon the FA of the original structure [14]. Such regional analyses rely partly on *a priori* knowledge of boundaries between tissue subtypes (e.g., active tumor and necrosis), which may have different MD values [15]. DIPGs have indistinct borders and may contain areas of varying tumor activity, normal grey and/or white matter, edema, and necrosis, making it difficult to identify a region that best characterizes the tumor. In addition, DTI in the brainstem is especially challenging due to geometric distortions found at the air-tissue interface of the paranasal sinuses (i.e., susceptibility artifacts) and movement from cardiac pulsation (i.e., motion artifacts), both of which may produce spurious diffusion results [16]. A histogram can provide analysis of MD values across the entire tumor volume, giving a graphic, quantitative representation of the distribution of MD values from intratumoral heterogeneity. Changes in the distribution of MD values in different tumor regions may reflect changes in tissue subtypes over the course of treatment (e.g., increase in proportion of necrotic tissue compared to proportion of active tumor). MD histogram analyses have been used to differentiate high-grade and low-grade tumors in adults [17, 18]. Studies of adult high-grade gliomas have used MD histograms to predict patient outcome and treatment response [19–22]. Patients in these studies frequently receive corticosteroids, with variable doses among patients [19, 21, 22]. Corticosteroids have a known effect on diffusion parameters, reducing the magnitude of diffusion within brain tumors [23, 24]; yet reports of MD histograms in adults with gliomas have not accounted for corticosteroid use when interpreting treatment-response. Corticosteroids are commonly used to manage clinical symptoms in children with DIPG. This study used a comprehensive DTI acquisition and processing method to determine if global MD measures and MD histograms could aid in assessment of treatment effects by determining corticosteroid-related changes and longitudinal changes in DIPG.

2. Methods

2.1. Patients. Patients or their legal guardians signed a document of informed consent for enrollment in a phase II study of Pegylated Interferon Alfa-2b (PEG-Intron) for children with DIPG [25]. The institution review board approved the study. Study eligibility criteria are described in Warren et al.'s [25]. Patients were required to enroll within 2–10 weeks after completion of radiation treatment and, if receiving corticosteroids, maintain a steady or decreasing dose for ≥1 week prior to study entry. DTI was acquired during standard MRI evaluations on a subset of patients.

2.2. MRI. Imaging data were acquired on a single GE Signa HDx 1.5T scanner (GE Medical Systems, Milwaukee WI) equipped with an eight-channel phased array coil. Clinical imaging sequences included pre- and postcontrast T1 spin echo (TR/TE = 450/13 ms, FOV = 220 × 220 mm, matrix = 256 × 192, thickness = 3 mm), T2-fast spin echo (T2-TSE; TR/TE = 3400/95 ms, FOV = 220 × 220 mm, matrix = 256 × 192, slice thickness = 3 mm), and fluid attenuated inversion recovery (FLAIR; TR/TE/TI = 10,000/140/2200 ms, FOV = 220 × 220 mm, matrix = 256 × 192, thickness = 3 mm). Precontrast whole-brain DTI datasets were acquired using a dual spin-echo preparation period and single shot spin-echo echo planar imaging (EPI) sequence (TR/TE = 17.6/89.3 ms, FOV = 240 × 240 mm, matrix = 96 × 96, thickness = 2.5 mm, no gap, 64 slices). Diffusion gradient encoding was applied in 60 noncollinear directions with maximum b-value = 1100 s/mm^2 and in 10 noncollinear directions with b-value = 300 s/mm^2 and b-value = 0 s/mm^2 (80 imaging volumes total).

2.3. DTI Processing and Analysis. Diffusion data were processed offline using TORTOISE [26]. T2-FSE images were used as the structural target for DTI data processing. T2-FSE images from the first time point were aligned to the hemispheric midline and the anterior and posterior commissures plane using MIPAV [27]. Follow-up scans were registered to the first time point. Diffusion weighted-imaging (DWI) data were corrected for rigid body motion, eddy-current distortion [28], and EPI distortion [29]. Corrected DWI data were registered to T2-FSE structural images. The DT [30–32] was calculated using a nonlinear least squares method with robust estimation of tensors by outlier rejection [33], which removes physiological effects like cardiac pulsation. MD maps were calculated from the DT.

2.4. Regions of Interest (ROI) Analysis. Precontrast FLAIR images and MD maps were coregistered via the T2-TSE structural target using MIPAV and imported into TORTOISE for ROI analysis. FLAIR images were used for ROIs based on a previous report of more consistent selection of tumor boundaries with FLAIR compared to T2 [34]. Enhancement was not considered in ROI selection given the highly variable and frequently absent contrast enhancement patterns found in DIPG. Regions of FLAIR abnormality on each axial slice were used to determine tumor involvement within the pons and surrounding tissue. FLAIR signal abnormality was frequently diffuse, without distinct borders. Therefore, slice ROIs were manually drawn to include the entire FLAIR signal abnormality and the affected anatomical structure, excluding regions of CSF (Figure 1). ROIs were applied to MD maps. Axial ROIs were combined to create a volumetric ROI. Global MD measures from the volumetric ROI data included median, mean, 5th percentile (lowest 5% of ROI values), and 95th percentile (highest 5% of ROI values).

2.5. DTI Histograms. MD values from volumetric ROIs were used to generate MD histograms, plotting the frequency of MD values as a proportion of total ROI voxels versus MD values (bin width of 0.025×10^{-3} mm^2/s). Analysis of MD histogram characteristics included (1) standard deviation; (2) skewness, measure of histogram asymmetry: length of left tail > right tail (negative skewness) or length of right tail > left tail (positive skewness), (3) peak location (mode), and

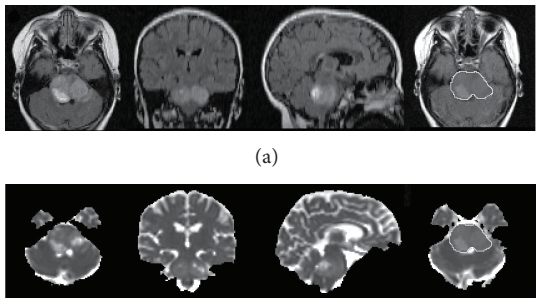

(a)

(b)

Figure 1: Coregistered axial, coronal, and sagittal (a) FLAIR images and (b) MD maps of the pons. ROIs were outlined on axial images ((a) and (b) far right) and combined to create a volumetric ROI covering the entire lesion.

(4) peak height. MD values were also fitted using a two-normal mixture distribution, a model reported in studies of adult glioblastoma [20–22]. From the two-normal mixture histograms we calculated the lower normal curve proportion (LCP), which represents the percentage of histogram data found within the lower curve, and the lower normal curve mean (LCM), that is, the mean MD value of the lower curve. Previous studies indicate that LCP reflects active, highly cellular areas of the tumor and the high normal curve proportion reflects necrotic or edematous regions [21, 22].

2.6. Statistical Analysis. We evaluated differences among patients using global MD measures and MD histogram characteristics at the first DTI scan and longitudinally. A linear mixed effect model was used with a random intercept and random slope to account for intraperson correlation due to multiple scans. We used an R^2 statistic for linear mixed models [35] to evaluate the association between MD measures and time. This same method was applied to evaluate the relationship between ROI volume and global and histogram parameters. Kaplan-Meier method was used to calculate the time to progression and overall survival relative to study entry. R^2 statistic for linear mixed models was used to examine the relationship between MD values and corticosteroid use, time to disease progression, and overall survival. We also applied univariate Cox proportional hazards models to explore the relationship of global measures and histogram parameters with progression and overall survival. P values of <0.05 were considered statistically significant. Data were analyzed using the statistical computing package, *R* (http://www.r-project.org/).

3. Results

3.1. Patients. Twelve patients (median age = 5 y, range = 4–8 y) underwent one or more DTI exams during the course of treatment with PEG-Intron (Table 1). Six patients received corticosteroids (dexamethasone), at the time of their initial DTI exam. Four of those patients continued to receive dexamethasone at subsequent time points, and, in each case, the dose was stable or decreased from the previous time point. Median time to disease progression was 28.1 weeks from study entry. Median overall survival was 45.7 weeks from study entry.

3.2. Global MD Measures. Global MD measures for all time points are shown in Figure 2(a). Median and mean MD values from the initial DTI scan were increased compared to those of normal brain tissue (MD of normal tissue = 0.7×10^{-3} mm^2/s), with considerable variability among patients: median MD range = 0.85–1.16 $\times 10^{-3}$ mm^2/s and mean MD range = 0.9–1.17 $\times 10^{-3}$ mm^2/s, respectively. Median and mean MD increased significantly over time ($R^2 = 0.29$, $P = 0.0369$ and $R^2 = 0.28$, $P = 0.0427$, resp.). The prognostic value of the median and mean MD did not reach statistical significance ($P > 0.1$). Fifth percentile MD values also increased significantly over time ($R^2 = 0.35$, $P = 0.0202$), with lower values at scans closer to study entry ($R^2 = 0.31$, $P = 0.0316$). Fifth percentile MD values appeared to be a strong predictor of progression and overall survival (HR > 20) but did not reach statistical significance ($P > 0.1$).

3.3. MD Histogram Measures. MD histogram measures for all time points are shown in Figure 2(b). MD histograms from initial DTI scans revealed heterogeneous distributions of MD values within each lesion, with no consistent histogram shape among patients (Figure 3(a)). Large differences in histogram shape and distribution were observed, even among patients at the same stage of their clinical course (Figure 3(b)). At subsequent scans, we continued to observe interpatient variation in histogram shape and distribution. As illustrated in Figure 4, changes in histograms for individual patients over time included a shift towards higher MD values and decreased peak height (i.e., shorter, broader peaks). Peak height was negatively associated with time from initial scan ($R^2 = 0.28$, $P = 0.0443$) and appeared to be a potentially strong predictor of progression and overall survival (HR > 20), but the association did not reach statistical significance ($P > 0.1$). Histogram standard deviation was associated with time from initial scan ($R^2 = 0.44$, $P = 0.0074$) and was lower in patients with scans closer to study entry ($R^2 = 0.44$, $P = 0.007$).

Unlike reports in adults, the two-normal mixture fitting of MD data resulted in large lower curves which included an overwhelming majority of MD histogram values for nearly all patients (median LCP = 92.98%, SD = 17.11%), with the exception of one patient in which the model was a poor fit for the histogram data (Figure 5). LCM MD values were higher than normal tissue for all patients, ranging from 0.88 to 1.16 $\times 10^{-3}$ mm^2/s (median = 0.95 $\times 10^{-3}$ mm^2/s, SD = 0.09 $\times 10^{-3}$ mm^2/s). Prognostic values of LCP and LCM at initial scan (HR < 1) and over time (HR < 1 and HR < 5, resp.) were not statistically significant ($P > 0.1$ for all analyses).

3.4. ROI Volume Measure. Volumetric ROIs ranged from 9.0 cm^3 to 63.6 cm^3. For patients with follow-up DTI, ROI volumes typically increased over time, though this trend did

Table 1: Patient characteristics.

Pt	Age (yr)	M/F	XRT (wks)	TTP (wks)	OS (wks)	DTI (wks)	Dexamethasone dose (mg/kg)
1	4	M	9	24	39	24	None
2	6	M	8	40	48	40	None
3	5	F	2	37	51	0	0.12
						27	0.11
4[1]	6	F	6	72	151+	12	None
						16	None
						32	None
						40	None
						56	None
						64	None
5	5	F	5	25	38	4	0.09
						16	0.01
6	5	F	9	9	23	4	0.08
7	6	F	5	16	31	0	0.01
						4	0.01*
						16	None
8	8	F	2	24	32	0	0.02
						4	0.01
						16	None
9	6	F	5	21	22	8	None
10	5	F	7	31	51	7	None
						12	None
						24	None
						28	None
11	4	M	4	16	24	4	0.27
12	5	F	8	15	49	0	None

[1]Patient went off study due to disease progression but continues to be followed.
XRT: radiation therapy (time from end of XRT to study entry).
TTP: time to disease progression (from study entry).
OS: overall survival (from study entry).
DTI: diffusion tensor imaging (time of scan from study entry).
*administered every other day.

not reach statistical significance ($P > 0.05$). Larger ROI volume was positively associated with increased time from study entry ($R^2 = 0.28$, $P = 0.0443$). ROI volume was inversely associated with positive histogram skewness ($R^2 = 0.27$, $P = 0.0478$) and positively associated with median MD ($R^2 = 0.52$, $P = 0.0025$) and mean MD ($R^2 = 0.51$, $P = 0.0027$). We identified a strong positive linear relationship between fifth percentile MD and ROI volume ($R^2 = 0.68$, $P < 0.001$), suggesting that larger tumors are more edematous or necrotic compared to smaller tumors. Clinical parameters, including use of corticosteroids, were not associated with ROI volume ($P > 0.05$).

3.5. Use of Corticosteroids and MD. Several differences in MD values were found for those patients receiving corticosteroids compared to those who were not (Table 2). Dexamethasone use was associated with lower median MD ($R^2 = 0.43$, $P = 0.0182$) and lower mean MD ($R^2 = 0.38$, $P = 0.0077$). MD histograms for patients receiving dexamethasone showed significantly more positive skewness ($R^2 = 0.38$, $P = 0.0136$)

Table 2: Use of corticosteroids and MD parameters.

MD parameter	No corticosteroids Median (SD)	+Corticosteroids Median (SD)
Median MD ($\times 10^{-3}$ mm^2/s)	0.96 (0.06)	0.90 (0.13)
Mean MD ($\times 10^{-3}$ mm^2/s)	1.0 (0.06)	0.95 (0.12)
Skewness	2.06 (0.46)	2.45 (1.32)
Peak Height	0.05 (0.01)	0.07 (0.03)

SD: standard deviation.

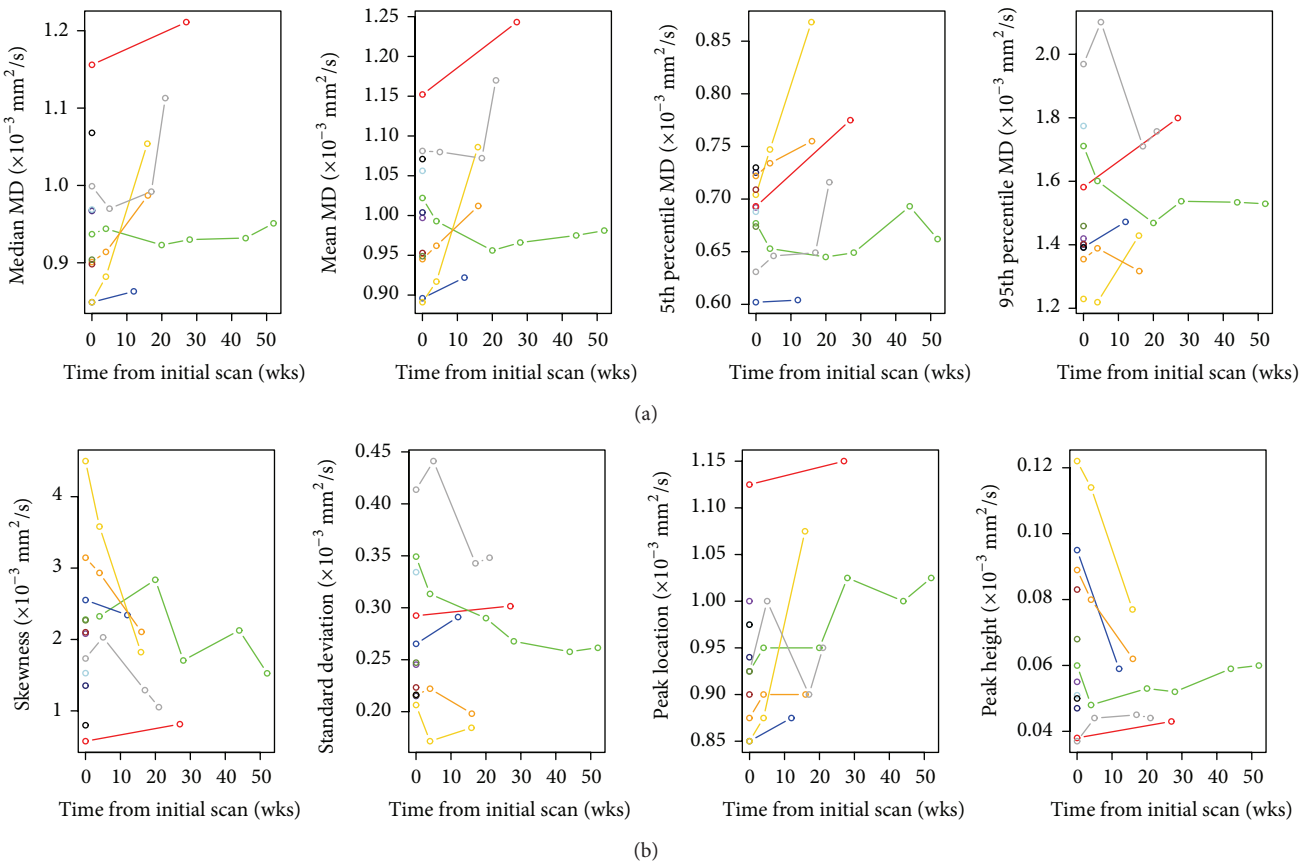

FIGURE 2: (a) Changes in global MD parameters over time for all patients. (b) Changes in MD histogram parameters over time for all patients.

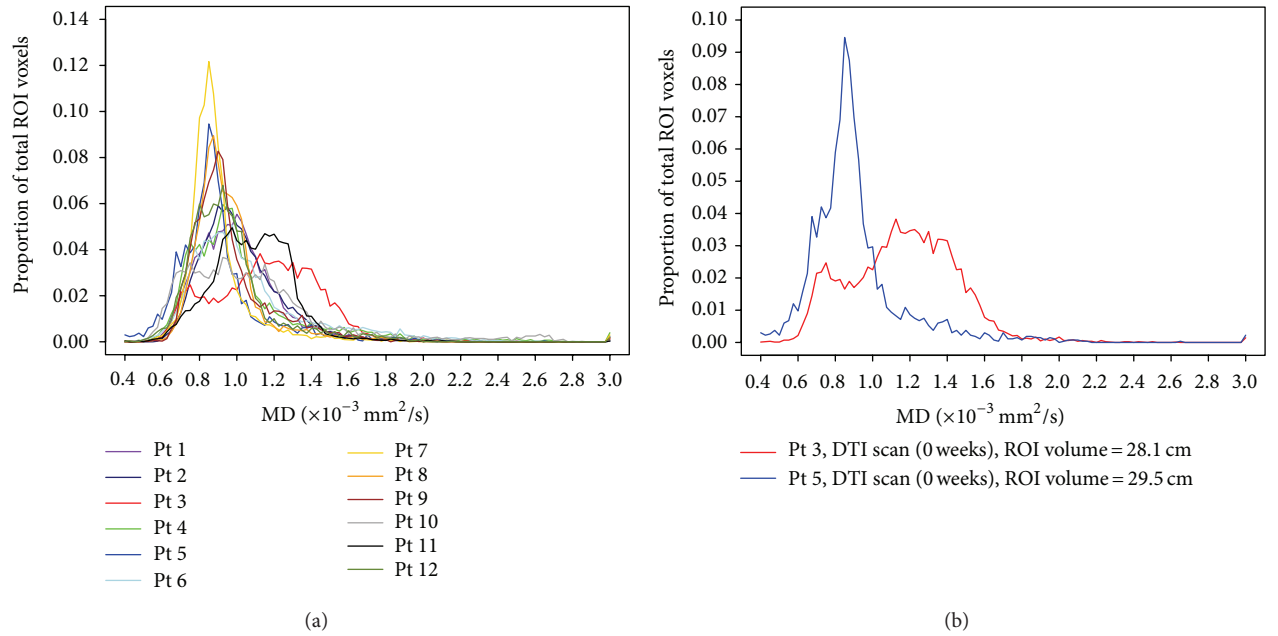

FIGURE 3: (a) Baseline MD histograms for all patients. (b) Baseline MD histograms for two patients, showing interpatient heterogeneity of baseline MD. DTI scans were performed two weeks after XRT and prior to PEG-Intron therapy for both patients. Both patients received dexamethasone at the time of scan.

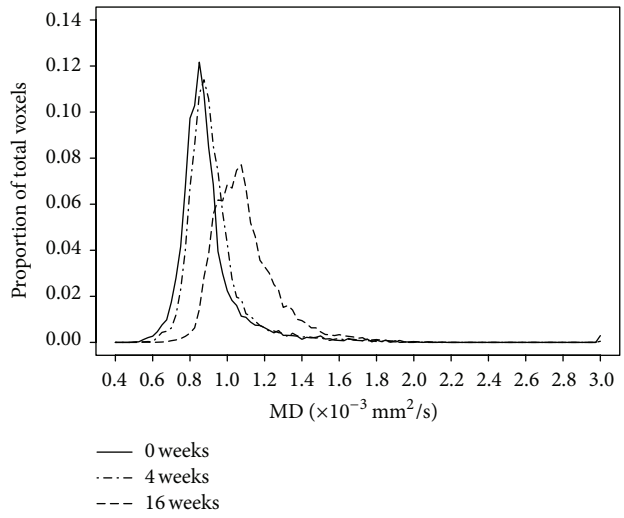

Figure 4: Changes in MD histogram over time for an individual patient.

and increased peak heights ($R^2 = 0.51$, $P = 0.0028$) compared to those of patients not receiving dexamethasone.

4. Discussion

With the increasing push for biopsy and development of targeted therapies for DIPG, more insight into the tumor environment is critical. In this study, we show that MD histogram analysis allowed further diffusion-related changes to be quantified and monitored over time compared to global ROI measures. Even in this small number of patients, we observed heterogeneous distributions of MD values, likely reflecting the known substantial interpatient biologic variation in DIPGs [3–5] and showed dynamic changes in tumor structure over time. Shape and appearance of MD histograms among patients varied greatly, even among patients at the same point in their treatment course. Histogram shape changed over time, though the observed patterns of change differed among patients. We observed a shift in histograms towards larger MD values and a decrease in peak height over time, particularly for patients with larger peak heights at their first DTI scan. This suggests an increase in tumor heterogeneity following treatment. We consistently saw an increase in MD values, though the relationship between MD values and progression and survival was not statistically significant. Increased MD was seen even in fifth percentile MD values, which represent regions with the lowest MD and, presumably, areas of greatest cellularity within the tumor ROI. The clinical significance of these findings is unknown but demonstrates that the tumor environment is dynamic, changing over time and course of therapy. Larger MD values could reflect an increase in extracellular water content compared to normal tissue either due to interstitial edema or the formation of cystic cavities associated with necrosis.

Studies in adult glioblastoma have applied a two-normal mixture model to MD histogram data and demonstrated a better fit of MD data and improved analysis for histogram measures, using MD values from the lower curve to stratify patients and predict treatment response [20–22]. For comparison, we applied the same model to our pediatric DIPG MD histogram data. Unlike reports in adults, the two-normal mixture model did not improve our analysis of pediatric DIPG. We observed relatively similar, large lower curves for almost all patients at all-time points and found no significant association between lower curve metrics and outcome.

In this study, changes in MD were clearly associated with use of corticosteroids. The effect of corticosteroids on diffusion properties in treatment-naïve adult patients with high-grade gliomas has been previously evaluated [23, 24], showing a decrease in MD with administration of corticosteroids. However, the effect on diffusion characteristics in patients undergoing concurrent treatment was previously unreported. Consistent with results from previous studies, diffusion parameters were significantly different when patients received dexamethasone, even in those patients receiving a steady or tapering dose. The primary effect of corticosteroids is a reduction or resolution of edema in tissue, reflected by overall lower MD values. Results from our study indicate that corticosteroid use in patients receiving antitumor therapy greatly impacts the DTI results and must be considered a confounding factor when using DTI to determine treatment response in this population.

Results of this study must be interpreted with consideration of limitations. Patients were enrolled in a clinical trial following standard radiation therapy; therefore, all DTI scans were performed following radiation and we were unable to assess changes in MD parameters before and after radiation therapy. Analysis of MD histograms to determine treatment response was limited by the number of patients who had longitudinal scans. We observed that over time the proportion of tissue with normal MD decreased in children with DIPG. The timing of DTI scans over the course of treatment was variable among patients due to scheduling limitations. Therefore, variation in MD histogram appearance at the initial scan cannot be solely attributed to differences in the tumors among patients, but also due, in part, to differences in the timing of scans relative to treatment. As is common in this population, use of corticosteroids varied among patients. We observed significantly lower MD values when corticosteroids were administered, which may reflect a reduction in edema within the tumor or may be a combination of the effect of corticosteroids and treatment response. Because correlation of diffusion parameters with tissue histology is not possible (due to restrictions on biopsy in children with DIPG), the biological interpretation of our findings is limited.

5. Conclusions

This study investigated both global MD measures, which are typically reported, and MD histogram characteristics, after comprehensive data processing, in children receiving treatment for DIPG. The most striking observations were the interpatient variation and intratumoral heterogeneity seen in MD and the significant effect of corticosteroids on MD. Our study shows that MD histogram analysis can be

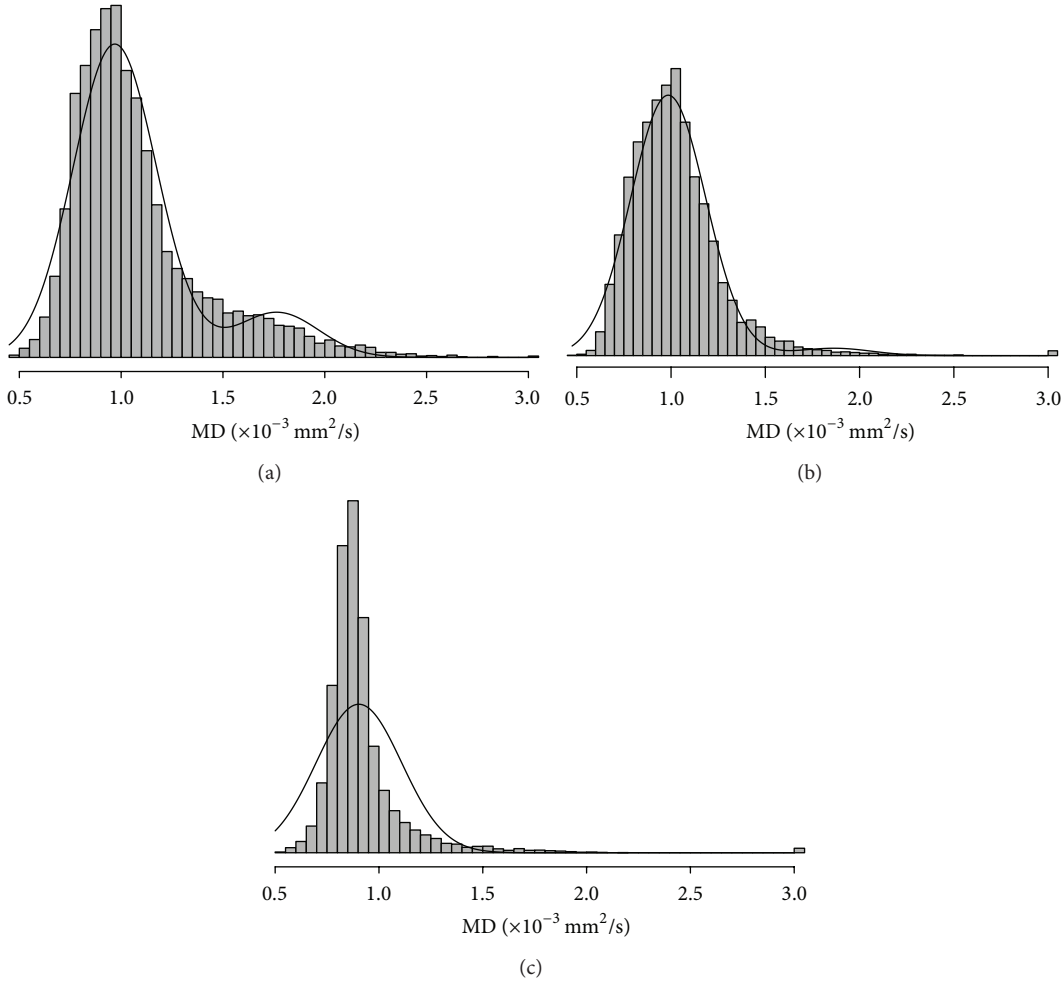

Figure 5: Two-normal mixture fitting for 3 patients on study. Overall, two-normal mixture histograms had large lower curves (a, b) with an acceptable overall fit to the distribution of data. However, for one patient with a very narrow peak (c), the model was not appropriate and excluded a large proportion of MD values.

used to visualize the known heterogeneity of DIPGs *in vivo* and to objectively quantify changes in tumor microstructure over the course of therapy that may not be captured using a global measure of MD values or findings on standard MRI. In addition, we caution that corticosteroid use in patients concurrently receiving antitumor therapy should be considered a confounding factor when analyzing DTI data.

Conflict of Interests

The authors declare that there is no conflict of interests regarding the publication of this paper.

Acknowledgments

This research was supported in part by the Intramural Research Program of the National Institutes of Health, National Cancer Institute, Center for Cancer Research. The views herein do not necessarily represent the official views of the National Cancer Institute, the National Institutes of Health, or the US Department of Health and Human Services, nor does the mention of trade names, commercial products, or organizations imply endorsement by the US Government. Dr. Joanna Shih performed the statistical analysis for this paper. Institutional Review Board approval was obtained. Written informed consent was obtained from all patients or their legal guardians. Results of the clinical trial were previously reported in Warren et al., *Cancer* 2012. This work was presented in part at the 2012 American Society for Neuroradiology Annual Meeting in New York City, NY.

References

[1] J. Grill, S. Puget, F. Andreiuolo, C. Philippe, L. MacConaill, and M. W. Kieran, "Critical oncogenic mutations in newly diagnosed pediatric diffuse intrinsic pontine glioma," *Pediatric Blood & Cancer*, vol. 58, no. 4, pp. 489–491, 2012.

[2] S. Puget, C. Philippe, D. A. Bax et al., "Mesenchymal transition and pdgfra amplification/mutation are key distinct oncogenic events in pediatric diffuse intrinsic pontine gliomas," *PLoS ONE*, vol. 7, no. 2, Article ID e30313, 2012.

[3] K. E. Warren, K. Killian, M. Suuriniemi, Y. Wang, M. Quezado, and P. S. Meltzer, "Genomic aberrations in pediatric diffuse intrinsic pontine gliomas," *Neuro-Oncology*, vol. 14, no. 3, pp. 326–332, 2012.

[4] J. Barrow, M. Adamowicz-Brice, M. Cartmill et al., "Homozygous loss of ADAM3A revealed by genome-wide analysis of pediatric high-grade glioma and diffuse intrinsic pontine gliomas," *Neuro-Oncology*, vol. 13, no. 2, pp. 212–222, 2011.

[5] M. Zarghooni, U. Bartels, E. Lee et al., "Whole-genome profiling of pediatric diffuse intrinsic pontine gliomas highlights platelet-derived growth factor receptor α and poly (ADP-ribose) polymerase as potential therapeutic targets," *Journal of Clinical Oncology*, vol. 28, no. 8, pp. 1337–1344, 2010.

[6] T. C. Hankinson, E. J. Campagna, N. O. K. Foreman, and M. H. Handler, "Interpretation of magnetic resonance images in diffuse intrinsic pontine glioma: a survey of pediatric neurosurgeons—clinical article," *Journal of Neurosurgery: Pediatrics*, vol. 8, no. 1, pp. 97–102, 2011.

[7] D. Hargrave, N. Chuang, and E. Bouffet, "Conventional MRI cannot predict survival in childhood diffuse intrinsic pontine glioma," *Journal of Neuro-Oncology*, vol. 86, no. 3, pp. 313–319, 2008.

[8] A. K. Liu, J. Brandon, N. K. Foreman, and L. Z. Fenton, "Conventional MRI at presentation does not predict clinical response to radiation therapy in children with diffuse pontine glioma," *Pediatric Radiology*, vol. 39, no. 12, pp. 1317–1320, 2009.

[9] L. Kornreich, M. Schwarz, B. Karmazyn et al., "Role of MRI in the management of children with diffuse pontine tumors: a study of 15 patients and review of the literature," *Pediatric Radiology*, vol. 35, no. 9, pp. 872–879, 2005.

[10] I. Yang, N. G. Huh, Z. A. Smith, S. J. Han, and A. T. Parsa, "Distinguishing glioma recurrence from treatment effect after radiochemotherapy and immunotherapy," *Neurosurgery Clinics of North America*, vol. 21, no. 1, pp. 181–186, 2010.

[11] M. D. Nelson Jr., D. Soni, and T. Z. Baram, "Necrosis in pontine gliomas: radiation induced or natural history?" *Radiology*, vol. 191, no. 1, pp. 279–282, 1994.

[12] K. J. Helton, N. S. Phillips, R. B. Khan et al., "Diffusion tensor imaging of tract involvement in children with pontine tumors," *American Journal of Neuroradiology*, vol. 27, no. 4, pp. 786–793, 2006.

[13] H. J. Chen, A. Panigrahy, G. Dhall, J. L. Finlay, M. D. Nelson Jr., and S. Blüml, "Apparent diffusion and fractional anisotropy of diffuse intrinsic brain stem gliomas," *American Journal of Neuroradiology*, vol. 31, no. 10, pp. 1879–1885, 2010.

[14] A. Virta, A. Barnett, and C. Pierpaoli, "Visualizing and characterizing white matter fiber structure and architecture in the human pyramidal tract using diffusion tensor MRI," *Magnetic Resonance Imaging*, vol. 17, no. 8, pp. 1121–1133, 1999.

[15] J. A. Brunberg, T. L. Chenevert, P. E. McKeever et al., "In vivo MR determination of water diffusion coefficients and diffusion anisotropy: correlation with structural alteration in gliomas of the cerebral hemispheres," *American Journal of Neuroradiology*, vol. 16, no. 2, pp. 361–371, 1995, Erratum in "In vivo MR determination of water diffusion coefficients and diffusion anisotropy: correlation with structural alteration in gliomas of the cerebral hemispheres", *American Journal of Neuroradiology*, vol. 16, no. 6, p. 1384, 1995.

[16] L. Walker, L.-C. Chang, C. G. Koay et al., "Effects of physiological noise in population analysis of diffusion tensor MRI data," *NeuroImage*, vol. 54, no. 2, pp. 1168–1177, 2011.

[17] Y. Kang, S. H. Choi, Y.-J. Kim et al., "Gliomas: histogram analysis of apparent diffusion coefficient maps with standard- or high-b-value diffusion-weighted MR imaging -correlation with tumor grade," *Radiology*, vol. 261, no. 3, pp. 882–890, 2011.

[18] A. Jakab, P. Molnár, M. Emri, and E. Berényi, "Glioma grade assessment by using histogram analysis of diffusion tensor imaging-derived maps," *Neuroradiology*, vol. 53, no. 7, pp. 483–491, 2011.

[19] M. Nowosielski, W. Recheis, G. Goebel et al., "ADC histograms predict response to anti-angiogenic therapy in patients with recurrent high-grade glioma," *Neuroradiology*, vol. 53, no. 4, pp. 291–302, 2011.

[20] W. B. Pope, H. J. Kim, J. Huo et al., "Recurrent glioblastoma multiforme: ADC histogram analysis predicts response to bevacizumab treatment," *Radiology*, vol. 252, no. 1, pp. 182–189, 2009.

[21] W. B. Pope, A. Lai, R. Mehta et al., "Apparent diffusion coefficient histogram analysis stratifies progression-free survival in newly diagnosed bevacizumab-treated glioblastoma," *American Journal of Neuroradiology*, vol. 32, no. 5, pp. 882–889, 2011.

[22] W. B. Pope, X. J. Qiao, H. J. Kim et al., "Apparent diffusion coefficient histogram analysis stratifies progression-free and overall survival in patients with recurrent GBM treated with bevacizumab: a multi-center study," *Journal of Neuro-Oncology*, vol. 108, no. 3, pp. 491–498, 2012.

[23] M. E. Bastin, T. K. Carpenter, P. A. Armitage, S. Sinha, J. M. Wardlaw, and I. R. Whittle, "Effects of dexamethasone on cerebral perfusion and water diffusion in patients with high-grade glioma," *American Journal of Neuroradiology*, vol. 27, no. 2, pp. 402–408, 2006.

[24] S. Minamikawa, K. Kono, K. Nakayama et al., "Glucocorticoid treatment of brain tumor patients: changes of apparent diffusion coefficient values measured by MR diffusion imaging," *Neuroradiology*, vol. 46, no. 10, pp. 805–811, 2004.

[25] K. Warren, R. Bent, P. L. Wolters et al., "A phase 2 study of pegylated interferon α-2b (PEG-Intron) in children with diffuse intrinsic pontine glioma," *Cancer*, vol. 118, no. 14, pp. 3607–3613, 2012.

[26] C. Pierpaoli, L. Walker, M. O. Irfanoglu et al., "TORTOISE: an integrated software package for processing diffusion MRI data," in *Proceedings of the 18th ISMRM Annual Meeting*, Stockholm, Sweden, 2010.

[27] M. J. McAuliffe, F. M. Lalonde, D. McGarry, W. Gandler, K. Csaky, and B. L. Trus, "Medical image processing, analysis & visualization in clinical research," in *Proceedings of the 14th IEEE Symposium on Computer-Based Medical Systems (CBMS '01)*, pp. 381–388, Bethesda, Md, USA, July 2001.

[28] G. K. Rohde, A. S. Barnett, P. J. Basser, S. Marenco, and C. Pierpaoli, "Comprehensive approach for correction of motion and distortion in diffusion-weighted MRI," *Magnetic Resonance in Medicine*, vol. 51, no. 1, pp. 103–114, 2004.

[29] M. Wu et al., "Comparison of EPI distortion correction methods in diffusion tensor MRI using a novel framework," in *Medical Image Computing and Computer-Assisted Intervention—MICCAI 2008*, vol. 5242 of *Lecture Notes in Computer Science*, pp. 321–329, 2008.

[30] P. J. Basser, J. Mattiello, and D. Lebihan, "Estimation of the effective self-diffusion tensor from the NMR spin echo," *Journal of Magnetic Resonance B*, vol. 103, no. 3, pp. 247–254, 1994.

[31] C. Pierpaoli and P. J. Basser, "Toward a quantitative assessment of diffusion anisotropy," *Magnetic Resonance in Medicine*, vol. 36, no. 6, pp. 893–906, 1996.

[32] C. Pierpaoli, P. Jezzard, P. J. Basser, A. Barnett, and G. di Chiro, "Diffusion tensor MR imaging of the human brain," *Radiology*, vol. 201, no. 3, pp. 637–648, 1996.

[33] L.-C. Chang, D. K. Jones, and C. Pierpaoli, "RESTORE: robust estimation of tensors by outlier rejection," *Magnetic Resonance in Medicine*, vol. 53, no. 5, pp. 1088–1095, 2005.

[34] R. M. Hayward, N. Patronas, E. H. Baker, G. Vézina, P. S. Albert, and K. E. Warren, "Inter-observer variability in the measurement of diffuse intrinsic pontine gliomas," *Journal of Neuro-Oncology*, vol. 90, no. 1, pp. 57–61, 2008.

[35] L. J. Edwards, K. E. Muller, R. D. Wolfinger, B. F. Qaqish, and O. Schabenberger, "An R^2 statistic for fixed effects in the linear mixed model," *Statistics in Medicine*, vol. 27, no. 29, pp. 6137–6157, 2008.

Hindawi Publishing Corporation
BioMed Research International
Volume 2014, Article ID 657953, 10 pages
http://dx.doi.org/10.1155/2014/657953

Clinical Study

Salvage Radiosurgery for Selected Patients with Recurrent Malignant Gliomas

Miguel Martínez-Carrillo,[1] Isabel Tovar-Martín,[1] Mercedes Zurita-Herrera,[1] Rosario Del Moral-Ávila,[1] Rosario Guerrero-Tejada,[1] Enrique Saura-Rojas,[2] Juan Luis Osorio-Ceballos,[3] Juan Pedro Arrebola-Moreno,[1] and José Expósito-Hernández[1]

[1] *Radiation Oncology Department, Virgen de las Nieves University Hospital, 18014 Granada, Spain*
[2] *Neurosurgery Department, Virgen de las Nieves University Hospital, 18014 Granada, Spain*
[3] *Medical Physics Department, Virgen de las Nieves University Hospital, 18014 Granada, Spain*

Correspondence should be addressed to Isabel Tovar-Martín; aris.tovar@gmail.com

Received 13 February 2014; Revised 13 April 2014; Accepted 16 April 2014; Published 7 May 2014

Academic Editor: Giuseppe Lombardi

Purpose. To analyse the survival after salvage radiosurgery and to identify prognostic factors. *Methods*. We retrospectively reviewed 87 consecutive patients, with recurrent high-grade glioma, that underwent stereotactic radiosurgery between 1997 and 2010. We evaluated the survival after initial diagnosis and after reirradiation. The prognostic factors were analysed by bivariate and multivariate Cox regression model. *Results*. The median age was 48 years old. The primary histology included anaplastic astrocytoma (47%) and glioblastoma (53%). A margin dose of 18 Gy was administered in the majority of cases (74%). The median survival after initial diagnosis was 21 months (39 months for anaplastic astrocytoma and 18.5 months for glioblastoma) and after reirradiation it was 10 months (17 months for anaplastic astrocytoma and 7.5 months for glioblastoma). In the bivariate analyses, the prognostic factors significantly associated with survival after reirradiation were age, tumour and treatment volume at recurrence, recursive partitioning analyses classification, Karnofsky performance score, histology, and margin to the planning target volume. Only the last four showed significant association in the multivariate analyses. *Conclusion*. stereotactic radiosurgery is a safe and may be an effective treatment option for selected patients diagnosed with recurrent high-grade glioma. The identified prognostic factors could help individualise the treatment.

1. Introduction

Gliomas are primary malignant brain tumours that arise from glial cells. The World Health Organization (WHO) has classified gliomas into four grades of ascending malignancy [1]. According to this classification, grade III and grade IV, also known as anaplastic astrocytoma (AA) and glioblastoma multiforme (GBM), respectively, are the most aggressive and are termed high-grade gliomas (HGG) [1]. The current standard treatment for glioblastoma patients includes maximal surgical resection, followed by temozolomide (TMZ) concomitant with external beam radiation (EBRT), and then subsequently with additional TMZ cycles, following the Stupp protocol [2]. Despite significant improvements in neuroimaging, surgical techniques, radiotherapy, and chemotherapy, the prognosis for these patients is still poor, with a median survival of 14.6 months and an overall survival of 27% after 2 years, dropping then to under 10% after 5 years [2].

Recurrence occurs in more than 90% of the patients [3] and its treatment is not clearly established with a median survival of 3–6 months without treatment [4]. Different options of treatment include: repetition of surgical resection, reirradiation with EBRT, brachytherapy or stereotactic radiosurgery (SRS), chemotherapy, novel therapies, or a combination of the above. Due to the highly invasive nature of HGG

and the subsequent difficulty to delineate it, local treatment does not seem to make sense. However, the majority of treatment failures are within the irradiated field; up to 90% of recurrences occurred within 2 cm of the tumour margins [5]. For this reason, local control is one of the main goals of the treatment of recurrent HGG.

Tumour resection is a good option for salvage treatment, but it is associated with many postoperative complications. EBRT exposes the brain to a high risk of radiation-related toxicity and necrosis. Brachytherapy is also associated with serious side effects like infections or risk of haemorrhage. All of this suggests a potential key role for SRS in the management of recurrent HGG; in addition, these tumours are relatively hypoxic with low α/β and a priori good responders to hypofractionated irradiation [4–6].

First conceived by Lars Leksell in 1951, stereotactic radiosurgery (SRS) is an irradiation modality that combines stereotactic technique with highly focused high-energy radiation treatments, making it possible to deliver large doses of radiation to an extremely small target [7].

The experience of reirradiation with radiosurgery for recurrent HGG is limited. At our institution, we have performed single fraction reirradiation (SRS) in selected patients with relatively well defined recurrent tumors as seen on imaging studies, which have an adequate volume.

In this study, we investigated our clinical data to evaluate the efficacy of SRS as a salvage treatment and the potential prolongation of survival time in 87 patients. Additionally we reported the results of overall and post-SRS survival and prognostic factors in patients with recurrent HGG treated with linear accelerator- (LINAC-) based radiosurgery over a 12-year period.

2. Patients and Methods

2.1. Patients. Between 1997 and 2010, 87 consecutive adult patients were treated at Virgen de las Nieves University Hospital (Granada, Spain). All of them underwent SRS LINAC as salvage treatment for recurrent HGG with the following features: (1) pathologically confirmed diagnosis of AA or GBM at the time of initial management; (2) underwent subsequent fractionated radiotherapy treatment with radical intent; (3) developed new or increasing contrast-enhanced lesions at the margin of primary localization in the follow-up magnetic resonance imaging (MRI) after radiotherapy, indicating tumour recurrence or progression; and (4) the size of the lesion was <3 cm.

Data were retrospectively collected by reviewing medical records, last followup in the hospital, and MRI studies and contacting patients and/or families. This way, we obtained information about age, gender, recursive partitioning analyses (RPA) classification [8], Karnofsky performance status (KPS) score, histology as World Health Organization (WHO) grade 3 gliomas AA or GBM, time to relapse, tumour and treatment volume at recurrence, margin to the planning target volume, dose administered, and radiological and neurological responses. Dates of death were obtained from National Death Index (INDEF, Spanish initials).

2.2. Radiosurgery. Outpatient radiosurgery was indicated by a medical staff composed of neurosurgeons, radiologists, radiation oncologists, and physicists involved in treatment planning and target volume determination for all patients.

Treatment was planned on the image fusion of computed tomography (CT) and MRI data, for the contrast-enhancing regions on T1-weighted MRI images, and was delivered using a linear accelerator (LINAC) (Varian 2100) equipped with micro-multileaf collimators (MMC) using 6 MV photons. A BrainLAB stereotactic head frame (BrainLAB A.G., Heimstetten, Germany) was used for every patient. BrainLAB cones were used for the treatment until 2004 when dynamic micro-multileaf collimator was incorporated (Figure 1).

The prescribed dose for reirradiation was based on tumour volume, prior radiation dose, time since EBRT, and location of the lesion with proximity to eloquent brain or radiosensitive structures. The GTV (contrast-enhancing lesion in T1-weighted MR images) was expanded by 0–6 mm to generate the planning target volume (PTV). This expansion was related to the year of treatment (without any expansion during the first five years), in the size and location of the recurrence.

2.3. Followup. After SRS, patients were seen for a follow-up visit after 8 weeks and thereafter in 3 months intervals. Each follow-up appointment consisted of a thorough clinical examination, including a neurological assessment and a contrast-enhanced MRI. Local control (LC) was defined as stabilization or decrease of lesion size or enhancement on imaging and lack of consistently increased surrounding T2 signal changes on serial examinations. Local failure was defined as persistent increase in size of the contrast-enhancing lesion (>20% volume increase) or new contiguous areas at the margin of treatment and concomitant T2 signal change. Toxicity was also collected. Differentiating second-time recurrence tumour after SRS from radiation injury based on MRI is difficult. Progressive contrast enhancements over time may represent either a mixture of a viable tumour and radiation-induced necrosis or radiation injury only. Metabolic imaging, MR spectroscopy, and MR perfusion were used as supplements in some uncertain cases.

2.4. Statistical Analyses. The aim of these studies is to examine the overall survival, post-SRS survival, and the identification of prognostic factors with influence on survival after SRS.

Overall survival was calculated from the time of the primary diagnosis to the time of death or last followup. Survival after SRS was calculated from the time of SRS until the death of last followup, using the Kaplan-Meier method.

Bivariate statistical analyses were performed to examine the relationships between the duration of survival after SRS and different variables at the time of the treatment, using Cox regression models. In a first step, those variables which were statistically significant in the bivariate analyses were included in the multivariate model that was finally built using a backward stepwise technique. Diagnosis of the models was performed in order to ensure the goodness

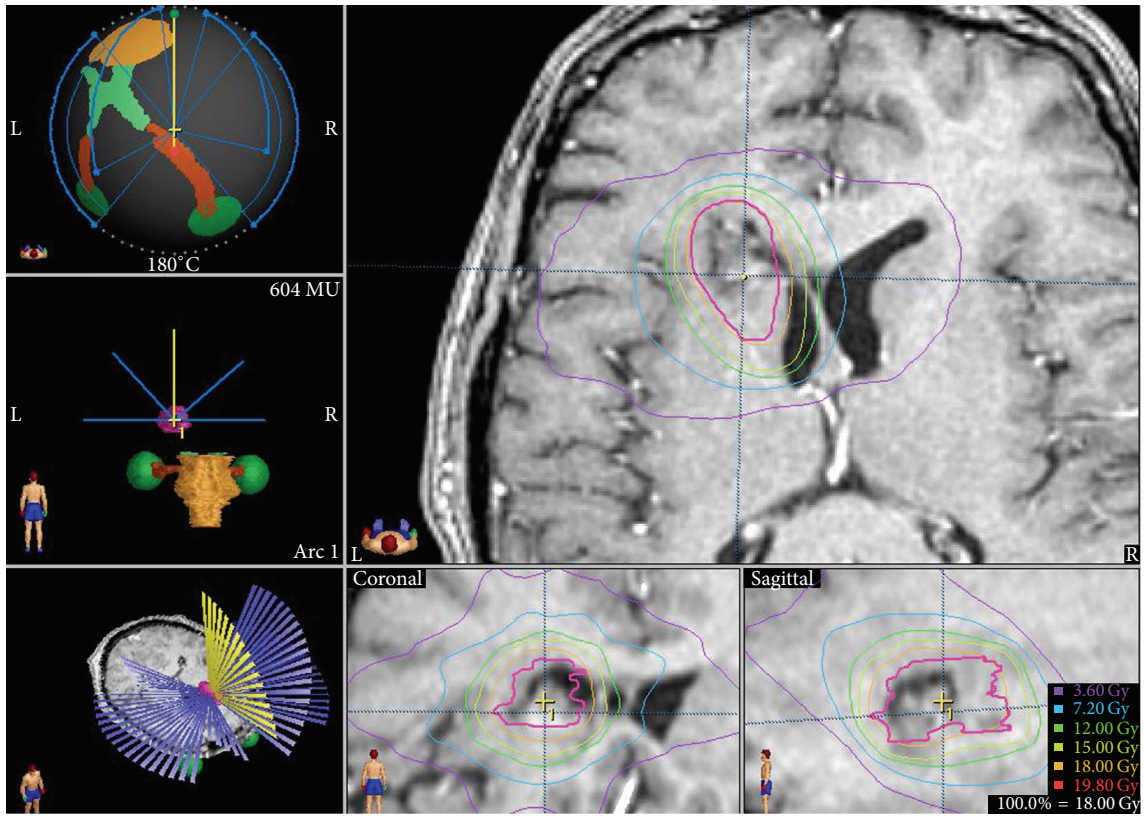

Figure 1: An example of radiosurgery treatment in our department.

Table 1: Initial treatment features.

Parameters	Number of patients (%)
Number or patients	87
Primary surgery	
Complete resection	43 (49.4)
Subtotal resection	23 (26.4)
Biopsy	21 (24.2)
Adjuvant therapy	
Stupp protocol	51 (58.6)
PCV + EBRT	12 (13.8)
EBRT without chemotherapy	24 (27.6)

of the fit and the fulfilment of implementation conditions. Hazard ratios (HRs) with 95% confidence intervals (CIs) were calculated. Two-sided P values less than 0.05 were considered significant. SPSS version 12 (SPSS, Chicago, IL) was used for statistical analyses, except for multivariate analyses that were performed by "R" version 3.0.2.

3. Results

3.1. Patients. The initial treatment characteristics are shown in Table 1. This initial treatment included: surgery, EBRT within 8–12 weeks after surgery with doses varying 54–66 Gy (mean 60 Gy), and adjuvant chemotherapy in 63 patients. Surgery with complete resection was performed in 43 patients (49.4%). From 1999 up to and including 2004, patients received EBRT alone or in combination with procarbazine, lomustine, and vincristine (PCV). From 2005, patients received the Stupp protocol [9] with temozolomide and EBRT, except for patients without good medical conditions who underwent exclusive EBRT. Thus, 51 patients (58.6%) were treated with the Stupp protocol, 12 patients (13.8%) were treated with EBRT in combination with PCV, and 24 patients (27.6%) were treated with EBRT alone.

Clinical features in recurrence are summarised in Table 2. Out of 87 patients, 43 were males and 44 females; median age was 49 years old; 41 patients with anaplastic astrocytoma (AA) and 46 with glioblastoma (GBM). The diagnosis was histologically confirmed in all patients. KPS score was higher than 80 in 40 patients. 51 patients (29 with AA and 20 with GBM) had surgery for the first recurrence and radiosurgery for the residual tumour seen on the postoperative MRI after reoperation or for a second recurrence. The median time interval from diagnosis to SRS treatment was 13.8 months (range 5–61 m).

3.2. Radiosurgery and Radiological and Clinical Responses. The median prescribed dose was 18 Gy (range 14–20). The median tumor volume and PTV volume were 4 cc and 6 cc, respectively. The margin of the GTV to create the PTV was 0 mm in the majority of treatments (48.3%) followed by 5 (20.7%). The treatment was administered by cones in 40.2% of cases and by MMC in 59.8%. The majority of patients

Table 2: Patient treatment characteristics at recurrence.

Parameters	Number of patients	Patients treated by Stupp protocol	Patients diagnosed with AA	Patients diagnosed with GBM
Numbers of patients	87	51	41	46
Gender				
Male	43 (49.4%)	27 (52.9%)	16 (39%)	27 (58.7%)
Female	44 (50.6%)	24 (47.1%)	25 (61%)	19 (41.3%)
Age (years)				
median (range)	48.7 (18–78)	47 (26–71)	45 (18–78)	49.5 (26–78)
KPS				
Mean (range)	83 (60–100)	90 (70–100)	90 (70–100)	80 (70–100)
KPS > 80	40 (46%)	28 (54.9%)	22 (53.7%)	18 (39.1%)
KPS ≤ 80	47 (50%)	23 (45.1%)	19 (46.3%)	28 (60.9%)
RPA				
Mean (range)	4.1 (3–5)	4 (3–5)	4 (3–5)	4 (3–5)
Histology				
Anaplastic astrocytoma	41 (47.1%)	25 (49%)	100%	0
Glioblastoma	46 (52.9%)	26 (51%)	0	100%
Time to recurrence (months)				
Mean (range)	13.8 (4–61)	11 (4–61)	10 (4–61)	10 (5–28)
≤8 months	29 (33.3%)	14 (27.4%)	12 (29.3%)	17 (36.9%)
9–12 months	30 (34.5%)	19 (27.3%)	15 (36.6%)	15 (32.6%)
>12 months	28 (32.2%)	18 (35.3%)	14 (34.1%)	13 (30.5%)
Tumour volume (cc)				
Mean (range)	8.7 (1–42.6)	4 (0.36–34.1)	5.2 (1–28)	4 (0.05–34.1)
<3 cc	29 (33.3%)	16 (31.4%)	12 (29.3%)	17 (37%)
4–7 cc	26 (29.9%)	22 (43.1%)	12 (29.3%)	14 (30.4%)
>7 cc	32 (36.8%)	13 (25.5%)	17 (41.4%)	15 (32.6%)
Location				
Unifocal	79 (90.8%)	45 (88.2%)	39 (95.1%)	40 (87%)
Multifocal	8 (9.2%)	6 (11.8%)	2 (4.9%)	6 (13%)
Dose radiosurgery				
Mean (range)	18.01 Gy (14–20)	18 Gy (16–20)	18 (15–20)	18 Gy (14–20)
Dose ≥ 18 Gy	76 (87%)	46 (90.2%)	35 (85.4%)	41 (89.1%)
PTV margin				
Mean (range)	1.67 mm (0–6)	2 mm (0–6)	2 mm (0–5)	0 mm (0–6)
0 mm	43 (49.4%)	20 (39.2%)	19 (46.3%)	24 (52.2%)
1–3 mm	22 (25.3%)	10 (19.6%)	12 (29.3%)	10 (21.7%)
>3 mm	22 (25.3%)	21 (41.2%)	10 (24.4%)	12 (26.1%)

received only one SRS treatment (89%), while the remainder underwent more than one course of SRS (9.8% two SRSs and 1.2% three SRSs).

The median follow-up after SRS was 10 months (range 1–141 months). The initial radiological response was complete in 7.8%, partial in 24.7%, stabilisation in 32.5%, and progression in 26%. In 9% of the patients the response could not be evaluated, because of death before the MRI. These patients are considered as nonresponders. At the initial evaluation after the SRS, 17.1% of patients were clinically better than before the treatment, 32.9% remained without change, 21.4% were neurologically worse, and 28.6% were not evaluated because of death before the first follow-up visit or incomplete data in the clinical record.

There were no cases of treatment-related adverse events or episodes of acute neurological toxicity. On the follow-up images (10%) there was an increasing oedema with a transient worsening of neurological function for the patients; all of this was considered as adverse radiation effects.

The treatment of local failure post-SRS consisted of surgical resection in three patients, changes in chemotherapy regimen in five patients, and no further treatment for the remainder.

3.3. Survival and Prognostic Factors. At the end of the study 7 patients (8%) were alive with no evidence of disease, 5 patients (5.7%) were alive with disease, and 75 patients (86.2%) were dead. The cause of death was the progression of the tumour in all patients.

Table 3 shows the information about survival. The median overall survival was 21 months (range 9–151 months), although patients treated by Stupp protocol had higher survival than patients treated by other treatments [10].

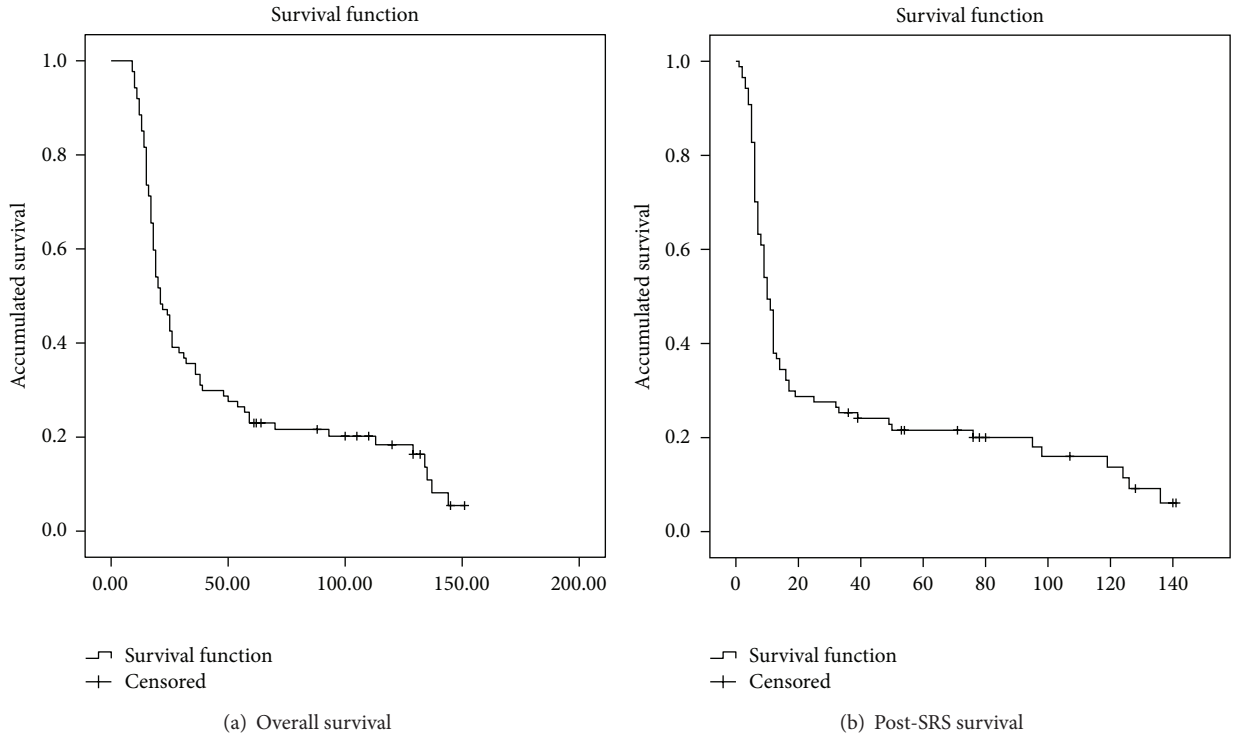

(a) Overall survival

(b) Post-SRS survival

Figure 2: Overall and post-SRS survival. Kaplan-Meier survival function.

Initial treatment (Stupp versus others) was not significantly associated with overall survival (HR = 0.79; 95 % CI = 0.49–1.25). The actuarial global survival rates after 12, 24, and 36 months were 88.5%, 46%, and 35.6%, respectively (Figure 2(a)). The median survival after SRS was 10 months (range 1–141 months), 7.5 months for GBM (range 1–140), and 17 months for AA (4–141). The actuarial survival after SRS rate was 37.9% after 12 months, 28.7% after 24 months, and 25.3% after 36 months (Figure 2(b)).

The variables included in the analyses of the prognostic factors of post-SRS survival were age (year old), gender, KPS score, RPA classification, histology (AA or GBM), initial surgery (complete or not), initial treatment (Stupp protocol versus other treatments), time of recurrence (months), focality (unifocal or multifocal), tumour volume (cubic centimeter), treatment volume (cubic centimeter), margin to the PTV (millimeter), and dose (Gy) administered. In the bivariate analyses (Table 4) the following variables were significantly associated with survival post-SRS: age (years old) (HR = 1.04; 95% CI = 1.01–1.05), KPS ≤ 80 versus > 80 (HR = 2.59; 95% CI = 1.55–4.3), RPA IV versus III (HR = 2.39; 95% CI = 1.18–4.82), RPA V versus III (HR = 6.32; 95% CI = 2.82–14.14), GBM versus AA (HR = 2.45; 95% CI = 1.53–3.94), tumour volume (cubic centimetre) (HR = 1.04; 95% CI = 1.01–1.07), treatment volume (cubic centimetre) (HR = 1.03; 95% CI = 1.01–1.06), and margin to the PTV (millimetre) (HR = 0.77; 95% CI = 0.67–0.87). In the multivariate analyses (Table 3) we found that the risk of sudden death was 2.08 times higher in KPS ≤ 80 than KPS > 80 (95% CI = 0.28–0.83) (Figure 3(a)), 3.13 times higher in GBM than AA (95% CI = 1.79–5.48) (Figure 3(b)), 3.46 times higher in RPA IV than RPA III (95% CI = 1.61–7.46), 7.29 times higher in RPA V than RPA III (95% CI = 3.23–16.34) (Figure 3(c)), and 3.19 times higher in PTV margin 0 than PTV ≥ 1 (95 % CI = 1.91–5.31).

4. Discussion

Poor prognosis of this HGG with high risk of relapse, mainly within 2 cm of the resection cavity, suggests there is a need to improve local treatment [4]. Hau et al. [11] compared patients who were treated with aggressive salvage therapy including SRS with a group of patients who received no salvage treatment. In that study, the median actuarial survival after recurrence was 8.2 months in the intervention group and 2.2 months in the nonintervention group, indicating that salvage treatment was beneficial.

Several authors have studied the optimal moment to administer SRS: as an initial treatment or as an adjuvant treatment for recurrence [6, 12]. Nowadays, the study with the highest level of evidence is Radiation Therapy Oncology Group 93-05 [12]. Although it was highly criticised, the conclusion was that the addition of SRS at the time of initial treatment did not appreciably enhance survival, quality of life, or neurocognition for GBM. However, Kong et al. [13] showed a survival benefit of SRS as salvage treatment compared with historic control. So far, the main role of SRS takes place at the time of recurrence, for this reason, our department does not recommend SRS as initial treatment.

Managing recurrent HGG is particularly challenging. Surgery is well established as newly diagnoses HGG; however,

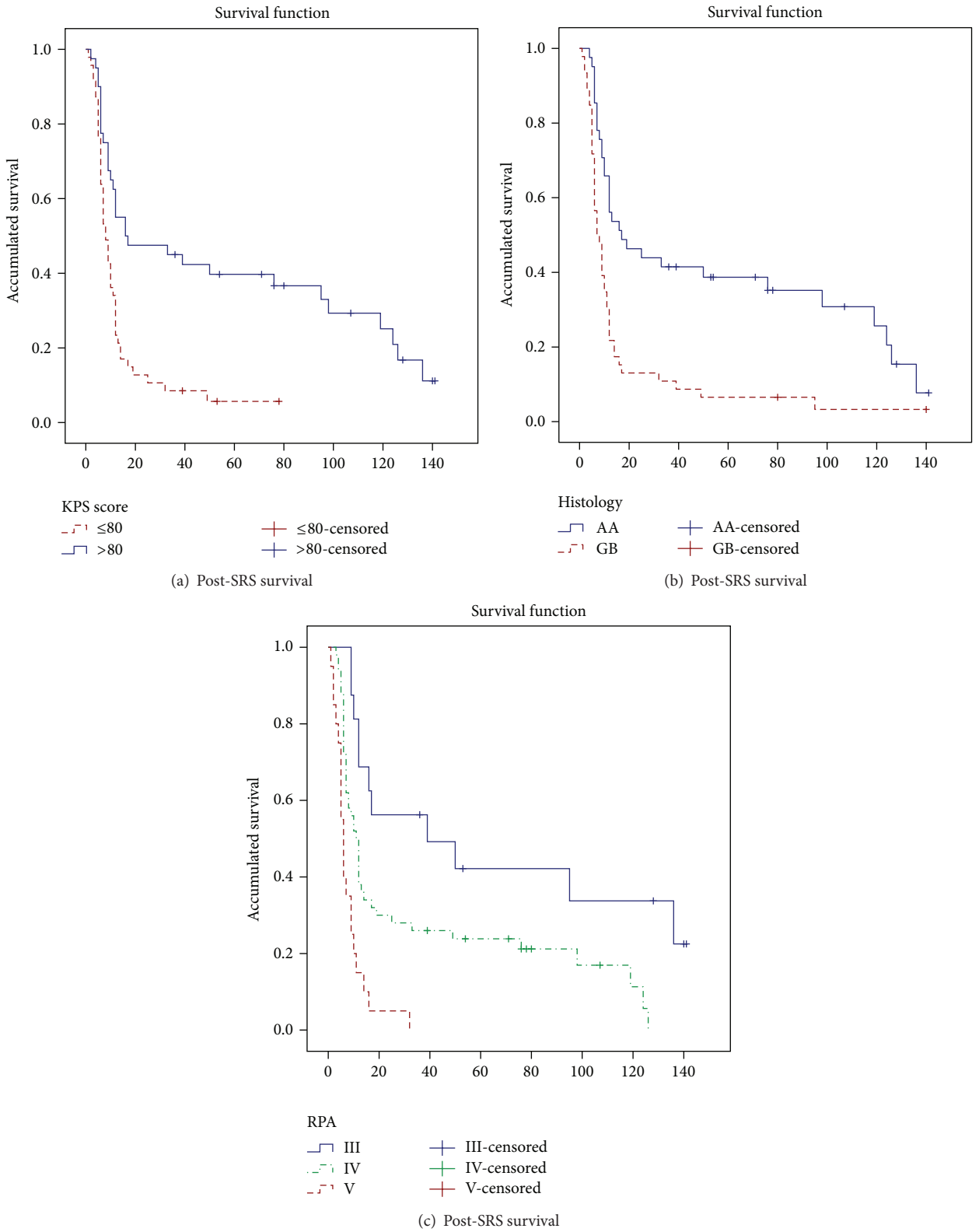

(a) Post-SRS survival

(b) Post-SRS survival

(c) Post-SRS survival

Figure 3: Prognosis factors, Kaplan-Meier survival function.

Table 3: Survival.

	Stupp protocol	Others Treatments	AA	GBM
OS (median)	21 months	19 months	39 months	18.5 months
Actuarial Sv				
12 m	88.5%	88.9%	95.1%	82.6%
24 m	46%	36.1%	41.5%	50%
36 m	35.6%	25%	30.9%	21.7%
Post-SRS Sv	10 months	9 months	17 months	7.5 months
Actuarial post-SRS Sv				
12 m	37.9%	30.6%	70.7%	30.4%
24 m	28.7%	19.4%	41.5%	13%
36 m	25.3%	16.7%	25.7%	10.9%

OS: overall survival and Sv: survival.

Table 4: Prognostic factors.

Variables	Bivariate analyses		Multivariate analyses	
	HR (95% CI)	P value	HR (95% CI)	P value
Age	1.04 (1.01–1.05)	$P < 0.001$	Not significant	
KPS (≤80 versus >80)	2.59 (1.55–4.3)	$P < 0.001$	2.08 (0.28–0.83)	$P = 0.008$
RPA				
IV versus III	2.39 (1.18–4.82)	$P = 0.015$	3.46 (1.61–7.46)	$P = 0.001$
V versus III	6.32 (2.82–14.14)	$P < 0.001$	7.29 (3.23–16.34)	$P < 0.001$
Histology (GBM versus AA)	2.45 (1.53–3.94)	$P < 0.001$	3.13 (1.79–5.48)	$P < 0.001$
Tumour volume	1.04 (1.01–1.07)	$P = 0.005$	Not significant	
Treatment volume	1.03 (1.01–1.06)	$P = 0.013$	*	
Margin to PTV				
0 versus ≥1	0.77 (0.67–0.87)	$P < 0.001$	3.19 (1.91–5.31)	$P < 0.001$

* This variable was not considered for the multivariate analyses because of the strong correlation (0.97 Spearman' s correlation coefficient) with tumour volume.

the reoperation has a low median postoperative survival and high complication rates due to the infiltrative growth pattern of gliomas [14–16]. Skeie et al. [17] reviewed patients treated with SRS, surgery, or both. For recurrent GBM the median survival for SRS was significantly better than surgery. Surgery could be used to decrease the size of a large tumour before SRS. This way, 59% of our patients underwent surgery as salvage treatment after recurrence that allowed the treatment with SRS for the residual tumour. EBRT increases the risk of late cumulative radiation injury, although the recent advances in radiotherapy that reduce the radiation to surrounding brain tissue can turn this treatment into a useful option for tumours with a larger volume [4]. Brachytherapy can have side effects as radiation necrosis, hemorrhage, and infection [4]. Thus, there is a clear advantage of SRS over brachytherapy: the noninvasive approach. There have been many studies suggesting that SRS is effective mainly for HGG [13, 18–20].

Related to adverse side effects due to reirradiation by SRS, early toxicity as headache, nausea, vomiting, and so forth is medically managed, while late complication involves radiation necrosis that typically develops one to three years after radiation. The incidence reported by the literature varies from 0% [21, 22] to 30% [23, 24] and is associated with tumour volume [24]. In our series, none of the patients had radiation necrosis, probably given the short life expectancy. In addition, we believe that SRS provides a highly precise delivery of radiation dose sufficient to induce tumour cell death while sparing surrounding host tissue. For this reason, we think reirradiation by SRS is safe for small tumours.

We analysed our series with 87 patients treated with SRS at the moment of the recurrence. We used a LINAC equipped with micro-multileaf collimators (MMC) using 6 MV photons and a BrainLAB stereotactic head frame. There are different SRS modalities (LINAC, Cyberknife and Gamma knife), and most of the published articles describe the experience with Gamma Knife. However, there is no evidence of which modality is better. The majority of patients received 18 Gy in one fraction, and as other authors pointed, because of the high radiation dose already given in the initial treatment with EBRT, it is difficult to administer a high dose [17]. Skeie et al. [17] did not find any difference in survival when they compared patients who received more than 12 Gy versus ≤12 Gy. In addition, the dose administered was not correlated to survival post-SRS in our study.

The median overall and post-SRS survival in our study is in accordance with the literature (Table 5). The median post-SRS survival varies between 6.5 months [25] and 26 months

Table 5: Studies of SRS as treatment for recurrent high-grade gliomas.

Study	*N*	Histological grade	Median dose (Gy)	Median volume (cm^3)	Median post-SRS survival (months)	Prognostic factors
Chamberlain et al., 1994 [34]	15	IV	13.4	17	8	NR
Hall et al., 1995 [35]	25	III–IV	20	28	6.5	Age, KPS
Shrieve et al., 1995 [27]	86	IV	13	10.1	12	Age, volume
Larson et al., 1996 [31]	93	IV	16	6.5	16.4	Age, grade, KPS, focality, and volume
Kondziolka et al., 1997 [36]	42	III–IV	15.5	6.5	21	Grade, volume
Cho et al., 1999 [23]	46	III–IV	17	10	11	Age, grade, KPS, and volume
Ulm et al., 2005 [30]	33	III–IV	15	—	—	Location, RPA
Hsieh et al., 2005 [24]	26	IV	12	21.6	10	KPS
Mahajan et al., 2005 [37]	41	IV	—	4.7	11	None
Combs et al., 2005 [21]	32	IV	15	10	10	None
Kong et al., 2008 [13]	114	III–IV	16	10.6	26 (III)–13 (IV)	Histology, volume
Patel et al., 2009 [18]	26	IV	18	10.4	8.5	None
Biswas et al., 2009 [38]	18	IV	15	8.4	5.3	NR
Villavicencio et al., 2009 [25]	26	IV	20	7	7	Extent of surgery
Pouratian et al., 2009 [22]	26	IV	6	21.3	9.4	KPS, PTV margin
Torok et al., 2011 [39]	14	IV	24	6.97	10	NR
Maranzano et al., 2011 [40]	13	IV	17.3	5.3	11	Radiation dose
Cuneo et al., 2012 [29]	63	III/IV	15	4.8	11	Age, KPS, and bevacizumab
Park et al., 2012 [41]	11	IV	16	13.6	17.9	None
Skeie et al., 2012 [17]	51	IV	12.2	12.4	19 (from initial diagnosis)	None
Martínez-Carrillo 2014	87	III/IV	18.01	8.7	10 (17 III–7.5 IV)	KPS, RPA, histology, and PTV margin

NR: not reported.

[13]. These differences may be due to the inhomogeneity among the studies (clinical features of the patients, histological type, modalities of treatment after SRS, and so forth). The study with the largest number of patients is Kong et al.'s study [13] with a post-SRS survival of 26 months for grade III gliomas and 13 months for grade IV gliomas, different data as RPA classifications were not reported.

Favourable prognostic factors derived from the most relevant studies published (Table 5) include higher prescription dose, adequate SRS margin, anaplastic astrocytoma, smaller tumour volume, younger age, higher KPS, better RPA, location in noneloquent area, unifocality, and concurrent chemotherapy. However, among the different prognosis factors analysed in the present study, only KPS score, RPA, histology, and margin to the PTV made statistically a significant influence on post-SRS survival in the multivariate analyses. The identification of prognostic factors varies among studies. The difference may be due, in part, to the definition and/or adherence of eligibility criteria, clinical features of the patients, characteristic of the treatment, and so on. Other molecular prognosis factors as O-6-methylguanine-DNA methyltransferase (MGMT) methylation, 1p/19q deletion, or isocitrate dehydrogenase 1/2 (IDH1/2) mutation [26] were not included in these studies, probably because the role of this molecular factors is fairly recent.

Shrieve et al. [27] showed that while under 40 years old patients had a median survival of 49 months; over 40 years old patients had a median survival of 18.2 months ($P < 0.001$). In our study the age was associated with the post-SRS survival only in the bivariate analyses; thus, for each extra year of life the risk of sudden death was multiplied by 1.04 (95% CI = 1.01–1.05). We did not find this correlation in the multivariate analyses, perhaps because the variability explained by this variable in the bivariate analyses was later explained by the RPA classification in the multivariate model.

The tumour and treatment volumes were identified as prognosis factor for the post-SRS survival in the bivariate analyses but not in the multivariate analyses. Kong et al. [13] and Combs et al. [28] obtained the similar results, although the latter treated patients with fractionated stereotactic radiotherapy instead of SRS.

According to our statistical analyses, higher KPS score was statistically significant correlated with post-SRS survival. In our study the cut-off point was KPS score of 80

(Figure 2(a)), while Cuneo et al. [29] reported the same correlation but with a cut-off point of 70 in the KPS score. Other authors have shown KPS score as prognosis factor for survival with a cut-off point of 90 [22, 24].

RPA classification was a significant predictive value of survival on bivariate and multivariate analyses in this series, reinforcing the predictive value of the RPA classification even with salvage treatments. A survival benefit from SRS for patients with class III through V has also been suggested by Ulm et al. [30] and Skeie et al. [17].

We found that the risk of sudden death was 3.13 times higher in GBM than AA (95% CI = 1.79–5.48) (Figure 2(b)). In HGG group, grade III presents a significant favourable prognosis with respect to grade IV, for overall and postsalvage SRS survival. Larson et al. [31] found that the post-SRS survival was 68 weeks and 38 weeks for grade III and grade IV gliomas, respectively. Kong et al. [13] found similar results with post-SRS survival of 26 months and 13 months for grades III and IV, respectively.

PTV margin was a statistical significant protective factor. Several authors defend the use of an "extended field" to cover the potential microscopic expansion [32, 33]. As mentioned above, this strategy is supported by the acknowledgment that this kind of tumours tend to progress within 2 cm of the contrast-enhancing edge. Koga et al. [32] found a statistically significant difference in the local control between conventional SRS (47%) and extended field (93%). However, the "extended field" depends on the tumour volume, location,and if there are close organs at risk, considering that in reirradiation the treatment volume has a strong correlation with the toxicity.

To obtain better results for this kind of tumours, different strategies are mentioned:

(i) Imaging to improve the target delineation and to evaluate the results after treatment.

(ii) New chemotherapy agents and targeted therapies as bevacizumab [29].

(iii) Molecular characterisation of these tumours as the determination of the methylation status of MGMT [26].

The main weakness of our study is the retrospective character of the study with a heterogeneous population and nonuniform treatment modalities and selection bias because patients who are candidates for salvage SRS treatment tend to have more favourable prognosis factors than those ineligible patients. However, due to the low incidence of these tumours, a prospective study is difficult and in clinical practice, patients diagnosed with this entity are not homogeneous and neither is the initial treatment which depends on the medical condition of the patients. You can find the same problem related to the homogeneity of the sample in other published articles [3, 4, 13]. In addition, our series has a large number of patients and the results are in accordance with the literature.

5. Conclusion

There is no class I evidence establishing a "standard of care" for recurrence. Because local recurrence remains the predominant pattern of failure in patients with HGGs, local salvage treatment with SRS is appropriate and safe and may contribute to a prolonged survival in young patients with AA histology who have a good KPS score and RPA classification, a small volume, and are treated with an adequate margin. In addition, it seems multimodality treatment is better than no salvage therapy, for this reason, we recommend second surgery to reduce the volume of the recurrence and to complete the treatment with SRS if possible.

Conflict of Interests

The authors declare that there is no conflict of interests regarding the publication of this paper.

References

[1] D. N. Louis, H. Ohgaki, O. D. Wiestler et al., "The 2007 WHO classification of tumours of the central nervous system," *Acta Neuropathologica*, vol. 114, no. 2, pp. 97–109, 2007.

[2] R. Stupp, M. E. Hegi, W. P. Mason et al., "Effects of radiotherapy with concomitant and adjuvant temozolomide versus radiotherapy alone on survival in glioblastoma in a randomised phase III study: 5-year analysis of the EORTC-NCIC trial," *The Lancet Oncology*, vol. 10, no. 5, pp. 459–466, 2009.

[3] T. Koga and N. Saito, "Efficacy and limitations of stereotactic radiosurgery in the treatment of glioblastoma," *Neurologia Medico-Chirurgica*, vol. 52, no. 8, pp. 548–552, 2012.

[4] R. E. Elliott, E. C. Parker, S. C. Rush et al., "Efficacy of gamma knife radiosurgery for small-volume recurrent malignant gliomas after initial radical resection," *World Neurosurgery*, vol. 76, no. 1-2, pp. 128–140, 2011.

[5] L. A. Marin, C. E. Smith, M. Y. Langston, D. Quashie, and L. E. Dillehay, "Response of glioblastoma cell lines to low dose rate irradiation," *International Journal of Radiation Oncology Biology Physics*, vol. 21, no. 2, pp. 397–402, 1991.

[6] A. L. Elaimy, A. R. Mackay, W. T. Lamoreaux et al., "Clinical outcomes of gamma knife radiosurgery in the salvage treatment of patients with recurrent high-grade glioma," *World Neurosurgery*, vol. 80, no. 6, pp. 872–878, 2013.

[7] L. Leksell, "Stereotactic radiosurgery," *Journal of Neurology Neurosurgery and Psychiatry*, vol. 46, no. 9, pp. 797–803, 1983.

[8] C. B. Scott, C. Scarantino, R. Urtasun et al., "Validation and predictive power of Radiation Therapy Oncology Group (RTOG) recursive partitioning analyses classes for malignant glioma patients: a report using RTOG 90-06," *International Journal of Radiation Oncology Biology Physics*, vol. 40, no. 1, pp. 51–55, 1998.

[9] R. Stupp, W. P. Mason, M. J. Van den Bent et al., "Radiotherapy plus concomitant and adjuvant temozolomide for glioblastoma," *The New England Journal of Medicine*, vol. 352, no. 10, pp. 987–996, 2005.

[10] F. Nava, I. Tramacere, A. Fittipaldo et al., "Survival effect of first- and second-line treatments for patients with primary glioblastoma: a cohort study from a prospective registry, 1997–2010," *Neuro-Oncology*, vol. 16, no. 5, pp. 719–727, 2014.

[11] P. Hau, U. Baumgart, K. Pfeifer et al., "Salvage therapy in patients with glioblastoma: is there any benefit?" *Cancer*, vol. 98, no. 12, pp. 2678–2686, 2003.

[12] L. Souhami, W. Seiferheld, D. Brachman et al., "Randomized comparison of stereotactic radiosurgery followed by conventional radiotherapy with carmustine to conventional radiotherapy with carmustine for patients with glioblastoma multiforme: report of Radiation Therapy Oncology Group 93-05 protocol," *International Journal of Radiation Oncology Biology Physics*, vol. 60, no. 3, pp. 853–860, 2004.

[13] D.-S. Kong, J.-I. Lee, K. Park, H. K. Jong, D.-H. Lim, and D.-H. Nam, "Efficacy of stereotactic radiosurgery as a salvage treatment for recurrent malignant gliomas," *Cancer*, vol. 112, no. 9, pp. 2046–2051, 2008.

[14] G. R. Harsh, V. A. Levin, P. H. Gutin, M. Seager, P. Silver, and C. B. Wilson, "Reoperation for recurrent glioblastoma and anaplastic astrocytoma," *Neurosurgery*, vol. 21, no. 5, pp. 615–621, 1987.

[15] E. S. Mandl, C. M. F. Dirven, D. R. Buis, T. J. Postma, and W. P. Vandertop, "Repeated surgery for glioblastoma multiforme: only in combination with other salvage therapy," *Surgical Neurology*, vol. 69, no. 5, pp. 506–509, 2008.

[16] P. Dirks, M. Bernstein, P. J. Muller, and W. S. Tucker, "The value of reoperation for recurrent glioblastoma," *Canadian Journal of Surgery*, vol. 36, no. 3, pp. 271–275, 1993.

[17] B. S. Skeie, P. Ø. Enger, J. Brøgger et al., "Gamma knife surgery versus reoperation for recurrent glioblastoma multiforme," *World Neurosurgery*, vol. 78, no. 6, pp. 658–669, 2012.

[18] M. Patel, F. Siddiqui, J.-Y. Jin et al., "Salvage reirradiation for recurrent glioblastoma with radiosurgery: radiographic response and improved survival," *Journal of Neuro-Oncology*, vol. 92, no. 2, pp. 185–191, 2009.

[19] E. Binello, S. Green, and I. M. Germano, "Radiosurgery for high-grade glioma," *Surgical Neurology International*, vol. 3, supplement 2, pp. 118–126, 2012.

[20] J. B. Clavier, J. Voirin, P. Kehrli, and G. Noël, "Systematic review of stereotactic radiotherapy for high-gliomas," *Cancer Radiothérapie: Journal de La Société Française de Radiothérapie Oncologique*, vol. 14, no. 8, pp. 739–754, 2010.

[21] S. E. Combs, V. Widmer, C. Thilmann, H. Hof, J. Debus, and D. Schulz-Ertner, "Stereotactic radiosurgery (SRS): treatment option for recurrent glioblastoma multiforme (GBM)," *Cancer*, vol. 104, no. 10, pp. 2168–2173, 2005.

[22] N. Pouratian, R. W. Crowley, J. H. Sherman, J. Jagannathan, and J. P. Sheehan, "Gamma Knife radiosurgery after radiation therapy as an adjunctive treatment for glioblastoma," *Journal of Neuro-Oncology*, vol. 94, no. 3, pp. 409–418, 2009.

[23] K. H. Cho, W. A. Hall, B. J. Gerbi, P. D. Higgins, W. A. McGuire, and H. B. Clark, "Single dose versus fractionated stereotactic radiotherapy for recurrent high-grade gliomas," *International Journal of Radiation Oncology Biology Physics*, vol. 45, no. 5, pp. 1133–1141, 1999.

[24] P. C. Hsieh, J. P. Chandler, S. Bhangoo et al., "Adjuvant gamma knife stereotactic radiosurgery at the time of tumor progression potentially improves survival for patients with glioblastoma multiforme," *Neurosurgery*, vol. 57, no. 4, pp. 684–692, 2005.

[25] A. T. Villavicencio, S. Burneikiene, P. Romanelli et al., "Survival following stereotactic radiosurgery for newly diagnosed and recurrent glioblastoma multiforme: a multicenter experience," *Neurosurgical Review*, vol. 32, no. 4, pp. 417–424, 2009.

[26] K. Masui, T. F. Cloughesy, and P. S. Mischel, "Review: molecular pathology in adult high-grade gliomas: from molecular diagnostics to target therapies," *Neuropathology and Applied Neurobiology*, vol. 38, no. 3, pp. 271–291, 2012.

[27] D. C. Shrieve, E. Alexander, P. Y. Wen et al., "Comparison of stereotactic radiosurgery and brachytherapy in the treatment of recurrent glioblastoma multiforme," *Neurosurgery*, vol. 36, no. 2, pp. 275–284, 1995.

[28] S. E. Combs, L. Edler, R. Rausch, T. Welzel, W. Wick, and J. Debus, "Generation and validation of a prognostic score to predict outcome after re-irradiation of recurrent glioma," *Acta Oncológica*, vol. 52, no. 1, pp. 147–152, 2013.

[29] K. C. Cuneo, J. J. Vredenburgh, J. H. Sampson et al., "Safety and efficacy of stereotactic radiosurgery and adjuvant bevacizumab in patients with recurrent malignant gliomas," *International Journal of Radiation Oncology Biology Physics*, vol. 82, no. 5, pp. 2018–2024, 2012.

[30] A. J. Ulm, W. A. Friedman, P. Bradshaw, K. D. Foote, and F. J. Bova, "Radiosurgery in the treatment of malignant gliomas: the University of Florida experience," *Neurosurgery*, vol. 57, no. 3, pp. 512–517, 2005.

[31] D. A. Larson, P. H. Gutin, M. McDermott et al., "Gamma knife for glioma: selection factors and survival," *International Journal of Radiation Oncology Biology Physics*, vol. 36, no. 5, pp. 1045–1053, 1996.

[32] T. Koga, K. Maruyama, M. Tanaka et al., "Extended field stereotactic radiosurgery for recurrent glioblastoma," *Cancer*, vol. 118, no. 17, pp. 4193–4200, 2012.

[33] S. Sirin, K. Oysul, S. Surenkok et al., "Linear accelerator-based stereotactic radiosurgery in recurrent glioblastoma: a single center experience," *Vojnosanitetski Pregled*, vol. 68, no. 11, pp. 961–966, 2011.

[34] M. C. Chamberlain, D. Barba, P. Kormanik, and W. M. Shea, "Stereotactic radiosurgery for recurrent gliomas," *Cancer*, vol. 74, pp. 1342–1347, 1994.

[35] W. A. Hall, H. R. Djalilian, P. W. Sperduto et al., "Stereotactic radiosurgery for recurrent malignant gliomas," *Journal of Clinical Oncology*, vol. 13, no. 7, pp. 1642–1648, 1995.

[36] D. Kondziolka, J. C. Flickinger, D. J. Bissonette, M. Bozik, and L. D. Lunsford, "Survival benefit of stereotactic radiosurgery for patients with malignant glial neoplasms," *Neurosurgery*, vol. 41, no. 4, pp. 776–785, 1997.

[37] A. Mahajan, I. E. McCutcheon, D. Suki et al., "Case-control study of stereotactic radiosurgery for recurrent glioblastoma multiforme," *Journal of Neurosurgery*, vol. 103, no. 2, pp. 210–217, 2005.

[38] T. Biswas, P. Okunieff, M. C. Schell et al., "Stereotactic radiosurgery for glioblastoma: retrospective analysis," *Radiation Oncology*, vol. 4, article 11, 2009.

[39] J. A. Torok, R. E. Wegner, A. H. Mintz, D. E. Heron, and S. A. Burton, "Re-irradiation with radiosurgery for recurrent glioblastoma multiforme," *Technology in Cancer Research and Treatment*, vol. 10, no. 3, pp. 253–258, 2011.

[40] E. Maranzano, P. Anselmo, M. Casale et al., "Treatment of recurrent glioblastoma with stereotactic radiotherapy: long-term results of a mono-institutional trial," *Tumori*, vol. 97, no. 1, pp. 56–61, 2011.

[41] K.-J. Park, H. Kano, A. Iyer et al., "Salvage gamma knife stereotactic radiosurgery followed by bevacizumab for recurrent glioblastoma multiforme: a case-control study," *Journal of Neuro-Oncology*, vol. 107, no. 2, pp. 323–333, 2012.

Hindawi Publishing Corporation
BioMed Research International
Volume 2014, Article ID 198697, 5 pages
http://dx.doi.org/10.1155/2014/198697

Research Article

IDH1^{R132H} Mutation Increases U87 Glioma Cell Sensitivity to Radiation Therapy in Hypoxia

Xiao-Wei Wang,[1,2,3] Marianne Labussière,[1,2,3] Samuel Valable,[4,5,6] Elodie A. Pérès,[4,5,6] Jean-Sébastien Guillamo,[4,5,6,7] Myriam Bernaudin,[4,5,6] and Marc Sanson[1,2,3,8,9]

[1] *Université Pierre et Marie Curie-Paris 6, Centre de Recherche de l'Institut du Cerveau et de la Moëlle épinière (CRICM), UMR-S975, 75013 Paris, France*
[2] *INSERM, U 975, 75013 Paris, France*
[3] *CNRS, UMR 7225, 75013 Paris, France*
[4] *CNRS, UMR 6301 ISTCT, CERVOxy group, GIP CYCERON, Boulevard Henri Becquerel, BP 5229, 14074 Caen cedex, France*
[5] *Université de Caen Basse-Normandie, UMR 6301 ISTCT, 14000 Caen, France*
[6] *CEA, DSV/I2BM, UMR 6301 ISTCT, 14000 Caen, France*
[7] *CHU de Caen, Service de Neurologie, Boulevard Côte de Nacre, 14000 Caen, France*
[8] *AP-HP, Groupe Hospitalier Pitié-Salpêtrière, Service de Neurologie 2, 75013 Paris, France*
[9] *Service de Neurologie 2, Groupe Hospitalier Pitié-Salpêtrière, 75651 Paris Cedex 13, France*

Correspondence should be addressed to Marc Sanson; marc.sanson@psl.aphp.fr

Received 12 February 2014; Accepted 6 April 2014; Published 7 May 2014

Academic Editor: Andrea Pace

Objective. *IDH1* codon 132 mutation (mostly Arg132His) is frequently found in gliomas and is associated with longer survival. However, it is still unclear whether *IDH1* mutation renders the cell more vulnerable to current treatment, radio- and chemotherapy. *Materials and Methods*. We transduced U87 with wild type *IDH1* or *IDH1*^{R132H} expressing lentivirus and analyzed the radiosensitivity (dose ranging 0 to 10 Gy) under normoxia (20% O_2) and moderate hypoxia (1% O_2). *Results*. We observed that *IDH1*^{R132H} U87 cells grow faster in hypoxia and were more sensitive to radiotherapy (in terms of cell mortality and colony formation assay) compared to nontransduced U87 and *IDH1*^{wt} cells. This effect was not observed in normoxia. *Conclusion*. These data suggest that *IDH1*^{R132H} mutation increases radiosensitivity in mild hypoxic conditions.

1. Introduction

The *IDH1* gene encoding the cytoplasmic NADP+-dependent isocitrate dehydrogenase—and more rarely *IDH2*, encoding the mitochondrial isoform—are frequently mutated in gliomas, especially low grade gliomas and secondary glioblastomas [1]. *IDH1/IDH2* mutation is associated with better clinical outcome, whatever the grade, but it is still not clear whether it is merely a prognostic marker or a predictor of the response to radiotherapy or chemotherapy [2–6]. Recent data *IDH1/IDH2* mutation results in a new enzyme function catalyzing the NADPH-dependent reduction of alpha-ketoglutarate to D-2-hydroxyglutarate (D-2HG) [7]. *IDH1/IDH2* mutations result in D-2HG accumulation and lowering NADPH levels. On one hand D-2HG inhibits various alpha-ketoglutarate dependant reactions, including histone and DNA demethylation, and is likely to promote—rather than inhibit—HIF1α degradation [8–11]. On the other hand, low NADPH levels might sensitize tumors to oxidative stress, potentiating response to radiotherapy, and may account for the prolonged survival of patients harboring the mutations.

Since the majority of gliomas are poorly responsive to current treatment regimens, the ability to enhance cell

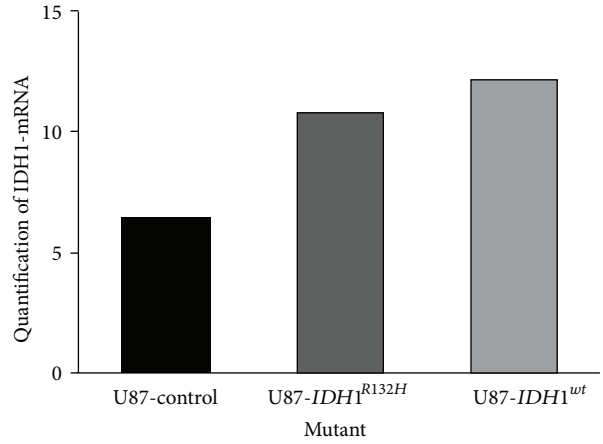

Figure 1: Real time PCR quantified the expression of the $IDH1^{wt}$ and $IDH1^{R132H}$ transduced genes.

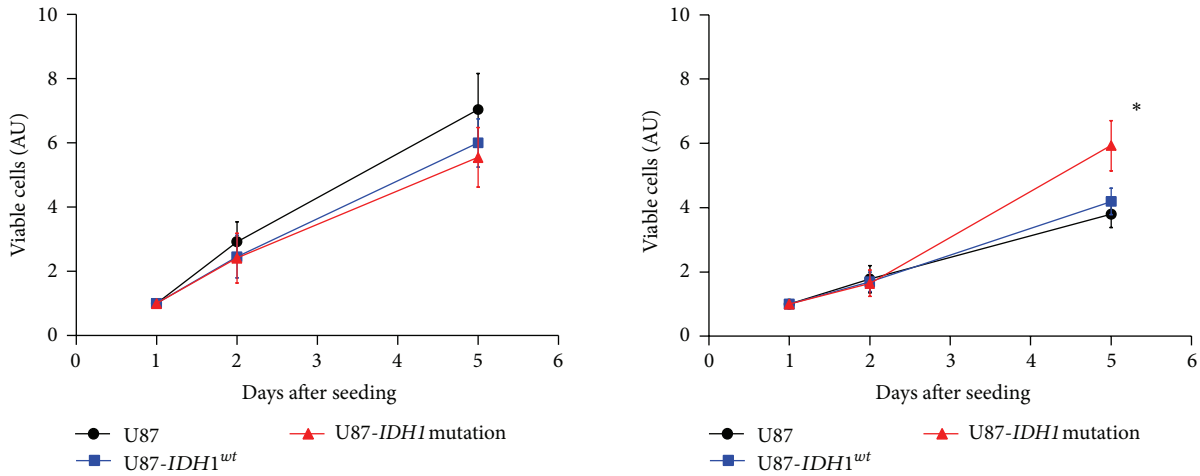

Figure 2: Effect of $IDH1^{R132H}$ on U87 cell proliferation. U87, $IDH1^{wt}$-U87, and $IDH1^{R132H}$-U87 cells were incubated in normoxia 20% (left) or hypoxia 1% (right) and cells were counted after 1, 3, and 7 days.

radio-chemosensitivity would be of clinical benefit. In this study, we characterized the impact of *IDH1* mutation on U87 glioma cell growth and radiosensitivity.

2. Methods and Materials

2.1. Cell Culture and Hypoxia Treatment. The human glioblastoma cell line U87 MG (HTB14) was obtained from the American Type Culture Collection (ATCC, Rockville, MD) and maintained in Dulbecco's modified Eagle's medium (DMEM), supplemented with 10% fetal bovine serum (FBS) and 1% penicillin/streptomycin. Normoxic cells (21% O_2) were grown in a humidified-air atmosphere incubator containing 95% air/5% CO_2 at 37°C. Hypoxia experiments were performed in a controlled atmosphere chamber (INVIVO2 1000, Ruskinn, Awel, France) set at 1% O_2, 94% N_2, and 5% CO_2 at 37°C.

2.2. Production of Recombinant Expression Lentiviruses. A recombinant pLenti7.3/V5-TOPO expression vector (Invitrogen's ViraPowerTM HiPerformTM Lentiviral Expression Systems; catalog number K5320-00) containing the human *IDH1* wild type and $IDH1^{R132H}$ cDNA was generated. The expression clones and the ViraPower Packaging Mix were cotransfected into the 293FT Cell line to produce lentiviral stocks, which were used to transduce the mammalian U87 cell line. U87-$IDH1^{wt}$ and U87-$IDH1^{R132}$ stable cell lines were acquired using EmGFP selection by flow cytometry. The constructs was verified by DNA sequencing and RT-qPCR analysis.

2.3. Cell Proliferation Assay in Normoxia and in Hypoxia. To evaluate the impact of *IDH1* mutation on cell growth in normoxia and in hypoxia by trypan blue dye exclusion method, U87, U87-$IDH1^{wt}$, and U87-$IDH1^{R132H}$ cells (4000/well) plated in 24-well plates (6 plates in total) were incubated at 37°C for six hours in normoxia to adhere; then 3 plates were removed at 37°C in the controlled atmosphere chamber overnight. At 1, 3, and 7 days after exposure to normoxia and hypoxia, the cells were trypsinized, and the number of viable cells

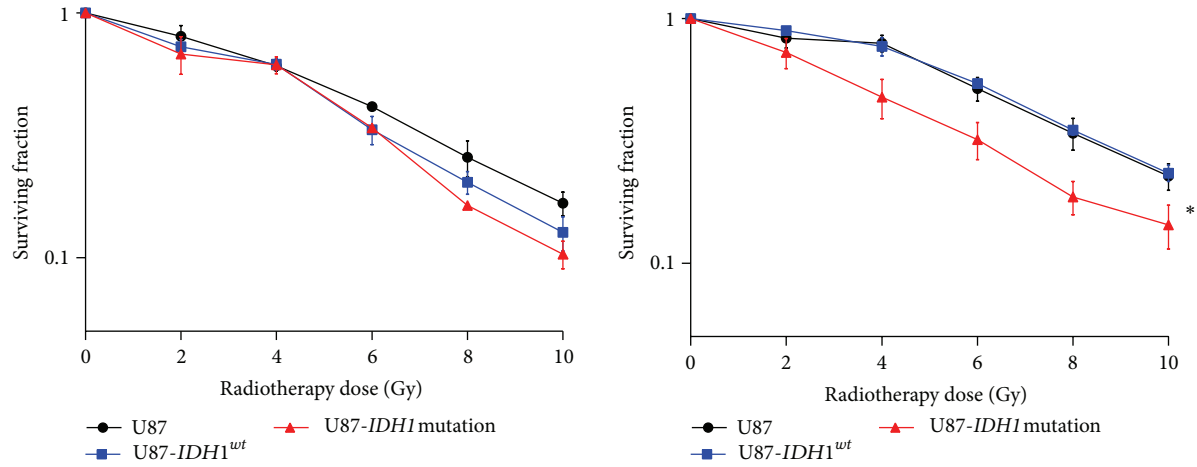

Figure 3: Effect of $IDH1^{R132H}$ on U87 cell viability after irradiation. Transduced cells were plated and then irradiated with doses ranging from 0 to 10 Gy, in normoxia (20%) (left) and in hypoxia (1%) (right). Cells were counted 5 days later.

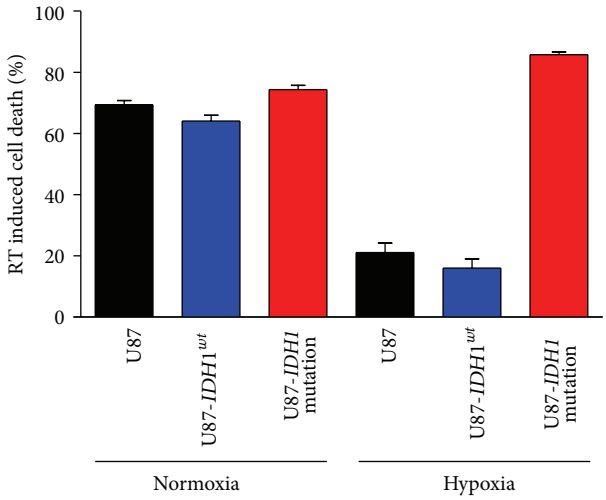

Figure 4: Cell viability after 8 Gy irradiation. Cells were counted before 8 Gy irradiation and 5 days after, in normoxia (20% O_2) (left) and in hypoxia (1% O_2) (right).

per well was determined by counting with trypan blue. The experiment was performed three times in triplicate each.

2.4. Comparative Cell Viability Assay after Irradiation, in Normoxia and in Hypoxia. To evaluate the effect of $IDH1^{R132H}$ in the response to radiotherapy, U87 cells, $IDH1^{wt}$-U87, and $IDH1^{R132H}$-U87 cells were plated (4.103 per well) in 24-well plates. Six hours later at 37°C in normoxia, plates were either kept in normoxia or incubated in the controlled atmosphere chamber 1% O_2 overnight. The next day, cells were irradiated with doses ranging from 0 to 10 Gy in order to determine the most discriminating dose. Cells were fixed in paraformaldehyde (PFA) 4%, then stained with Hoechst 33342 (10 μg/mL in PBS, Sigma-Aldrich, France) and photographed in a blinded fashion under fluorescence (4 wells per condition; 4 photographs per well) at 24 h, 48 h, and 120 h, respectively. Cells were counted with ImageJ software (Rasband, WS, ImageJ, US NIH).

2.5. Colony-Formation Assay in Normoxia and in Hypoxia. U87, $IDH1^{wt}$-U87, and $IDH1^{R132H}$-U87 cells were plated in 6-well containing 0.3% base agar layer. Six hours later, cells were either incubated in the hypoxic or normoxic chamber overnight. The next day, the cells were treated by radiotherapy at the Radiotherapy Department of the Centre de Lutte Contre le Cancer (CLCC) François Baclesse (Caen, France) using an X-ray generator with doses ranging 0–8 Gy (Therac 15-Saturne with a dose rate of 2 Gy/min) and then incubated again for colony formation. One month later, the colonies were fixed in 20% ethanol and stained with 0.05% crystal violet. Colonies that contained more than 50 cells were counted. Survival was calculated as the average number of colonies counted divided by the number of cells plated multiplicated by plating efficiency (PE), where PE is the fraction of colonies counted divided by cells plated without radiation. The clonogenic survival data were generated using JMP software. The experiment was performed five times in triplicate each.

2.6. Statistical Analysis. Results obtained *in vitro* were expressed as mean ± SEM Image analysis was performed with in-house macros under the ImageJ Software (Rasband, WS, ImageJ, US NIH). All statistical analyses were determined using post hoc tests after significant ANOVA. Values of $P < 0.05$ were considered statistically significant.

3. Results

3.1. Transduced Cells Express High Quantities of $IDH1^{wt}$ and $IDH1^{R132H}$. The presence of $IDH1^{R132H}$ transduced gene was confirmed by DNA sequencing. Real time PCR showed a high expression of gene $IDH1^{wt}$ and $IDH1^{R132H}$ in transduced U87 cells compared to nontransduced cells (Figure 1).

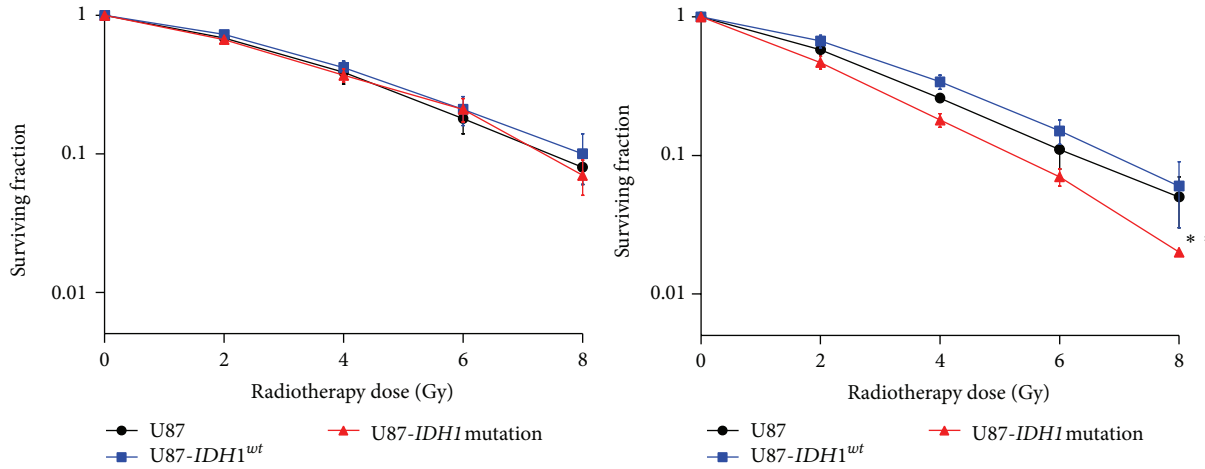

FIGURE 5: $IDH1^{R132H}$-U87 cells have a reduced colony forming cell ability after irradiation in hypoxia. U87, $IDH1^{wt}$-U87, and $IDH1^{R132H}$-U87 cells were plated 24 h before irradiation (0-2-4-6-8 Gy) in agar and incubated for one month in normoxia (20% O_2) and in hypoxia (1% O_2). The colonies were fixed in ethanol, stained with 0.05% crystal violet, and counted. Survival rate was estimated by the ratio between the colonies count and the number of cells plated, multiplicated by the plating efficiency.

3.2. $IDH1^{R132H}$ Expressing U87 Glioma Cells Grow Faster in Hypoxia. We determined whether $IDH1^{R132H}$ expression directly influences cell growth in normoxia and in hypoxia. The viable cell number per well was determined by counting with trypan blue at 1, 3, and 7 days after incubation in normoxia and in hypoxia. Proliferation rate of U87-$IDH1^{R132H}$ cells was significantly higher in normoxia than in hypoxia for all the three cell lines. In normoxia, U87, U87-$IDH1^{wt}$, and U87-$IDH1^{R132H}$ cells grew at the same rate, whereas U87-$IDH1^{R132H}$ grew faster than U87 and U87-$IDH1^{wt}$ in hypoxia (Figure 2).

3.3. Effect of Transduced $IDH1^{R132H}$ on Cell Viability upon Exposure to Doses Ranging 0 to 10 Gy in Normoxia and in Hypoxia. To evaluate the role of $IDH1^{R132H}$ in the response to radiotherapy, U87, U87-$IDH1^{wt}$, and U87-$IDH1^{R132H}$ were exposed to different doses (range: 0–10 Gy): in normoxia the three cell lines showed the same radiosensitivity profile, whereas in hypoxia, the viability of U87-$IDH1^{R132H}$ cells was significantly lower after 5 days compared to control cells and $IDH1^{wt}$ cells (Figure 3) (13% versus 23% and 22% for a dose of 10 Gy, $P < 0.001$), respectively. This result suggests that $IDH1^{R132H}$ makes the cells more radiosensitive in hypoxic, but not in normoxic conditions.

3.4. Effect of Transduced $IDH1^{R132H}$ on Cell Mortality over Time following 8 Gy Irradiation in Normoxia and in Hypoxia. We quantified then cell death at 24 h, 48 h, and 120 h after 8 Gy irradiation. There was no substantial cell death after 24 h. The effect appeared at 48 h in both normoxia and in hypoxia (data not shown) and was maximal after 5 days. Cell death was significantly higher for $IDH1^{R132H}$ transduced cells in hypoxia but not in normoxia (Figure 4).

3.5. Radiosensitivity of U87- $IDH1^{R132H}$ in Hypoxia Is Confirmed by Colony-Formation Assay. A colony-formation assay was used to confirm the effect of $IDH1^{R132H}$ on the response to radiotherapy. Cells were treated with graded doses of radiation (0, 2, 4, 6, and 8 Gy). Colony-forming efficiency was determined 1 month later and surviving fractions were calculated. In normoxia, U87, U87-$IDH1^{wt}$, and U87-$IDH1^{R132H}$ had the same colony-formation capacity after radiotherapy. In hypoxia, the colony number of U87-$IDH1^{R132H}$ after radiotherapy was significantly lower than U87 and U87-$IDH1^{wt}$ (Figure 5). Thus, U87-$IDH1^{R132H}$ significantly sensitized U87 glioma cells to radiation.

4. Discussion

We observed here that *IDH1* mutated U87 grew faster in moderate hypoxic conditions (1% O_2) than in normoxia (21% O_2). This contrast with data obtained in normoxia, $IDH1^{R132H}$ overexpression in established glioma cell lines *in vitro*, resulted in a marked decrease in proliferation and mice injected with $IDH1^{R132H}$-U87 cells had prolonged survival compared to mice injected with $IDH1^{wt}$-U87 cells [12].

We found then that $IDH1^{R132H}$-U87 were more sensitive to radiotherapy in hypoxic condition. Indeed a high rate of cell proliferation is *per se* a sensitive factor of the radiation therapy response. But on the other hand, *IDH1/IDH2* mutated cells may be more sensitive to oxidative stress. The role of isocitrate dehydrogenase in cellular defense against oxidative stress has been suggested [13]. Indeed, *IDH1/IDH2* serves as a major source of cytosolic and mitochondrial NADPH production necessary to regenerate reduced glutathione (GSH) by glutathione reductase and for the activity of NADPH-dependent thioredoxin system, both are important in the protection of cells from oxidative damage [14, 15]. Thus, the

decrease of NADPH in *IDH1/IDH2* mutated cells might result in an increase of ROS that can damage DNA. Partially in line with our results, U87 cells transduced with $IDH1^{R132H}$ or $IDH2^{R172K}$ demonstrated increased sensitivity to radiation but the effect observed in normoxia and hypoxic conditions was not investigated [16].

Despite hypoxia being considered as a factor of radioresistance, we observed here a radiosensitizing effect of $IDH1^{R132H}$ in glioblastoma cell line in hypoxic but not in normoxic condition. Until recently, *IDH1/2* mutations were believed to result in the stabilization of HIF1α [10, 17]. Interestingly Koivunen et al. [11] showed that D-2HG (but not L-2HG) instead of being an inhibitor of EGLN (HIF prolyl 4-hydroxylases) activity acts as a partial agonist of EGLN and promotes the degradation of HIF1α. Because HIF protects cells from irradiation therapy under hypoxic condition, we may hypothesize that *IDH* mutation, by inducing an inappropriate degradation of HIF, could make the mutated cell more vulnerable to RT.

In conclusion, this study suggests a radiosensitizing effect of $IDH1^{R132H}$ in glioblastoma cell lines U87 grown under mild hypoxic conditions, which are close to *in vivo* conditions. We need to confirm this finding on clinical setting: the 1p19q codeletion is a known marker of chemosensitivity. Whether the *IDH1/2* mutation is a marker of radiosensitivity should be determined. The ongoing EORTC trial on low grade gliomas, which randomizes radiotherapy versus chemotherapy in low grade gliomas at progression and includes also a prospective observational cohort, will be pivotal to answer this question.

Conflict of Interests

The authors declare that there is no conflict of interests regarding the publication of this paper.

Acknowledgments

This work was supported by Grants from the Institut National du Cancer (INCA; PL 046), the Association pour la Recherche sur le Cancer, the Centre National de la Recherche Scientifique (CNRS), the University of Caen-Basse Normandie, the Conseil Régional de Basse-Normandie. The authors wish to thank the Radiotherapy Department of the CLCC François Baclesse (Caen, France), especially A. Batalla and P. Chevallier for giving them an access to the irradiator.

References

[1] D. W. Parsons, S. Jones, X. Zhang et al., "An integrated genomic analysis of human glioblastoma multiforme," *Science*, vol. 321, no. 5897, pp. 1807–1812, 2008.

[2] M. Sanson, Y. Marie, S. Paris et al., "Isocitrate dehydrogenase 1 codon 132 mutation is an important prognostic biomarker in gliomas," *Journal of Clinical Oncology*, vol. 27, no. 25, pp. 4150–4154, 2009.

[3] M. J. Van Den Bent, H. J. Dubbink, Y. Marie et al., "IDH1 and IDH2 mutations are prognostic but not predictive for outcome in anaplastic oligodendroglial tumors: a report of the European Organization for Research and Treatment of Cancer Brain Tumor Group," *Clinical Cancer Research*, vol. 16, no. 5, pp. 1597–1604, 2010.

[4] C. Houillier, X. Wang, G. Kaloshi et al., "IDH1 or IDH2 mutations predict longer survival and response to temozolomide in low-grade gliomas," *Neurology*, vol. 75, no. 17, pp. 1560–1566, 2010.

[5] M. J. van den Bent, A. A. Brandes, M. J. B. Taphoorn et al., "Adjuvant PCV chemotherapy in newly diagnosed anaplastic oligodendroglioma—long term follow-up of EORTC Brain Tumor Group study 26951," *Journal of Clinical Oncology*. In press.

[6] J. G. Cairncross, M. Wang, R. B. Jenkins et al., "Benefit from procarbazine, lomustine, and vincristine in oligodendroglial tumors is associated with mutation of IDH," *Journal of Clinical Oncology*, vol. 32, no. 8, pp. 783–790, 2014.

[7] L. Dang, D. W. White, S. Gross et al., "Cancer-associated IDH1 mutations produce 2-hydroxyglutarate," *Nature*, vol. 462, no. 7274, pp. 739–744, 2009.

[8] C. Lu, P. S. Ward, G. S. Kapoor et al., "IDH mutation impairs histone demethylation and results in a block to cell differentiation," *Nature*, vol. 483, no. 7390, pp. 474–478, 2012.

[9] S. Turcan, D. Rohle, A. Goenka et al., "IDH1 mutation is sufficient to establish the glioma hypermethylator phenotype," *Nature*, vol. 483, no. 7390, pp. 479–483, 2012.

[10] W. Xu, H. Yang, Y. Liu et al., "Oncometabolite 2-hydroxyglutarate is a competitive inhibitor of α-ketoglutarate-dependent dioxygenases," *Cancer Cell*, vol. 19, no. 1, pp. 17–30, 2011.

[11] P. Koivunen, S. Lee, C. G. Duncan et al., "Transformation by the (R)-enantiomer of 2-hydroxyglutarate linked to EGLN activation," *Nature*, vol. 483, no. 7390, pp. 484–488, 2012.

[12] L. B. C. Bralten, N. K. Kloosterhof, R. Balvers et al., "IDH1 R132H decreases proliferation of glioma cell lines in vitro and in vivo," *Annals of Neurology*, vol. 69, no. 3, pp. 455–463, 2011.

[13] H. L. Jin, Y. K. Sung, S. K. In, and J.-W. Park, "Regulation of ionizing radiation-induced apoptosis by mitochondrial NADP+-dependent isocitrate dehydrogenase," *Journal of Biological Chemistry*, vol. 282, no. 18, pp. 13385–13394, 2007.

[14] J. Shi, H. Zuo, L. Ni et al., "An IDH1 mutation inhibits growth of glioma cells via GSH depletion and ROS generation," *Neurological Sciences*. In press.

[15] I. V. Mohrenz, P. Antonietti, S. Pusch et al., "Isocitrate dehydrogenase 1 mutant R132H sensitizes glioma cells to BCNU-induced oxidative stress and cell death," *Apoptosis*, vol. 18, pp. 1416–1425, 2013.

[16] S. Li, A. P. Chou, W. Chen et al., "Overexpression of isocitrate dehydrogenase mutant proteins renders glioma cells more sensitive to radiation," *Neuro-Oncology*, vol. 15, pp. 57–68, 2013.

[17] S. Zhao, Y. Lin, W. Xu et al., "Glioma-derived mutations in IDH1 dominantly inhibit IDH1 catalytic activity and induce HIF-1α," *Science*, vol. 324, no. 5924, pp. 261–265, 2009.

Hindawi Publishing Corporation
BioMed Research International
Volume 2014, Article ID 351252, 7 pages
http://dx.doi.org/10.1155/2014/351252

Clinical Study

Activity and Safety of Bevacizumab Plus Fotemustine for Recurrent Malignant Gliomas

V. Vaccaro,[1] A. Fabi,[1] A. Vidiri,[2] D. Giannarelli,[3] G. Metro,[4] S. Telera,[5] S. Vari,[1] F. Piludu,[2] M. A. Carosi,[6] V. Villani,[7] F. Cognetti,[1] A. Pompili,[5] L. Marucci,[8] C. M. Carapella,[5] and A. Pace[7]

[1] *Department of Medical Oncology, Regina Elena National Cancer Institute, Via Elio Chianesi 53, 00144 Rome, Italy*
[2] *Diagnostic Oncology Department, Regina Elena National Cancer Institute, Via Elio Chianesi 53, 00144 Rome, Italy*
[3] *Biostatistic Unit, Regina Elena National Cancer Institute, Via Elio Chianesi 53, 00144 Rome, Italy*
[4] *Division of Medical Oncology, Santa Maria della Misericordia Hospital, Azienda Ospedaliera di Perugia, Perugia, Italy*
[5] *Division of Neurosurgery, Regina Elena National Cancer Institute, Via Elio Chianesi 53, 00144 Rome, Italy*
[6] *Department of Pathology, Regina Elena National Cancer Institute, Via Elio Chianesi 53, 00144 Rome, Italy*
[7] *Division of Neurology, Regina Elena National Cancer Institute, Via Elio Chianesi 53, 00144 Rome, Italy*
[8] *Department of Radiation Oncology, Regina Elena National Cancer Institute, Via Elio Chianesi 53, 00144 Rome, Italy*

Correspondence should be addressed to A. Fabi; alessandra.fabi@virgilio.it

Received 14 February 2014; Revised 9 April 2014; Accepted 14 April 2014; Published 4 May 2014

Academic Editor: Roberta Rudà

Background. No established chemotherapeutic regimen exists for the treatment of recurrent malignant gliomas (rMGs). Herein, we report the activity and safety results of the bevacizumab (B) plus fotemustine (FTM) combination for the treatment of rMGs. *Patients and Methods*. An induction phase consisted of B 10 mg/kg days 1, 15 plus FTM 65 mg/m^2 days 1, 8, and 15. Nonprogressive patients entered the maintenance phase with B 10 mg/kg plus FTM 75 mg/m^2 every 3 weeks. The primary endpoint was response rate; secondary endpoints included safety, progression free survival (PFS), and overall survival (OS). *Results*. Twenty-six patients affected by recurrent MGs (50% glioblastoma) were enrolled. Eight partial responses (31%) were observed. Median PFS and OS were 4 (95% C.I.: 2.8–5.1) and 6 months (95% C.I.: 4.2–7.8), respectively. Responses were significantly associated with both improved PFS and OS ($P = 0.002$ and $P = 0.001$, resp.). Treatment adverse events were mostly mild to moderate in intensity. Bevacizumab-related adverse events included grade 3 venous thromboembolic event (8%), grade 2 epistaxis (4%), hypertension (8%), and gastrointestinal perforation (4%). *Conclusions*. Bevacizumab plus FTM showed activity and good tolerability in pretreated MGs. Further investigations are needed in order to verify the benefits deriving from the addition of B to a cytotoxic in this clinical setting of patients.

1. Introduction

Malignant gliomas (MGs) account for roughly 50% of all malignant primary brain tumors in adults. Active treatments include resection of the tumor to the extent that is surgically feasible, radiotherapy, and chemotherapy. Glioblastoma multiforme (GBM) represents the most common form of malignant gliomas [1]. Its aggressive clinical behavior leads to a dismal prognosis, with a median survival of approximately 14 months. The standard of care for surgically resected patients with newly diagnosed GBM is based on the concurrent administration of radiation plus temozolomide (TMZ) followed by TMZ maintenance up to 6 months [2, 3]. However, long-term survival is rarely achieved and the disease almost invariably recurs. Nowadays, there are no established therapeutic options for the treatment of rMGs. Nitrosourea compounds such as carmustine, lomustine, and the third generation nitrosourea derivative fotemustine (FTM) are associated with response rates ranging from 15 to 30% and a median progression free survival (PFS) that rarely exceeds

6 months [4, 5]. Notwithstanding, FTM has been shown to cross the blood-brain barrier because of its lipophilic profile and in the population of patients with recurrent GBM demonstrated a good activity and a favorable safety profile, mielosuppression being the most prevalent side effect [4–8].

Recent progress in the understanding of the molecular characteristics of GBM has prompted the development of targeted therapeutic approaches. As compared to normal brain tissue, rMGs show an intense vascular proliferation with high expression of the vascular endothelial growth factor (VEGF) [9]. Vessel density degree and VEGF level expression have been shown to directly correlate with the biologic aggressiveness of gliomas and a worse prognosis [10–13]. Furthermore, it has been demonstrated that VEGF inhibition leads to a decreased growth of glioma cell lines and that antiangiogenic agents can reduce both peritumoral edema and the need for corticosteroid therapy [13, 14]. On this basis, a strong rationale existed for the use of bevacizumab, an anti-VEGF monoclonal antibody, for treatment of rMGs (recurrent malignant gliomas). A bevacizumab combination regimen was first evaluated in recurrent GBM in association with irinotecan in either prospective phase II or retrospective studies that showed encouraging response rates and relevant clinical benefit (CB) [9, 11, 12, 15, 16]. Also, the activity of bevacizumab has been demonstrated when administered as a single agent [12].

Currently, few data are available on the combination of bevacizumab with nitrosoureas; therefore, we conducted an observational prospective study evaluating the activity and safety of bevacizumab plus FTM for the treatment of recurrent MG patients.

2. Materials and Methods

Patients with histologically proven MGs and clinicoradiological progression after no more than two previous chemotherapy lines, temozolomide plus radiotherapy, must have been the upfront therapy. Progression had to be documented by magnetic resonance imaging (MRI). Inclusion criteria were evaluable and/or measurable disease; at least 12 weeks from a second intracranial surgery and/or radiotherapy and 4 weeks from first or second-line chemotherapy; age between 18 and 80 years; Karnofsky performance status (KPS) $\geq$ 60; and adequate hematological, liver, and renal function. Treatment with low dose of heparin for antithrombotic prophylaxis was permitted. Previous treatment including either bevacizumab or FTM and evidence of hemorrhage at baseline MRI excluded patients from the study. Other exclusion criteria were pregnancy or nursing, clinically significant cardiovascular diseases, such as congestive heart failure (NYHA classes II, III, and IV), unstable angina pectoris or myocardial infarction within 6 months prior to study entry, uncontrolled hypertension (systolic blood pressure > 150 mmHg and/or diastolic blood pressure > 100 mmHg on treatment) or history of hypertensive crises or hypertensive encephalopathy, history of stroke or transient ischemic attack within 6 months prior to study entry, clinically significant vascular disease or symptomatic peripheral vascular disease, presence or history of recurrent thromboembolism (>1 episode of deep venous thrombosis or peripheral embolism) during the past 2 years, inherited bleeding diathesis or coagulation disorder, intestinal perforation or the presence of other condition that would have made the treatment unsafe, active infections or other uncontrolled diseases, and psychiatric disorders. The trial was conducted in agreement with the Declaration of Helsinki and International Committee on Harmonization guidelines for good clinical practice. All enrolled patients were amenable to compliance with testing and were informed of the investigational nature of the study. The study was approved by a local ethics committee and a signed informed consent was obtained by the patients.

2.1. Treatment Plan. All patients received FTM in combination with bevacizumab. The treatment consisted of an induction phase with bevacizumab i.v. at the dose of 10 mg/kg every three weeks plus FTM i.v. at the dose of 65 mg/mq over 1 hour on days 1, 8, and 15 followed after a 3-week interval by maintenance phase with bevacizumab at 10 mg/kg i.v. plus FTM 75 mg/mq every three weeks. Ten minutes before each infusion of FTM, a 5-HT3 receptor antagonist was administered for antiemetic prophylaxis. Antiepileptic drugs were given during the study period as medically indicated. Glucocorticoids were used to the dose necessary for neurologic stability. Study treatment was continued until disease progression, withdrawal of the patient, or unacceptable toxicity.

2.2. Study Assessment. MRI of the brain was uniformly adopted for tumor assessment and evaluation of the response. Magnetic resonance imaging was performed on a 1.5-T system (Optima MR450w, GE Healthcare, Milwaukee, WI) with dedicated 16-channel receive-only RF coils; slice thickness 4 mm and matrix size of 512 $\times$ 512 were used. Spin-echo (SE) sequences T1, T2, and FLAIR before contrast medium infusion in coronal plane (SE T2) and axial planes (SE T1, T2, and FLAIR) were performed; a three-dimensional volumetric T1-weighted sequence (fast-spoiled- gradient-echo sequence with fat saturation pulse), after the administration of gadopentetate dimeglumine contrast agent (Magnevist, Bayer Schering Pharma AG, Berlin, Germany), at a dosage of 0.1 mmol/kg of body weight, was performed. Both FLAIR and contrast-enhanced T1-weighted sequences were considered for the response assessment to treatment according to RANO criteria [17]. MRI examination was performed within 2 weeks before study begins. Further evaluations were performed after the completion of the induction phase every nine weeks during the maintenance phase or whenever disease progression was clinically suspected.

Toxicity was assessed before each drug administration by medical history, physical examination, hematology, and biochemistry. Adverse events were graded 1 to 4 according to the National Cancer Institute (NCI) common toxicity criteria (NCICT-CAE) version 3.0 [18]. Reduction in the bevacizumab dose was not permitted; dose delays were allowed for reversible and preventable toxicities.

FTM administration was omitted in case of grade 3-4 thrombocytopenia and/or neutropenia and grade 3-4 nonhematological toxicity except for nausea/vomiting. At recovery, treatment was resumed with a 25% dose reduction. Granulocyte colony-stimulating factor (G-CSF) was allowed. Data were collected for up to 12 months after the last bevacizumab/FTM infusion for the following specific adverse events: hypertension, proteinuria, arterial and venous thromboembolic events, congestive heart failure, central nervous system bleeding, other hemorrhages, wound-healing complications, and gastrointestinal perforations and fistulae.

2.3. MGMT Gene Promoter Methylation Analysis. Genomic DNA was isolated from one paraffin section of tissue collected at the time of initial diagnosis (Ex-Wax DNA Extraction Kit S4530, Chemicon), proteinase digestion lasting a maximum of 6 hours. DNA was denatured with sodium hydroxide and subjected to bisulfite treatment in a volume of 350 μL (4.4 M sodium bisulfite and 20 mM hydroquinone) for five hours at 55°C and then purified. Unmethylated cytosine, but not its methylated counterpart, is modified into uracil by the treatment. The methylation-specific PCR was performed in a two-step approach. The results were confirmed in an independent experiment, starting with reisolation of DNA from the tumor.

2.4. Statistical Analysis. The primary endpoint of the study was the response rate. The study was designed according to A'Hern [18] to refuse a response rate of 10% when the true response rate was 30%. At a significance level of 5% with a power of 80% we needed 25 patients. The study would have been considered positive if at least 6 responses had been observed. Rates statistics were used to summarize pertinent study information. Rates are reported with their 95% confidence interval. The time to event analysis is measured from the start of treatment and is performed according to the Kaplan-Meier method. The disease control rate (DCR) was the sum of partial responses plus stable disease and clinical benefit (CB) was evaluated measuring steroid reduction and clinical status associated with the stability or response lasting ≥3 months. Progression free survival (PFS) was the time elapsing from the start of study treatment to the date of disease progression or death of the patient in the absence of documented disease progression. Overall survival (OS) was estimated from the first day of treatment to the date of death of the patient due to any cause. If a patient progressed/died, the progression and survival were censored at the time of the last visit.

3. Results

3.1. Patients' Characteristics. Patients' characteristics are reported in Table 1. Twenty-six patients were recruited. Median age was 38 years (range 25–68) and median KPS was 80 (range 70–100). GBM was the most represented histotype (13 patients, 50% of cases); 15 (57.5%) patients performed primary surgery and all the GBM patients received concomitant radiotherapy and temozolomide followed by temozolomide (Stupp regimen) after diagnosis. Non-GBM patients received radiotherapy and temozolomide after diagnosis or progression of disease. Eleven patients (42%) had been treated with two previous chemotherapy lines (7 patients had continuative low dose temozolomide after first line temozolomide failure and 4 patients were given PCV polychemotherapy as second line). Patients received a median of 6 (range 2–15) cycles of bevacizumab plus FTM. MGMT status was assessable in 19 patients (73%), 14 on primary tumor tissue and 5 in the recurrent tumor tissue; MGMT resulted methylated in 10 (53%) cases and unmethylated in 9 (35%) cases.

Table 1: Patient characteristics.

Characteristics	All patients (26)
Median age, years (range)	38 (range: 25–68)
Gender (%)	
Female	11 (42)
Male	15 (58)
Median baseline KPS	80 (70–100)
Histotype (%)	
GBM	13 (50)
Anaplastic astrocytoma	7 (27)
Anaplastic oligodendroglioma	2 (8)
Anaplastic oligoastrocytoma	4 (15)
Prior surgery (%)	
Biopsy	11 (42.5)
Partial resection	11 (42.5)
Total resection	4 (15)
Prior radiotherapy	26 (100)
Second surgery	7 (27)
Prior lines of chemotherapy (%)	
1	26 (100)
2	11 (42)
Type of prior chemotherapy (%)	
TMZ	26 (100)
PCV	4 (15)
MGMT gene promoter methylation status (%)	
Evaluable	19 (73)
Unmethylation	10 (53)
Methylation	9 (47)

KPS: Karnofsky performance status; TMZ: temozolomide; PCV: procarbazine, carmustine, and vincristine; MGMT: methylguanine methyltransferase.

3.2. Activity. All patients were evaluable for activity. No case of complete response was observed; eight patients (31%) achieved partial response while 16 (61.5%) patients had disease stabilization, for a disease control rate of 92.5%. Two (7.5%) patients progressed, both at the end of induction phase. Responses or stability was observed in all histotypes (10 GBM, 8 AA, and 6 AOD/AOA) (Figure 1). In particular, partial responses were achieved in 2 GBM and 6 anaplastic gliomas, while stability was showed in 5 GBM and in 11 anaplastic gliomas.

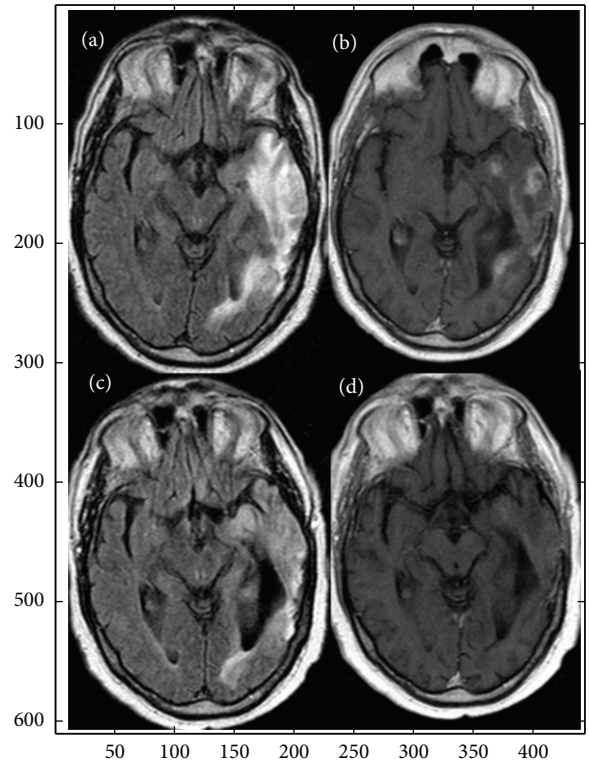

Figure 1: Before treatment MRI SE FLAIR (a) and T1 after contrast medium infusion (b) shows a large lesion in the left temporal lobe, hyperintense on FLAIR image with multiple focal enhancement areas after c.m. infusion. There is a compression on ventricle trigone. MRI FLAIR (c) and T1 (d) after contrast medium (c.m.), after treatment, show marked reduction of the hyperintensity area on the FLAIR sequence with disappearance of the enhancement areas on T1 sequence after c.m. The ventricle trigone is enlarged.

Sixteen patients (60%) achieved clinical benefit; in all of them, a significant decrease of corticosteroid dose at the time of response was observed (median dose of dexamethasone from 12 to 4 mg every day; $P = 0.001$). Patients had no significant change of Mini Mental Status from the start to the end of treatment, while a significant benefit in terms of improvement of KPS was observed from the first to the last cycle of treatment ($P = 0.02$).

3.3. Progression Free Survival and Overall Survival. At a median follow-up of 6 months (range 2–13), the median PFS was 4 months (95% C.I.: 2.8–5.1). The rate of patients who were free of progression at 6 and 12 months was 23.1% and 11.5%, respectively. PFS differed with regard to response: 6 months (95% C.I.: 2.4–9.6) for responsive patients, 4 months (95% C.I.: 1.4–6.6) for patients achieving stable response, and 1 month (95% C.I.: ne) for progressive patients ($P = 0.002$) (Figure 2(a)). The median OS was 6 months (95% C.I.: 4.2–7.8). At 6 and 12 months, 49.2% and 20.5% of patients were alive, respectively. OS differed with regard to response: 8 months (95% C.I.: 5.1–10.9) for responsive patients, 6 months (95% C.I.: 4.7–7.3) for patients achieving stable disease, and 3 months (95% C.I.: 1.4–4.5) for progressive patients ($P = 0.001$) (Figure 2(b)). Regarding the different outcome related to histotypes, progression free survival in GBM and anaplastic gliomas was 3 months (95% C.I.: 0.7–5.4) and 4 months (95% C.I.: 3.2–4.8), respectively.

3.4. Activity according to MGMT. Among patients with assessment of MGMT methylation, 33% and 10% of responses were observed in MGMT methylated and unmethylated tumors, respectively.

3.5. Safety. All patients were evaluable for toxicity. Treatment-related adverse events are summarized in Table 2. The most common toxicities (all grades) were neutropenia in 6 (23%) patients, thrombocytopenia in 4 (15%) patients, and increase of AST and ALT in 3 (11.5%) patients. Grade 4 adverse events were neutropenia in 2 (8%) patients, leucopenia in 2 (8%) patients, and grade 3 thrombocytopenia in 2 (8%) patients. No case of severe anemia was observed. Hematological toxicity was mostly confined to the induction phase (data not shown). In fact in the maintenance phase only one patient (4%) developed a case of severe toxicity, namely, grade 3 thrombocytopenia. Severe nonhematological toxicity was uncommon: one case (4%) of grade 3 hypertransaminasemia and one case (4%) of nausea/vomiting. Toxicities associated with bevacizumab included grade 3 venous thromboembolic event occurring in 2 (8%) patients, grade 2 nose bleeding in 1 case (4%), grade 2 hypertension in 2 cases (8%), and grade 2 gastrointestinal (GI) perforation in 1 patient (4%), solved with medical treatment. Neither intracranial hemorrhage nor proteinuria occurred. The FTM dose was reduced by 25% in 4 patients. Causes for dose reduction were thrombocytopenia,

Table 2: Grade 3-4 toxicities per patient (total: 26).

	Number of patients (%)
Grade 3-4 haematologic toxicity	
Neutropenia	2 (8)
Leucopenia	2 (8)
Thrombocytopenia	2 (8)
Grade 3-4 nonhaematologic toxicity	
Venous thromboembolism	2 (8)
CNS hemorrhage*	1 (4)
Hepatic^	1 (4)
Emesis	1 (4)

*Asymptomatic central nervous system hemorrhage.
^Transaminase increasing.

neutropenia, and hypertransaminasemia. No drug-related deaths were reported (as being related to the study drug), nor any patients were permanently discontinued from the study due to toxicity. The reason for not proceeding into maintenance phase in six patients was disease progression.

4. Discussion

This is the final analysis of the observational, prospective study of bevacizumab and FTM combination in rMGs. Our finding showed that the association of bevacizumab plus FTM achieved a partial response of 31% with a disease control rate of 92% and a clinical benefit of 60%, reaching our preplanned goal; a 6-month PFS rate of 23% was observed.

Recently, several prospective and retrospective studies provided clinical data on bevacizumab activity both as single agent and in combination therapy, establishing this antiangiogenetic agent as a valuable and active treatment option in rMGs.

In phase II trials regarding the association of bevacizumab with chemotherapeutic agents including also irinotecan, the response rates ranged from 38% to 57% [12, 16] and activity achieved a percentage of about 32% [9]. Among the experiences with bevacizumab combination regimens in GBM, the 6-month PFS ranged from 37% to 50% [9, 12, 16, 19, 20]. Bevacizumab is also active as a single agent in patients with recurrent GBM reporting objective response rate ranging from 25% to 42% and 6-month PFS of 29–42% [12, 13, 21, 22]. Published data are heterogeneous in terms of efficacy in the different histotypes. In GBM tumors, bevacizumab obtained responses between 25% and 48%, while higher activity was seen in recurrent MGs (34%–68% of responses) [23].

A standard regimen has not been established for the recurrent/progressive MGs treatment. We chose fotemustine as nitrosourea to be combined with bevacizumab taking into account the rationale that bevacizumab could improve the activity of cytotoxic molecules without worsening primary toxicities of each agent. Several different experiences have been reported with this drug. Phase II trials demonstrated activity of nitrosoureas, such as FTM, in relapsing GBM patients previously treated with TMZ plus radiotherapy as first line treatment [4]. Recently Brandes et al. experienced use of FTM, in progressive GBM patients, at a conventional dose of 100 mg/mq for both induction and maintenance phase, reporting a 6-month PFS rate of 21%, a median OS of 6 months, and a partial response of 7% [5]. At the dose of 100 mg/mq, FTM has been reported to show a 30% of responses, a DCR of 62%, and a 6-PFS rate of 48–52% [24, 25]. The most frequent toxicities of full dose FTM were grade 3-4 thrombocytopenia and neutropenia observed in about 20% of patients. At lower dose, as demonstrated by Italian experiences in second-line treatment of rMGs, FTM did not reduce therapeutic activity; conversely, safety profile, mainly emathological, was improved [7]. All these results have defined FTM as an optimal therapeutic option in rMGs.

The only previous experience on the combination of FTM and bevacizumab in recurrent GBM was recently reported by Soffietti et al. Fotemustine was administered at a dose of 75 mg/m^2 on days 1 and 8; bevacizumab was given at a dose of 10 mg/kg every two weeks; both were followed, after an interval of 3 weeks, by a maintenance phase of the combination with the same doses every 3 weeks. The authors showed a response rate of 52%, a median PFS of 5.2 months, and PFS rate at 6 months of 42.6%. The authors reported a median OS of 9.1 months and at 6 and 12 months the OS rates were 75.9% and 29.7%, respectively [26]. Although having the same schedule and dose, the different results of our study from those of Soffietti's trial might be due, probably, to the mixed histotype included in our population and to the patients' characteristics. Taking into account the previous chemotherapeutic lines administered, 42% of the patients were at the second recurrence and were heavily pretreated with temozolomide and combination regimens such as procarbazine, lomustine, and vincristine.

The comparison of our results with previous published data on the use of FTM as a single agent seems to show no further advantage in terms of both response rate and PFS when the drug is combined with bevacizumab.

Interestingly, in the present study bevacizumab plus FTM produced better results in terms of DCR (65.1%) than those reported with FTM as a single agent (47.5%), suggesting that the antiangiogenetic role of the drug, delaying the intravascular invasion and inhibiting the neovascularization [6], can result in a better disease control. Furthermore, our results confirm the relationship between response and patient outcome in terms of PFS and OS [7]. Overall these data highlight the importance of treating, if amenable, the MGs patients beyond the first relapse with further active drugs.

Within the second-line treatment of rMGs the safety profile of the regimen used is paramount. The combination of bevacizumab plus FTM used herein is well tolerated. Most frequent grade 3-4 toxicities were primarily related to chemotherapy. Bevacizumab-related toxicities were consistent with those reported in other trials. In our cohort 8% of patients experienced grade 3 venous thromboembolic events, while epistaxis, hypertension, and GI perforation were reported in a low percentage of patients (4%).

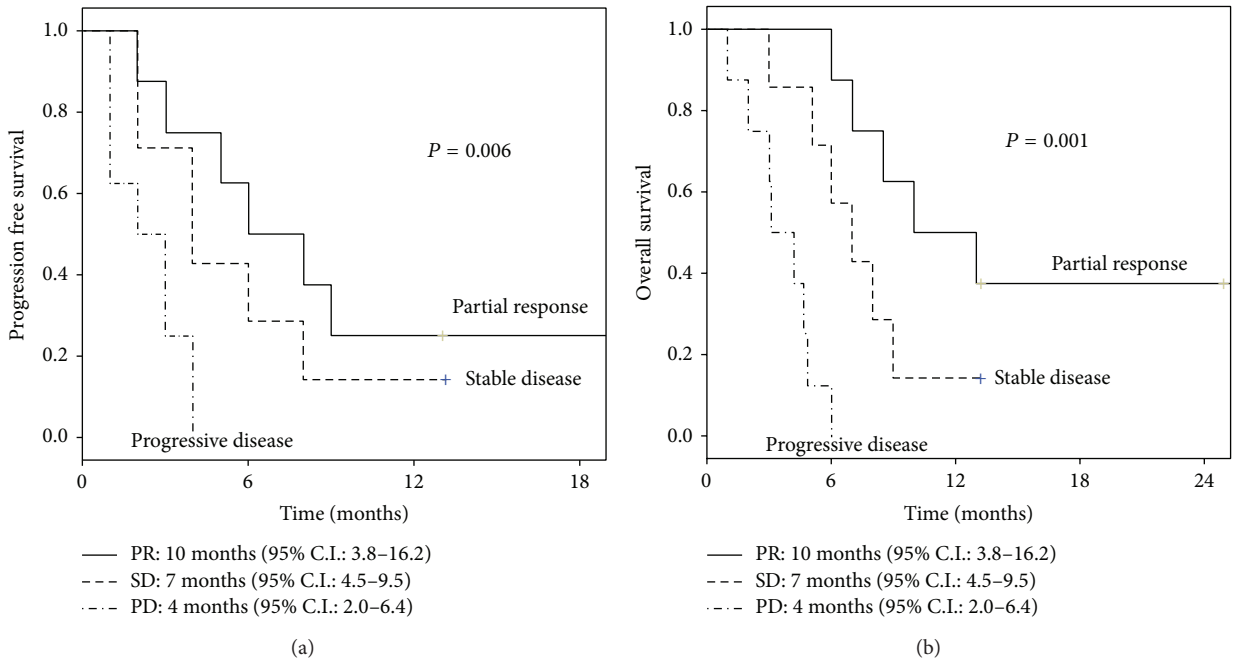

Figure 2: (a) Progression free survival according to response. (b) Overall survival according to response.

In this experience no intracranial hemorrhage was seen, although heavy pretreated patients (43.5%) were included in the population.

On the other hand, in this analysis a significant improvement in terms of clinical benefit was reported. This translates in the achievement of a better clinical status, even in the absence of evident radiological responses. The clinical benefit plays an important role in MGs patients and could represent one of the best evaluation parameters of antiangiogenic drugs activity.

Preliminary results of the Dutch phase II (BELOB trial), randomized trial on firstly recurrent GBMs comparing bevacizumab plus lomustine versus either lomustine or bevacizumab alone, showed a better outcome in terms of 6-month PFS and OS for the combination. Primary endpoint for the combination treatment with bevacizumab and lomustine met the prespecified criterion for further investigation: 9-month OS rate of 59%, 6-month PFS rate of 41%, and median PFS of 4 months (at lower dose of lomustine) were achieved [27].

Further analysis is needed to clarify the real benefit of bevacizumab either as combination or as a single agent treatment. Many of the unanswered questions regarding the use of antiangiogenetic drugs in MGs are being addressed by ongoing clinical trials, namely, the MD Anderson randomized phase II trial [28], the recently opened EORTC 26101 study [29], and the ML25739 Italian study [30]; all of them are comparing the role of bevacizumab alone or in combination with nitrosourea with the attempt to define prospectively the benefit of the biological drug in comparison to chemotherapy.

Conflict of Interests

The authors declare that there is no conflict of interests regarding the publication of this paper.

Authors' Contribution

V. Vaccaro and A. Fabi contributed equally to this work.

References

[1] R. Siegel, D. Naishadham, and A. Jemal, "Cancer statistics, 2012," *CA Cancer Journal for Clinicians*, vol. 62, no. 1, pp. 10–29, 2012.

[2] R. Stupp, M. E. Hegi, W. P. Mason et al., "Effects of radiotherapy with concomitant and adjuvant temozolomide versus radiotherapy alone on survival in glioblastoma in a randomised phase III study: 5-year analysis of the EORTC-NCIC trial," *The Lancet Oncology*, vol. 10, no. 5, pp. 459–466, 2009.

[3] R. Stupp, W. P. Mason, M. J. van den Bent et al., "Radiotherapy plus concomitant and adjuvant temozolomide for glioblastoma," *The New England Journal of Medicine*, vol. 352, no. 10, pp. 987–996, 2005.

[4] R. Addeo, M. Caraglia, M. S. De Santi et al., "A new schedule of fotemustine in temozolomide-pretreated patients with relapsing glioblastoma," *Journal of Neuro-Oncology*, vol. 102, no. 3, pp. 417–424, 2011.

[5] A. A. Brandes, A. Tosoni, E. Franceschi et al., "Fotemustine as second-line treatment for recurrent or progressive glioblastoma after concomitant and/or adjuvant temozolomide: a phase II trial of Gruppo Italiano Cooperativo di Neuro-Oncologia (GICNO)," *Cancer Chemotherapy and Pharmacology*, vol. 64, no. 4, pp. 769–775, 2009.

[6] A. Fabi, G. Metro, M. Russillo et al., "Treatment of recurrent malignant gliomas with fotemustine monotherapy: impact of dose and correlation with MGMT promoter methylation," *BMC Cancer*, vol. 9, article 101, 2009.

[7] A. Fabi, G. Metro, A. Vidiri et al., "Low-dose fotemustine for recurrent malignant glioma: a multicenter phase II study," *Journal of Neuro-Oncology*, vol. 100, no. 2, pp. 209–215, 2010.

[8] D. Khayat, B. Giroux, J. Berille et al., "Fotemustine in the treatment of brain primary tumors and metastases," *Cancer Investigation*, vol. 12, no. 4, pp. 414–420, 1994.

[9] P. L. Nghiemphu, W. Liu, Y. Lee et al., "Bevacizumab and chemotherapy for recurrent glioblastoma: a single-institution experience," *Neurology*, vol. 72, no. 14, pp. 1217–1222, 2009.

[10] M. C. Chamberlain, "Bevacizumab for the treatment of recurrent glioblastoma," *Clinical Medicine Insights: Oncology*, vol. 5, pp. 117–129, 2011.

[11] A. Desjardins, D. A. Reardon, J. E. Herndon II et al., "Bevacizumab plus irinotecan in recurrent WHO grade 3 malignant gliomas," *Clinical Cancer Research*, vol. 14, no. 21, pp. 7068–7073, 2008.

[12] H. S. Friedman, M. D. Prados, P. Y. Wen et al., "Bevacizumab alone and in combination with irinotecan in recurrent glioblastoma," *Journal of Clinical Oncology*, vol. 27, no. 28, pp. 4733–4740, 2009.

[13] J. J. Raizer, S. Grimm, M. C. Chamberlain et al., "A phase 2 trial of single-agent bevacizumab given in an every-3-week schedule for patients with recurrent high-grade gliomas," *Cancer*, vol. 116, no. 22, pp. 5297–5305, 2010.

[14] M. C. Chamberlain, "Bevacizumab for recurrent malignant gliomas: efficacy, toxicity, and patterns of recurrence," *Neurology*, vol. 72, no. 8, pp. 772–774, 2009.

[15] J. J. Vredenburgh, A. Desjardins, J. E. Herndon II et al., "Phase II trial of bevacizumab and irinotecan in recurrent malignant glioma," *Clinical Cancer Research*, vol. 13, no. 4, pp. 1253–1259, 2007.

[16] J. J. Vredenburgh, A. Desjardins, J. E. Herndon II et al., "Bevacizumab plus irinotecan in recurrent glioblastoma multiforme," *Journal of Clinical Oncology*, vol. 25, no. 30, pp. 4722–4729, 2007.

[17] P. Y. Wen, D. R. Macdonald, D. A. Reardon et al., "Updated response assessment criteria for high-grade gliomas: response assessment in neuro-oncology working group," *Journal of Clinical Oncology*, vol. 28, no. 11, pp. 1963–1972, 2010.

[18] R. P. A'Hern, "Sample size tables for exact single-stage phase II designs," *Statistics in Medicine*, vol. 20, no. 6, pp. 859–866, 2001.

[19] A. D. Norden, G. S. Young, K. Setayesh et al., "Bevacizumab for recurrent malignant gliomas: efficacy, toxicity, and patterns of recurrence," *Neurology*, vol. 70, no. 10, pp. 779–787, 2008.

[20] M. R. Gilbert, M. Wang, K. Aldape et al., "RTOG 0625: a phase II study of bevacizumab with irinotecan in recurrent glioblastoma (GBM)," *Journal of Clinical Oncology*, vol. 27, supplement 15, 2009, ASCO Meeting Abstracts, abstract: 2011.

[21] M. C. Chamberlain and S. K. Johnston, "Salvage therapy with single agent bevacizumab for recurrent glioblastoma," *Journal of Neuro-Oncology*, vol. 96, no. 2, pp. 259–269, 2010.

[22] T. N. Kreisl, L. Kim, K. Moore et al., "Phase II trial of single-agent bevacizumab followed by bevacizumab plus irinotecan at tumor progression in recurrent glioblastoma," *Journal of Clinical Oncology*, vol. 27, no. 5, pp. 740–745, 2009.

[23] M. C. Chamberlain, "Emerging clinical principles on the use of bevacizumab for the treatment of malignant gliomas," *Cancer*, vol. 116, no. 17, pp. 3988–3999, 2010.

[24] M. G. Fabrini, G. Silvano, I. Lolli et al., "A multi-institutional phase II study on second-line Fotemustine chemotherapy in recurrent glioblastoma," *Journal of Neuro-Oncology*, vol. 92, no. 1, pp. 79–86, 2009.

[25] S. Scoccianti, B. Detti, A. Sardaro et al., "Second-line chemotherapy with fotemustine in temozolomide-pretreated patients with relapsing glioblastoma: a single institution experience," *Anti-Cancer Drugs*, vol. 19, no. 6, pp. 613–620, 2008.

[26] R. Soffietti, E. Trevisan, L. Bertero et al., "Bevacizumab and fotemustine for recurrent glioblastoma: a phase II study of AINO (Italian Association of Neuro-Oncology)," *Journal of Neuro-Oncology*, vol. 116, pp. 533–541, 2014.

[27] W. Taal, H. M. Oosterkamp, A. M. E. Walenkamp et al., "A randomized phase II study of bevacizumab versus bevacizumab plus lomustine versus lomustine single agent in recurrent glioblastoma: The Dutch BELOB Study," *Journal of Clinical Oncology*, vol. 31, supplement, 2013, ASCO Meeting Abstracts, abstract: 2001.

[28] "Standard Dose Bevacizumab Versus Low Dose Bevacizumab Plus Lomustine (CCNU) for Recurrent Glioblastoma Multiforme (GBM)," NCT01067469, http://clinicaltrials.gov/ct2/show/NCT01067469.

[29] "Bevacizumab and Lomustine in Treating Patients with Glioblastoma Multiforme in First Recurrence," NCT01290939, http://clinicaltrials.gov/show/NCT01290939.

[30] "A Study of Avastin (Bevacizumab) and Fotemustine in Patients with Recurrent Glioblastoma," NCT01474239, http://clinicaltrials.gov/show/NCT01474239.

Hindawi Publishing Corporation
BioMed Research International
Volume 2014, Article ID 540236, 7 pages
http://dx.doi.org/10.1155/2014/540236

Research Article

IDH Mutations: Genotype-Phenotype Correlation and Prognostic Impact

Xiao-Wei Wang,[1,2,3] Pietro Ciccarino,[1,2,3] Marta Rossetto,[1,2,3] Blandine Boisselier,[1,2,3] Yannick Marie,[4] Virginie Desestret,[1,2,3,5] Vincent Gleize,[1,2,3] Karima Mokhtari,[1,2,3,5] Marc Sanson,[1,2,3,6,7] and Marianne Labussière[1,2,3]

[1] *Université Pierre et Marie Curie-Paris 6, Centre de Recherche de l'Institut du Cerveau et de la Moëlle épinière (CRICM) UMR-S975, 75013 Paris, France*
[2] *INSERM U 975, 75013 Paris, France*
[3] *CNRS, UMR 7225, 75013 Paris, France*
[4] *Institut du Cerveau et de la Moëlle épinière (ICM), Plateforme de Génotypage Séquençage, 75013 Paris, France*
[5] *AP-HP, Groupe Hospitalier Pitié-Salpêtrière, Laboratoire de Neuropathologie R. Escourolle, 75013 Paris, France*
[6] *AP-HP, Groupe Hospitalier Pitié-Salpêtrière, Service de Neurologie 2, 75013 Paris, France*
[7] *Fédération de Neurologie Mazarin, Groupe Hospitalier Pitié-Salpêtrière, 75651 Paris Cedex 13, France*

Correspondence should be addressed to Marc Sanson; marc.sanson@psl.aphp.fr

Received 14 February 2014; Accepted 7 April 2014; Published 30 April 2014

Academic Editor: Emeline Tabouret

IDH1/2 mutation is the most frequent genomic alteration found in gliomas, affecting 40% of these tumors and is one of the earliest alterations occurring in gliomagenesis. We investigated a series of 1305 gliomas and showed that *IDH* mutation is almost constant in 1p19q codeleted tumors. We found that the distribution of $IDH1^{R132H}$, $IDH1^{nonR132H}$, and *IDH2* mutations differed between astrocytic, mixed, and oligodendroglial tumors, with an overrepresentation of *IDH2* mutations in oligodendroglial phenotype and an overrepresentation of $IDH1^{nonR132H}$ in astrocytic tumors. We stratified grade II and grade III gliomas according to the codeletion of 1p19q and *IDH* mutation to define three distinct prognostic subgroups: 1p19q and *IDH* mutated, *IDH* mutated—which contains mostly *TP53* mutated tumors, and none of these alterations. We confirmed that *IDH* mutation with a hazard ratio = 0.358 is an independent prognostic factor of good outcome. These data refine current knowledge on *IDH* mutation prognostic impact and genotype-phenotype associations.

1. Introduction

The WHO Classification of Tumors of the Central Nervous System is the universal standard for classifying and grading brain neoplasms [1]. According to the presumed cell of origin, gliomas have been classified into three major groups: astrocytomas, oligodendrogliomas, and mixed oligoastrocytomas. Based on the presence or absence of malignant features: cell density, nuclear atypia, mitosis, microvascular proliferation, and necrosis, the WHO classification distinguishes grades I, II (LGG), III (anaplastic), and IV (glioblastomas, GBM) [2]. However, this classification suffers from a lack of reproducibility, with a high interobserver variability, often leading to discordant results between centers [3–5].

In these settings, there is a need for the identification of additional prognostic markers to refine the WHO classification in order to define more homogeneous subgroups. Mutations in the *IDH1* (isocitrate dehydrogenase 1) gene have been first reported in 2008 [6]. Since then, the *IDH1* mutation has been recognized as the most frequent alterations in gliomas, occurring in 40% of glial tumors [7–9] and is the most powerful prognostic factor ever described in gliomas [10, 11]. Less frequently the mitochondrial isoform *IDH2* is mutated.

We have investigated the mutational status of *IDH1* and *IDH2* in a cohort of 1305 glioma patients and correlated it with the genomic profile and the outcome.

2. Patients and Methods

2.1. Patients and Tissue Samples. Patients were selected retrospectively according to the following criteria: histologic diagnosis of grade II to grade IV glioma; clinical data and follow-up available in the neurooncology database; and written informed consent. The inclusion period extends from May 1987 to October 2010. Tumor DNA was extracted from both frozen and paraffin embedded formalin fixed tumors, when available, using the QIAmp DNA minikit, as described by the manufacturer (Qiagen). CGH-array analysis, LOH (loss of heterozygosity) analysis, *EGFR* amplification, and *P16* deletion assessment were performed as previously described [12].

2.2. Determination of IDH1 and IDH2 Mutational Status. The genomic regions spanning wild-type R132 of *IDH1* and wild-type R172 of *IDH2* were analyzed by direct sequencing using the following primers: IDH1f 5-AGAAGAGGGTTGAGGAGTTCAA, IDH1r 5-CACATACAAGTTGGAAATTTCTGG, IDH2f 5-AGCCCATCATCTGCAAAAAC, and IDH2r 5-CTAGGCGAGGAGCTCCAGT, as previously described [10]. Forward and reverse chains were analyzed on an ABI prism 3730 DNA analyzer (Perkin Elmer).

IDH2 mutational status was determined by Sanger sequencing and by PCR HRM. The latter approach allowing only the detection of an *IDH2* mutation presence, we have only the type of base substitution for 15 tumors. HRM was performed as previously described [13].

2.3. MGMT Status and TP53 Mutations Determination. DNA methylation status of the *MGMT* promoter was determined by bisulfite modification and subsequent nested MSP, a two-stage PCR approach, as previously described [14].

TP53 gene mutations were screened for exons 5–8 by using previously reported primers and methods [15].

2.4. Statistical Analysis. The χ^2 test (or Fisher's exact test when one subgroup was <5) was used to compare the genotype distribution. The association with continuous variables was calculated with a Mann-Whitney test.

Overall survival (OS) was defined as the time between the diagnosis and death or last follow-up. Patients who were still alive at last follow-up were considered as a censored event in analysis. Progression free survival (PFS) was defined as the time between the diagnosis and recurrence or last follow-up. Patients who were recurrence-free at last follow-up were considered as a censored event in analysis. To find clinical and/or genomic factors related to OS (or PFS), survival curves were calculated according to the Kaplan-Meier method and differences between curves were assessed using the log-rank test. Variables with a significant P value were used to build multivariate Cox model.

3. Results

We have screened for the presence of codon-132 mutations in the *IDH1* gene in a large cohort of 1305 gliomas, including 436 WHO grade II, 394 WHO grade III, and 475 WHO grade IV gliomas. The presence of *IDH2* mutation was investigated in a cohort of 980 gliomas (379 grade II, 289 grade III, 312 grade IV). In the whole cohort, sex ratio was 1.3 and median age at diagnosis was 49.2 years (range, 16.1 to 89.1 years). The characteristics of the population are indicated in Table 1.

Table 1: Patients demographics and clinical characteristics.

Characteristics	Glioma by grade		
	II (n = 436)	III (n = 394)	IV (n = 475)
Age, years			
Median	38.1	47.8	58.5
Range	16.1–77.0	19.1–89.1	18.2–89.1
KPS			
Median	90	90	80
Range	50–100	60–100	40–100
Biopsy (%)	25.6	28.7	26.6
Tumor removal (%)	74.4	71.3	73.4
Overall survival, months			
Median	121.9	41.7	14.5
Range	0.1–238.9	0.1–249.3	0.1–89.1
Progression free survival, months			
Median	38.8	19.5	8.2
Range	0.1–189.7	0.1–249.3	0.1–80.5

KPS: Karnofsky performance score; PFS: progression-free survival.

Taken together we found 609/1305 *IDH1* and 30/980 *IDH2* mutations (global mutation rates of 46.7% and 3.1%, resp.). No tumor harbored both *IDH1* and *IDH2* mutations (Supplementary Table 1 available online at http://dx.doi.org/10.1155/2014/540236). Patients with IDH1 mutations were younger for the whole series (median age 40.6 years for IDH1 mutated patients versus 55.9 years; $P < 0.0001$) and also for grades III and IV separately (median age at diagnosis 44.4 and 47.8 years for grades III and IV *IDH* mutated tumors, versus 51.5 and 59.0 years for grades III and IV nonmutated gliomas; $P = 0.0012$ and $P < 0.0001$, resp.).

3.1. Genotype-Phenotype Correlations. *IDH1* mutations affected 72.5% (316/436) grade II, 63.7% (251/394) grade III, and 8.8% (42/475) grade IV gliomas. We looked then for association between glioma subtypes (astrocytic, mixed, and oligodendroglial tumors) and $IDH1^{R132H}$, $IDH1^{nonR132H}$ mutations, and *IDH2* mutations. In grades II and III gliomas, *IDH2* mutations were overrepresented in oligodendrogliomas (22 IDH2 mutations out of 330 *IDH* mutated tumors; 6.7%), compared to astrocytomas (1/60; 1.7%) and mixed gliomas (6/176; 3.4%) ($P = 0.049$). In contrast, we found that $IDH1^{nonR132H}$ mutations were more frequent in astrocytic (6/60, 10.0% *IDH* mutated tumors) and mixed tumors (15/176, 8.5%), compared to oligodendroglial tumors (15/332, 4.5%, $P = 0.037$).

Table 2: Comparison of histologic distribution, molecular alterations, and prognostic impact between *IDH* mutated and wild type patients.

		n	*IDH1* mutated tumors*	*IDH2* mutated tumors	*IDH* wild type tumors
Histologic subtypes	Astrocytic tumors	**448**	**87**	**2**	**359**
	AII	61	43 (2)	1	17
	AIII	33	17 (4)	0	16
	GBM	354	27 (1)	1	326
	Oligodendroglial tumors	**584**	**347**	**22**	**215**
	OII	243	182 (10)	15	46
	OIII	220	150 (5)	7	63
	GBMO	121	15 (1)	0	106
	Mixed tumors	**275**	**176**	**6**	**93**
	OAII	134	92 (6)	5	37
	OAIII	141	84 (9)	1	56
Molecular alterations	*MGMT* promoter methylation	587	195/256 (76.2%)		172/331 (52.0%)
	EGFR amplification	1248	9/609 (1.5%)		196/639 (30.7%)
	Complete 10q loss	1148	57/572 (10.0%)		359/576 (62.3%)
	P16 deletion	1232	63/595 (10.6%)		203/637 (31.8%)
	TP53 mutation	396	64/178 (35.9%)		49/218 (22.5%)
Prognostic impact	Overall survival				
	Grade II	309	136.5		67.0[a]
	Grade III	303	136.9		20.1[b]
	Grade IV	435	26.6		14.2[c]
	Progression free survival				
	Grade II	309	41.3		28.5[d]
	Grade III	303	31.9		10.4[e]
	Grade IV	435	10.0		8.1[f]

*For histologic subtypes, the number in parentheses indicates the number of $IDH1^{nonR132H}$ mutations. [a,b,e]$P < 0.0001$; [c]$P = 0.0004$; [d]$P = 0.0363$; [f]$P = 0.0008$.

3.2. IDH Mutations Are Associated with Tumor Genomic Profile. We have then evaluated the association of *IDH* mutation with the molecular alterations commonly found in gliomas (Table 2). We found that *IDH* mutations were significantly associated with *MGMT* promoter methylation ($P < 0.0001$). In contrast, there was a strong association between the absence of *IDH* mutation and complete loss of chromosome 10q, *EGFR* amplification and *P16* deletion ($P < 0.0001$ in each case).

Complete 1p19q codeletion was found in 150 gliomas: the *IDH1* gene was mutated in 137 cases (91.3%) and the *IDH2* gene was mutated in 12 of the 13 remaining tumors. Taken together, the *IDH* genes were altered in 99.3% (149/150) of the 1p19q codeleted tumors.

TP53 mutation was analyzed by Sanger sequencing in 396 tumors: 64/178 (35.9%) *IDH* mutated tumors were also mutated on *TP53*, versus 49/218 (22.5%) of the nonmutated tumors ($P = 0.0036$). *TP53* mutation was correlated with astrocytic histology: 95 tumors out of 286 (33.2%) astrocytic and mixed gliomas were *TP53* mutated, whereas only 16.4% (18/110) of oligodendrogliomas were mutated on *TP53* ($P = 0.0008$). *TP53* mutation was rarely associated with 1p19q codeletion: 1p19q codeleted gliomas were less frequently *P53* mutated (4/52, 7.7%), as compared to the noncodeleted tumors (103/170, 60.6%; $P < 0.0001$). When excluding 1p19q codeleted tumors (considered as the hallmark of oligodendrogliomas), *TP53* mutation was even more strongly correlated with IDH mutation: 57/98 (58.2%) of *IDH* mutated tumors was also mutated on *TP53*, versus 46/175 (26.2%, $P < 0.0001$) in nonmutated gliomas.

3.3. IDH1 Mutation Is an Independent Prognostic Factor of Good Outcome. We investigated the prognostic impact of *IDH* status in grade II, grade III, and grade IV gliomas. For each grade, *IDH* mutated patients have significantly longer overall survival and progression free survival than *IDH* normal patients (Figure 1 and Table 2).

We then entered the following factors as candidate variables in the multivariate Cox proportional hazards regression model analysis: *IDH* mutation, *P16* deletion, 1p19q codeletion, extent of surgery, Karnofsky index, and age at diagnosis (Table 3). *IDH* mutation was a strong and independent predictor of a better outcome (hazard ratio for overall survival= 0.358; 95% CI, 0.248 to 0.517; $P < 0.0001$).

Moreover, as previously described [16], we stratified the grade II and grade III tumors according to 1p19q codeletion and *IDH* status, thus defining three prognostic groups: 1p19q codeleted (and *IDH* mutated), *IDH* mutated, and others (Figure 2).

Whatever the grade, patients harboring the 1p19q codeletion have a significantly longer survival (median OS: 150.9 months) than patients only harboring *IDH* mutation (69.0 months) or none of these alterations (25.4 months). We looked then at *TP53* mutation in these three prognostic

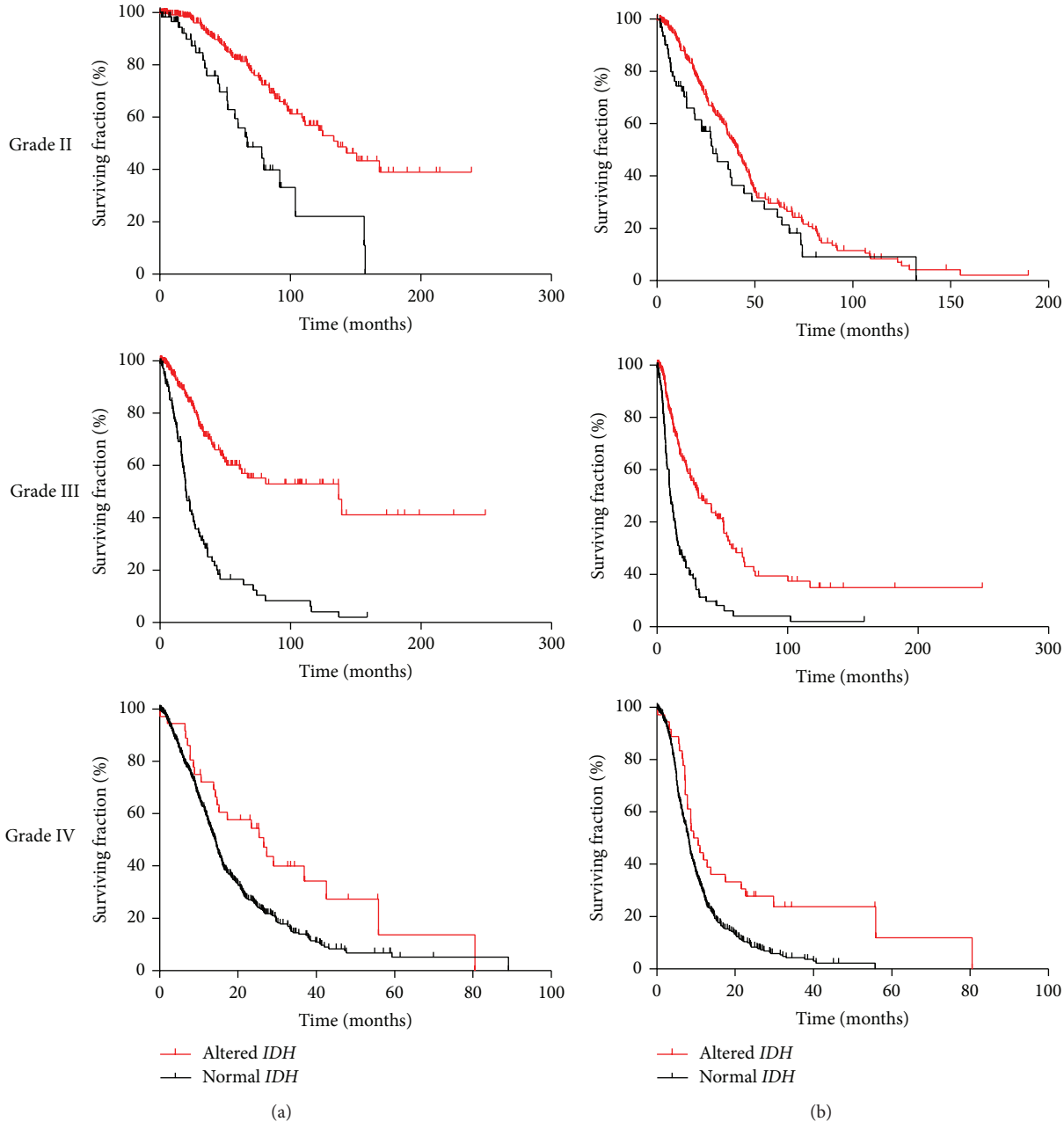

Figure 1: Prognostic impact of *IDH* status on overall survival (a) and progression free survival (b) in grade II to IV gliomas.

Table 3: Multivariate Cox proportional hazards regression model analysis of survival of the 1305 glioma patients cohort. *MGMT* promoter methylation was not included in this analysis due to a low number of evaluable patients for this parameter.

Parameter	Overall survival			Progression free survival		
	HR	95% CI for HR	*P*	HR	95% CI for HR	*P*
Age > 60 years	1.831	1.358 to 2.467	0.0001	1.479	1.158 to 1.889	0.0018
Surgery extent	0.775	0.588 to 1.021	0.0715	1.045	0.823 to 1.326	0.7199
1p19q codeletion	0.202	0.098 to 0.415	<0.0001	0.491	0.326 to 0.739	0.0007
IDH mutation	0.358	0.248 to 0.517	<0.0001	0.467	0.348 to 0.627	<0.0001
IK > 70	0.419	0.315 to 0.556	<0.0001	0.489	0.375 to 0.636	<0.0001
P16 deletion	1.513	1.168 to 1.960	0.0018	1.471	1.165 to 1.858	0.0013

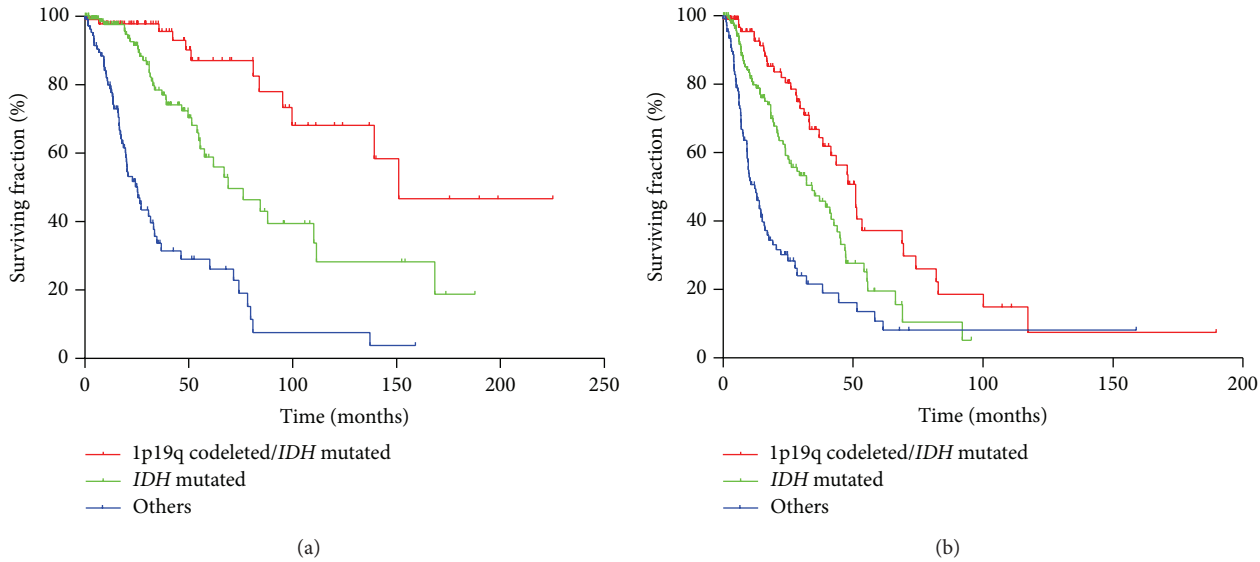

Figure 2: Overall survival (OS, (a)) and progression free survival (PFS, (b)) for grade II and III gliomas patients stratified according to 1p19q codeletion and presence of IDH mutations. Median OS were 150.9, 69.0, and 25.4 months for 1p19q/IDH mutated, IDH mutated, and other groups, respectively. Median PFS were 51.1, 34.3, and 12.2 months for 1p19q/IDH mutated, IDH mutated, and other groups, respectively.

Table 4: Association of *TP53* mutation with 1p19q codeleted tumors and *IDH* mutated tumors.

		TP53			
		Mutated	Normal	Percentage	Difference to *IDH* mutated group (*P*)
Grade II	1p19q/*IDH* mutated	3	31	8.8%	*<0.0001*
	IDH mutated	31	22	58.5%	—
	others	5	13	27.8%	*0.0309*
Grade III	1p19q/*IDH* mutated	1	16	6.3%	*0.0002*
	IDH mutated	21	13	61.8%	—
	others	11	24	31.4%	*0.0160*

groups and found *P53* mutation strongly associated with group 2 in both grades II and III (Table 4). For example in grade II gliomas, *TP53* was mutated in 58.5% in group 2, versus 8.8% and 27.8% in groups 1 and 3, respectively ($P < 0.0001$ and $P = 0.031$, resp.).

4. Discussion

In this large series, we investigated the place of *IDH1*/*IDH2* mutation in gliomas, in particular in different genotypes and phenotypes. As a first result, we confirmed the strong association of *IDH* mutations with the tumor genomic profile [10]: virtually all 1p19q codeleted tumors are *IDH* mutated [17, 18] whereas *IDH* mutation is extremely rare in gliomas with *EGFR* amplification. Secondly, we showed that the type of mutation is related to the molecular profile. The $IDH1^{R132H}$ mutation represents 90% of all *IDH* mutations. However, we found here that $IDH1^{nonR132H}$ mutations are associated with astrocytic tumors [19], whereas *IDH2* mutations are associated with oligodendrogliomas. The 1p19q codeletion is a hallmark of oligodendroglial phenotype and we found similar results when tumors are stratified according to histological subtype.

The association of *IDH* mutation with *TP53* mutation has been widely studied in literature and has led to contradictory results. *IDH* mutation was found associated with *TP53* mutation in several studies [11, 18, 20–24] but other authors did not find such an association [10, 25]. We found an association between *IDH* and *TP53* mutations, but we showed *TP53* mutation correlated with astrocytic phenotype, in contrast with *IDH* mutation more associated with the oligodendroglial phenotype. Therefore, when excluding 1p19q codeleted tumors, mostly oligodendroglial, and rarely *TP53* mutated, we found a stronger positive association between *IDH* and *TP53* mutations. This result is concordant with the data of Gravendeel et al. who found a correlation between *TP53* mutation and $IDH1^{nonR132H}$ mutation [26].

Confirming previous data obtained on smaller cohorts [10, 16], our findings showed that gliomas patients harboring an *IDH1* mutated tumor present an improved outcome, compared to patients with an *IDH1* normal tumor. The multivariate analysis shows that *IDH* status is an independent prognostic factor in a 1332 glioma patients cohort. To further explore the prognostic impact of *IDH1* mutation, we subdivided both grade II and III gliomas patients in three prognostic subgroups, based on the 1p19q codeletion

and *IDH1* mutation status ((i) *IDH* mut/1p19qdel, (ii) *IDH* mut/1p19qnon del, (iii) *IDH* non mut/1p19qnon del.). In line with a recent study [22], we found that *TP53* mutation characterizes the group 2 (IDH mut non 1p19q codeleted). The third group with the worst prognosis contains mainly triple negative gliomas (non 1p19q codeleted, non *IDH* mutated, non *TP53* mutated) [22].

Taken together, our results show that *IDH* mutation combined with other genomic marker can be used to refine the prognostic classification of gliomas, independently of tumor grade. With the recent results of randomized trial, *IDH1* mutation has become, with 1p19q codeletion, a predictive marker of the response to chemotherapy [27–29].

Conflict of Interests

The authors declare that there is no conflict of interests regarding the publication of this paper.

Acknowledgments

This paper is supported by Grants from the Institut National du Cancer (INCA; PL 046) and the Ligue Nationale contre le Cancer. The authors are indebted to Anne-Marie Lekieffre and Muriel Brandel for their assistance in the study. All authors had full access to the original data, reviewed the data analyses, read, and approved the final paper.

References

[1] D. N. Louis, H. Ohgaki, O. D. Wiestler et al., "The 2007 WHO classification of tumours of the central nervous system," *Acta Neuropathologica*, vol. 114, pp. 97–109, 2007.

[2] D. Figarella-Branger and C. Bouvier, "Histological classification of human gliomas: state of art and controversies," *Bulletin du Cancer*, vol. 92, no. 4, pp. 301–309, 2005.

[3] S. W. Coons, P. C. Johnson, B. W. Scheithauer, A. J. Yates, and D. K. Pearl, "Improving diagnostic accuracy and interobserver concordance in the classification and grading of primary gliomas," *Cancer*, vol. 79, pp. 1381–1393, 1997.

[4] J. M. Kros, "Grading of gliomas: the road from eminence to evidence," *Journal of Neuropathology and Experimental Neurology*, vol. 70, no. 2, pp. 101–109, 2011.

[5] M. J. van den Bent, "Interobserver variation of the histopathological diagnosis in clinical trials on glioma: a clinician's perspective," *Acta Neuropathologica*, vol. 120, no. 3, pp. 297–304, 2010.

[6] D. W. Parsons, S. Jones, X. Zhang et al., "An integrated genomic analysis of human glioblastoma multiforme," *Science*, vol. 321, no. 5897, pp. 1807–1812, 2008.

[7] J. Balss, J. Meyer, W. Mueller, A. Korshunov, C. Hartmann, and A. von Deimling, "Analysis of the IDH1 codon 132 mutation in brain tumors," *Acta Neuropathologica*, vol. 116, no. 6, pp. 597–602, 2008.

[8] F. E. Bleeker, S. Lamba, S. Leenstra et al., "IDH1 mutations at residue p.R132 (IDH1R132) occur frequently in high-grade gliomas but not in other solid tumors," *Human Mutation*, vol. 30, no. 1, pp. 7–11, 2009.

[9] H. Ohgaki and P. Kleihues, "Genetic alterations and signaling pathways in the evolution of gliomas," *Cancer Science*, vol. 100, no. 12, pp. 2235–2241, 2009.

[10] M. Sanson, Y. Marie, S. Paris et al., "Isocitrate dehydrogenase 1 codon 132 mutation is an important prognostic biomarker in gliomas," *Journal of Clinical Oncology*, vol. 27, no. 25, pp. 4150–4154, 2009.

[11] H. Yan, D. W. Parsons, G. Jin et al., "IDH1 and IDH2 mutations in gliomas," *The New England Journal of Medicine*, vol. 360, no. 8, pp. 765–773, 2009.

[12] A. Idbaih, Y. Marie, C. Lucchesi et al., "BAC array CGH distinguishes mutually exclusive alterations that define clinicogenetic subtypes of gliomas," *International Journal of Cancer*, vol. 122, no. 8, pp. 1778–1786, 2008.

[13] B. Boisselier, Y. Marie, M. Labussière et al., "COLD PCR HRM: a highly sensitive detection method for IDH1 mutations," *Human Mutation*, vol. 31, no. 12, pp. 1360–1365, 2010.

[14] S. Everhard, G. Kaloshi, E. Crinière et al., "MGMT methylation: a marker of response to temozolomide in low-grade gliomas," *Annals of Neurology*, vol. 60, no. 6, pp. 740–743, 2006.

[15] A. Idbaih, B. Boisselier, M. Sanson et al., "Tumor genomic profiling and TP53 germline mutation analysis of first-degree relative familial gliomas," *Cancer Genetics and Cytogenetics*, vol. 176, no. 2, pp. 121–126, 2007.

[16] M. Labussière, A. Idbaih, X.-W. Wang et al., "All the 1p19q codeleted gliomas are mutated on IDH1 or IDH2," *Neurology*, vol. 74, no. 23, pp. 1886–1890, 2010.

[17] M. Labussiere, M. Sanson, A. Idbaih, and J.-Y. Delattre, "IDH1 gene mutations: a new paradigm in glioma prognosis and therapy?" *Oncologist*, vol. 15, no. 2, pp. 196–199, 2010.

[18] T. Watanabe, S. Nobusawa, P. Kleihues, and H. Ohgaki, "IDH1 mutations are early events in the development of astrocytomas and oligodendrogliomas," *American Journal of Pathology*, vol. 174, no. 4, pp. 1149–1153, 2009.

[19] C. Hartmann, J. Meyer, J. Balss et al., "Type and frequency of IDH1 and IDH2 mutations are related to astrocytic and oligodendroglial differentiation and age: a study of 1,010 diffuse gliomas," *Acta Neuropathologica*, vol. 118, no. 4, pp. 469–474, 2009.

[20] K. Ichimura, D. M. Pearson, S. Kocialkowski et al., "IDH1 mutations are present in the majority of common adult gliomas but rare in primary glioblastomas," *Neuro-Oncology*, vol. 11, no. 4, pp. 341–347, 2009.

[21] T. Labuda, J. P. Christensen, S. Rasmussen et al., "MEK kinase 1 is a negative regulator of virus-specific $CD8^+$ T cells," *European Journal of Immunology*, vol. 36, no. 8, pp. 2076–2084, 2006.

[22] P. Metellus, B. Coulibaly, C. Colin et al., "Absence of IDH mutation identifies a novel radiologic and molecular subtype of WHO grade II gliomas with dismal prognosis," *Acta Neuropathologica*, vol. 120, no. 6, pp. 719–729, 2010.

[23] S. Nobusawa, T. Watanabe, P. Kleihues, and H. Ohgaki, "IDH1 mutations as molecular signature and predictive factor of secondary glioblastomas," *Clinical Cancer Research*, vol. 15, no. 19, pp. 6002–6007, 2009.

[24] M. Weller, J. Felsberg, C. Hartmann et al., "Molecular predictors of progression-free and overall survival in patients with newly diagnosed glioblastoma: a prospective translational study of the German Glioma Network," *Journal of Clinical Oncology*, vol. 27, no. 34, pp. 5743–5750, 2009.

[25] H. J. Dubbink, W. Taal, R. van Marion et al., "IDH1 mutations in low-grade astrocytomas predict survival but not response to temozolomide," *Neurology*, vol. 73, no. 21, pp. 1792–1795, 2009.

[26] L. A. M. Gravendeel, N. K. Kloosterhof, L. B. C. Bralten et al., "Segregation of non-p.R132H mutations in IDH1 in distinct molecular subtypes of glioma," *Human Mutation*, vol. 31, no. 3, pp. E1186–E1199, 2010.

[27] G. Cairncross, M. Wang, E. Shaw et al., "Phase III trial of chemoradiotherapy for anaplastic oligodendroglioma: long-term results of RTOG 9402," *Journal of Clinical Oncology*, vol. 31, pp. 337–343, 2013.

[28] M. J. van den Bent, A. A. Brandes, M. J. Taphoorn et al., "Adjuvant procarbazine, lomustine, and vincristine chemotherapy in newly diagnosed anaplastic oligodendroglioma: long-term follow-up of EORTC brain tumor group study 26951," *Journal of Clinical Oncology*, vol. 31, pp. 344–350, 2013.

[29] J. G. Cairncross, M. Wang, R. B. Jenkins et al., "Benefit from procarbazine, lomustine, and vincristine in oligodendroglial tumors is associated with mutation of IDH," *Journal of Clinical Oncology*, 2014.

Hindawi Publishing Corporation
BioMed Research International
Volume 2014, Article ID 549742, 8 pages
http://dx.doi.org/10.1155/2014/549742

Review Article

BMPs as Therapeutic Targets and Biomarkers in Astrocytic Glioma

Pilar González-Gómez,[1] Nilson Praia Anselmo,[1,2] and Helena Mira[1]

[1] *Unidad de Neurobiología Molecular, UFIEC, Instituto de Salud Carlos III, Carretera Majadahonda-Pozuelo, Km. 2.2, Majadahonda, 28220 Madrid, Spain*
[2] *Laborotório de Biologia Molecular da UFPA "Francisco Mauro Salzano", Instituto de Ciências Biológicas, Universidade Federal do Pará, 66075-900 Belém, PA, Brazil*

Correspondence should be addressed to Helena Mira; hmira@isciii.es

Received 13 February 2014; Accepted 15 March 2014; Published 28 April 2014

Academic Editor: Alessandro Della Puppa

Astrocytic glioma is the most common brain tumor. The glioma initiating cell (GIC) fraction of the tumor is considered as highly chemoresistant, suggesting that GICs are responsible for glioma relapse. A potential treatment for glioma is to induce differentiation of GICs to a more benign and/or druggable cell type. Given BMPs are among the most potent inducers of GIC differentiation, they have been considered as noncytotoxic therapeutic compounds that may be of use to prevent growth and recurrence of glioma. We herein summarize advances made in the understanding of the role of BMP signaling in astrocytic glioma, with a particular emphasis on the effects exerted on GICs. We discuss the prognostic value of BMP signaling components and the implications of BMPs in the differentiation of GICs and in their sensitization to alkylating drugs and oncolytic therapy/chemotherapy. This mechanistic insight may provide new opportunities for therapeutic intervention of brain cancer.

1. Introduction

Astrocytic glioma is the most common tumor of the adult central nervous system. It comprises pilocytic astrocytoma (grade I), low grade astrocytoma (A, grade II), anaplastic astrocytoma (AA, grade III), and glioblastoma (GBM, grade IV) [1]. Glioblastoma is further subdivided into primary GBM, which arises de novo in older patients in the absence of a preexisting low grade lesion, and secondary GBM, which most often develops in younger adults through malignant progression from low grade A, to AA and finally to GBM [2]. Despite recent advances made in both diagnostic modalities and therapeutic strategies, astrocytic glioma remains as one of the deadliest human cancers. The 5-year survival rate in patients with this type of solid tumor is among the lowest for all cancers. The median survival for patients with GBM is about one year [3].

The major obstacle to develop more robust molecular signatures and better therapies for GBM patients arises from the high intra- and intertumor cellular heterogeneity. As in many types of solid cancers, diversity of glioma may be a consequence of genetic changes, clonal evolution, different environment, and the existence of a cellular hierarchy in which a minority of stem-like cells generate nontumorigenic more differentiated cells [4]. The Tumor Initiating Cell (TIC) model of cancer development and progression states that tumors, like normal adult tissues, contain a subset of cells characterized by three main properties: (1) self-renewal, this is, the capacity to produce more TICs, so they can maintain tumor growth indefinitely; (2) differentiation, since they give rise to differentiated progeny thereby generating all the various cell types that comprise the tumor, and (3) TICs are capable of initiating tumor growth *in vivo* [5, 6]. In the field of glial tumors, they are referred to as glioma initiating cells (GICs), and they were among the first solid tumor TICs described [7, 8]. The main hallmarks of the TIC theory are widely accepted for GICs, including their clonogenicity and capability for multilineage differentiation, activation of DNA repair mechanisms, and expression of drug transporters that might enable them to survive standard cytotoxic

therapies [7, 9, 10]. Nevertheless, some studies have suggested that GICs are not a minority of the tumor cell mass and that multiple cohorts of tumor-initiating cells might be active in GBM, each one characterized by distinct functional phenotypic features and molecular profiles [11, 12]. Whatever the case, this model has generated a considerable interest because GICs appear to possess properties that make them clinically relevant. GICs have been considered as the most chemoresistant cell fraction of the tumor bulk, suggesting that they are responsible for tumor relapse.

As described above, GICs share many properties with normal neural stem cells (NSCs). Moreover GICs, like NSCs, are sensitive to developmental signaling pathways such as the Bone Morphogenetic Protein (BMP), Notch, and Wnt pathways [13]. Knowing that any therapy that fails to eliminate GICs will result in recurrence of the tumor, it is clear that new drugs that specifically target these cells are urgently needed. A potential treatment for glioma is thus to exploit developmental pathways in order to induce differentiation of GICs to a more benign phenotype that would be amenable to standard therapy. The specific focus of this review is the role of BMP proteins and their receptors in astrocytic glioma pathogenesis because: (1) some members of the BMP family of ligands have been found differentially expressed in tumors *versus* healthy tissue with a neat clinical relevance, (2) activation of the BMP pathway reduces glioma cell proliferation *in vitro* and *in vivo* and induces differentiation of the glioma initiating cells (GICs), and (3) BMPs render GICs more susceptible to conventional therapy, so BMP treatment is being considered as a promising therapeutic tool against GBM.

2. The BMP Signaling Pathway

Bone morphogenetic proteins are a family of proteins that were originally identified to induce bone and cartilage formation in ectopic skeletal sites *in vivo* [14, 15]. Today we know that BMPs belong to the TGFb superfamily of cytokines and that they are pleiotropic molecules that exert a variety of effects in the whole body due to the high degree of promiscuity in the interaction of ligands with their receptors and regulators (reviewed by Kim and Choe [16]). For instance, it has been demonstrated that some BMPs are implicated in the development of several cancers, sometimes being ligated to tumor progression while others playing a role as tumor suppressors [17].

BMP ligands exert their activities by way of serine-threonine kinase receptors. Prior to that they have to be cut in the cytoplasm and secreted. The receptors form a tetrameric complex composed of two type II receptors (BMPRII) and two type I receptors, the prototypic ones being BMPRIA (ALK3) and BMPRIB (ALK6) [18]. BMPRIA preferentially binds BMP ligands of the Dpp subclass (BMP2/4) whereas BMPRIB has preference for members of the 60A subclass (BMP5/6/7/8). Once a BMP ligand is bound to the receptors, BMPRII phosphorylates BMPR type I, which triggers the signaling cascade by releasing and phosphorylating R-Smads. Phospho-R-Smad1,5,8 in turn oligomerize with Smad4 to form a complex that translocates to the nucleus where it starts the transcriptional response through the activation or repression of BMP-specific target genes [18].

3. Expression and Clinical Significance of BMP Signaling Pathway in Astrocytic Glioma

As we summarize in Table 1, BMP proteins and BMP signaling components are arising in recent studies as novel biomarkers with important therapeutic implications for astrocytic glioma. One of the largest studies exploring the value of BMPs was performed in 2013 by Wu and Yao [20]. They evaluated the expression status of BMP4 in a total of 630 patients with glioma and correlated this dataset with clinical prognosis. By both WB and RTqPCR analysis, they showed that BMP4 expression was significantly lower in tumor tissue than in adjacent healthy tissue. Moreover, BMP4 was downregulated in high grade glioma when compared with low grade glioma. Univariate analysis showed that low BMP4 levels correlated with high expression of the cell cycle marker Ki67, as well as with high tumor grade ($P < 0.001$ for both correlations). Kaplan-Meier analysis showed that patients with high BMP4 expression had significantly better prognosis ($P < 0.001$), highlighting the relevance of BMP4 as a predictor of survival [20].

In the same year, Bao et al. [21] had access to the whole genome mRNA expression microarray data of 220 glioma samples from the Chinese Glioma Genome Atlas (CGGA) database [21]. They found that BMP4 overexpression was significantly associated with low grade tumors. The correlation was validated in previously published microarray datasets from three additional databases (The Cancer Genome Atlas, TCGA; the Repository for Molecular Brain Neoplasia Data, Rembrandt; and GSE16011). Besides, they determined the protein expression level of BMP4 in an independent cohort of 77 glioma patients by immunohistochemistry (IHC), further demonstrating that BMP4 showed a low grade glioma preference both at the mRNA and protein level. The associations of BMP4 expression with clinical-pathological factors and prognosis of glioma patients were also statistically analyzed by Bao and coworkers [21]. Kaplan-Meier survival curves from the CGGA database data and also from the other 3 datasets indicated that high BMP4 expression was significantly associated with lower mortality, particularly when analyzing high grade tumors (AA and GBM). They also found a preferential expression of BMP4 in patients with isocitrate dehydrogenase 1 (IDH1) gene mutation [34], as well as in patients with a molecular signature corresponding to a proneural GBM subtype or G1 subtype, all of them features of a better prognostic GBM [35–37].

In 2009, Liu et al. reported that an active BMP signaling pathway could be beneficial for the outcome of GBM patients [19]. Using Smad1,5,8 phosphorylation as a readout, they reported that BMP signaling was significantly decreased in AA and GBM samples when compared with normal brain and low grade astrocytomas. The expression of the BMPRIB receptor was also downregulated in high grade gliomas. Moreover, Kaplan-Meier survival curves

Table 1: Clinical significance of BMP signaling pathway.

Molecule	Expression data in high grade gliomas	No patients	Methods	Clinical significance	Authors	Reference
BMP2	UP	98	IHQ	↓BMP2: ↑survival time (tumor grade independent)	Liu et al. 2009	[19]
BMP4	DOWN	630	RTqPCR/WB/IHQ	↓BMP4: ↓survival time (all grades together)	Wu and Yao 2013	[20]
	DOWN	220/77	Microarray/IHQ	↓BMP4: ↓survival time (grades III and IV)	Bao et al. 2013	[21]
BMPRIB	DOWN	64	WB	n.d	Liu et al. 2009	[19]
P-Smad 1,5,8	DOWN	64	WB	↓p-Smad: ↓survival time (tumor grade independent)	Liu et al. 2009	[19]

*Bao et al. [21] validated the data using Rembrandt database and GSE16011 microarray data. N.d.: not determined.

and log-rank analysis showed that patients with a low P-Smad1,5,8/total Smad1,5,8 ratio had statistically shorter survival times, reinforcing the negative correlation between P-Smad/BMPRIB and the malignant grade of glioma. In line with this finding, Lee et al. [38] demonstrated that astroglial differentiation of GIC-like cell lines is impaired in a subset of GBMs due to the epigenetic silencing of BMPRIB, strengthening the view that loss of BMP signaling contributes to the pathogenesis of glioma.

But not all reports associate strong BMP signaling or BMP levels with a better clinical outcome of glioma patients. In 2009, Liu and coworkers reported that BMP2 expression became significantly higher as the glioma's grade advanced ($P < 0.001$) and the Karnofsky Performance Status (KPS) score decreased [39]. Univariate analyses of each factor with the Cox log-rank showed that the median survival of patients with a high BMP2 expression level was significantly shorter than those with a low BMP2 expression level ($P < 0.0001$). Liu et al. claimed that BMP2 was not only a significant predictor of survival in high grade gliomas but also in lower grade gliomas. Although these authors concluded that BMP2 is a highly sensitive biomarker for glioma prognosis, this work was done in a relatively small cohort of 98 glioma patients that were all classified as primary glioma cases, since the onset of the disease was less than three months before diagnosis and there was no prior history of malignant astrocytoma. Additional studies employing larger microarray databases available nowadays should confirm the view that the role of BMP4 and BMP7 in glioma differs from that of BMP2. Future studies may also address whether or not BMP function differs between primary and secondary gliomas.

4. BMP Effects on Glioma Initiating Cells

The discovery of GICs and GIC regulation has been fundamental to our current understanding of glioma recurrence. A number of pathways that are commonly deregulated in glioma, including the BMP pathway, are also involved in differentiation of normal NSCs, raising the idea that it is possible to force GICs to differentiate upon restoration of or exposure to the appropriate signals.

In the developing central nervous system, BMP signaling is critical for progenitor cell specification and maintenance of a particular phenotype through dynamic transcriptional regulation [40]. In NSCs derived from early embryos, BMPs appear to promote proliferation and neuronal differentiation. In contrast, NSCs derived from older animals undergo either astrocytic differentiation or quiescence in response to BMPs [41–43]. The same regulatory networks may be important for GICs.

In a seminal study by the Vescovi group, BMPs were shown to block proliferation and promote differentiation of NSCs and GICs, thereby inhibiting tumor growth [23]. Amongst all the BMP ligands tested, BMP4 elicited the strongest effect. BMP4 effectively reduced the *in vitro* proliferation of CD133+ cells (a marker frequently used to isolate GICs) without affecting apoptosis. Accordingly, results from our group employing five different primary GBM cultures indicate that BMP4 inhibits both GIC proliferation and self-renewal (González-Gómez and Mira, unpublished data). Most importantly, the Vescovi group also demonstrated that *in vivo* delivery of BMP4 inhibits tumor growth. Mice intracranially injected with untreated glioma cells died after three to four months, but nearly all mice injected with BMP4-treated cells survived until the end of the experiment [23].

Zhou et al. [24] observed that BMP4 may act as a key inhibitory regulator of cancer initiation and therefore may be used in combined stem cell-based therapy as a noncytotoxic therapeutic agent. The CD133+ GIC fraction used in this study was isolated from the human glioma cell line U87 by using vincristine and was exposed to the BMP4 protein. They showed that BMP4 inhibited U87 GIC proliferation ($P < 0.01$) via downregulation of cyclin D1 level and promoted GIC apoptosis through induction of Bax expression and inhibition of Bcl-2 and Bcl-xL levels.

BMP4 signaling in GICs may be enhanced by means of the inhibition of metabotropic glutamate receptors (mGluRs). These receptors are predominantly involved in maintaining cellular homeostasis in the central nervous system, but evidences suggesting other functional roles in human malignancies have pointed to mGluRs as novel cancer targets [44]. Purified GICs express mGlu3 receptor, the activation of which restrains the prodifferentiating activity of BMP4 *via* a mechanism of receptor-receptor interaction. Systemic treatment with an mGlu2/3 receptor antagonist reduces the growth of brain tumors originating from U87MG

glioma cells [45] or human GICs in mice [46]. The antagonist limits the growth of GIC xenografts and promotes astroglial differentiation mediated by BMP4 [46], suggesting that inhibition of mGluRs may be exploited as a tool to enhance BMP signaling/GIC differentiation. More recent findings suggest that mGlu3 receptor antagonists act synergistically with DNA-alkylating agents (Temozolomide) in killing GICs [47]. Together these data highlight a novel crosstalk between mGluR3 and BMP4 and suggest that mGlu3 receptor blockade may be combined with BMP delivery as a strategy for the treatment of malignant gliomas. This is an attractive approach that warrants further investigation [44].

Chirasani et al. [29] clearly demonstrated *in vivo* and *in vitro* that BMP7, another member of the bone morphogenetic protein family, may be therapeutically useful by the same criteria used for BMP4. These authors showed that BMP7 (released by neural precursor cells) stimulates a canonical BMP response in stem-like glioblastoma cells. This interfered with all the key functions of GICs, reducing their ability to maintain a cellular hierarchy (the markers of undifferentiated cells CD133, Nestin, and Olig2 were lost, whereas the differentiation marker GFAP was induced), their self-renewal capacity (attenuated ability to form spheres), and their potential for tumor-initiation *in vivo*.

Klose et al. [30] focused on analyzing the effects of BMP7 during glioma cell proliferation *in vitro* and *in vivo*. In a glioma cell line (Gli36ΔEGFR-LITG) that overexpresses EGFR, they observed that BMP7 treatment decreased proliferation up to 50% through cell cycle arrest in the G1 phase but not by induction of apoptosis. This effect was mediated by the modulation of the expression and phosphorylation of cyclin-dependent kinase 2, cyclin-dependent kinase inhibitor p21, and downstream retinoblastoma protein. Furthermore, *in vivo* optical imaging of luciferase activity of Gli36ΔEGFR-LITG cells implanted intracranially into nude mice in the presence or absence of BMP7 treatment corroborated the antiproliferative effects of this cytokine. This report clearly underlines the tumor-suppressive role of BMP7 in glioma-derived cells.

Moreover, Tate et al. [31] demonstrated that a BMP7 variant (BMP7v) inhibits GBM growth *in vitro* and *in vivo*. *In vitro*, this BMP7v decreased primary human GIC proliferation, angiogenesis, and stem cell marker expression while enhancing neuronal and astrocyte differentiation marker expression. In subcutaneous and orthotopic GIC xenografts, which closely reproduce the human disease, BMP7v decreased tumor growth and stem cell markers, while enhancing astrocyte and neuronal differentiation compared with control mice. In addition, BMP7v reduced brain invasion, angiogenesis, and the associated mortality in an orthotopic glioma model.

Taken together, these results suggest that BMP4/7 may be explored as potential therapeutic agents for glioma (Table 2). However, this therapeutic approach must be viewed with caution given BMPs are mitogenic in a subset of tumors with repressed BMPRIB expression. Lee et al. [38] reported that 20% of GBM tumors display epigenetic silencing of BMPRIB due to CpG methylation in its promoter regions. In these primary human GBMs, GICs resemble a very early embryonic NSC that is apparently blocked from further stem cell development and differentiation due to an aberration in the BMP signaling pathway. As in NSCs from early developmental stages, BMP treatment of these GICs increases proliferation. Conversely, forced expression of the methylated-promoter-repressed BMPRIB restores the normal differentiation capacity of the GICs, halting proliferation and inducing their terminal differentiation. Thus, Lee and coworkers provide an example of a temporally deregulated and aberrantly fixed stem-like cell, with a developmental differentiation blockade, that is contributing to the pathogenesis of glioma. These observations therefore identify BMPRIB as a promising molecular therapeutic target in a subset of GBMs. The recovery of BMPRIB expression in GBM cells and the development of BMPRIB specific agonists are worthy of further investigation [38].

5. BMPs as Therapeutic Targets in Astrocytic Glioma

With the advent of molecular biology and the consequent improved understanding of basic tumor biology, targeted therapies have become cornerstones for cancer treatment. As we explained above, BMPs have been shown to promote GIC differentiation and to reduce GBM proliferation *in vitro* and *in vivo* [23, 24, 29–31, 38], so they are becoming promising therapeutic tools that could be used in combination with other conventional treatments (Figure 1). This has been recently explored by several groups.

Persano and coworkers [22] found that BMP2 was not only an effective prodifferentiation treatment for GBM-derived stem cells but also that the BMP2-mediated differentiation made the tumor cells more sensitive to Temozolomide (TMZ) treatment. In fact, BMP2 or TMZ delivered separately did not promote GBM apoptosis, but both treatments together exerted a synergistic effect, causing a dramatic increase in cell death. This occurred because BMP2 decreased hypoxia-inducible factor 1 alpha (HIF1α) stability and consequently downregulated O-6-methylguanine-DNA methyltransferase (MGMT), a HIF1α target, thereby allowing the TMZ alkylating action [22].

Liu et al. [25] reported that BMP4 could reverse the multidrug resistance (MDR) phenotype of tumor cells. They generated a TMZ resistant U251 glioma cell line and observed a reduction of the BMP4 protein levels. Treating the cells with BMP4 abolished the MDR phenotype, sensitizing the cells again to TMZ and other treatments. They also corroborated this finding *in vivo*. Resistant cells were transfected with GFP-BMP4 and injected into nude mice brain. The treatment with TMZ was effective only in the mice overexpressing BMP4 [25].

BMP4 treatment has been combined with bevacizumab in GBM mouse models [26]. Bevacizumab is a humanized monoclonal antiangiogenic antibody against vascular endothelial growth factor A (VEGF-A). Although bevacizumab treatment results in a significant reduction of the tumor size and a temporary patient benefit, the prolonged antiangiogenic treatment generates progressive hypoxia,

Table 2: BMP effects on glioma initiating cells.

Subclass	Ligand	Function *in vitro*	Function *in vivo*	Authors	Reference
Dpp 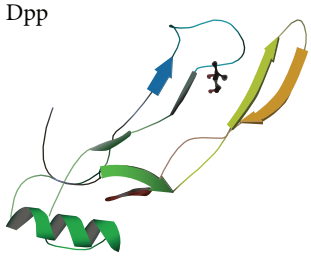	BMP2	↑Differentiation ↑Sensitivity to TMZ		Persano et al. 2012	[22]
		↑Differentiation	↓Tumor growth ↑Survival	Piccirillo et al. 2006	[23]
		↓Proliferation ↑Apoptosis		Zhou et al. 2011	[24]
		↓MDR phenotype ↑Sensitivity to TMZ		Liu et al. 2013	[25]
	BMP4		↓Tumor growth ↓Invasion	Rahman et al. 2013	[26]
			BMP4-oncolytic virus ↓Tumor size ↓Recurrence ↑Survival	Duggal et al. 2013	[27]
Scheufler et al. 1999 [28]		↓Proliferation ↓Sphere formation ↓Self-renewal		González-Gómez et al. (unpublished data)	
60A 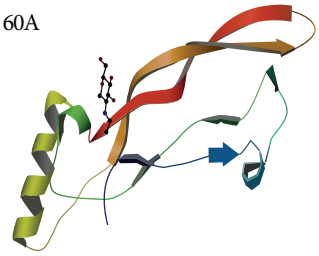	BMP7	↑Differentiation ↓Proliferation ↓Self-renewal	↓Tumor formation	Chirasani et al. 2010	[29]
		↓Proliferation = Apoptosis	↓Tumor growth	Klose et al. 2011	[30]
		↑Differentiation ↓Proliferation ↓Angiogenesis	↓Tumor growth ↑Differentiation ↓Brain invasion ↓Angiogenesis ↓Mortality	Tate et al. 2012	[31]
			BMP7 in microparticles ↓Tumor size	Reguera-Nuñez et al. 2014	[32]
Griffith et al. 1996 [33]		↓Proliferation ↓Sphere formation ↓Self-renewal	BMP7 in microparticles ↓Tumor size primary GICs from patients	González-Gómez et al. (unpublished data)	

which promotes tumor resistance, increased invasion, and finally tumor recurrence [48]. In fact, two recent studies showed that bevacizumab does not increase the overall survival of GBM patients although there is an improvement on the progression-free survival times [49, 50]. Novel strategies designed to overcome the proinvasive effects of bevacizumab may still be useful, since antiangiogenic therapies not only diminish tumor size but also improve blood flow, which is important for oxygen and drug delivery [51]. Rahman et al. [26] implanted human GBM cells in the striatum of immunocompromised mice and treated them with bevacizumab and BMP4 to test whether BMP4 could prevent diffuse tumor infiltration induced by bevacizumab in a malignant glioma xenograft model. It was possibly not the best model to assess the aim, because bevacizumab treatment did not result in diffuse infiltration of human GBM in the mouse brain parenchyma. Nevertheless they observed that BMP4 did have a favorable effect on GBM: it reduced tumor size and tumor invasion although there was no synergistic effect with bevacizumab treatment [26].

Effective treatment with BMPs or any other chemotherapeutic agent is limited due to the presence of the blood-brain barrier (BBB) that tightly regulates the diffusion of endogenous molecules but also of xenobiotics. Tumor-targeted drug delivery is one of the major areas in cancer research and viruses and biomaterials have already been used to deliver BMPs with good results. Duggal and colleagues developed an oncolytic vaccinia virus that overexpressed BMP4 and tested its activity *in vitro* and in an orthotopic xenograft model of GBM. The virus overexpressing BMP4 promoted cell differentiation of primary GIC cultures derived from tumor biopsies. Interestingly, GIC differentiation further increased the replication capacity of the oncolytic virus. intracranial inoculation of the BMP4-virus at the same coordinates as the tumor cells (implanted two weeks earlier) resulted in a rapid tumor regression and improved survival of the mice.

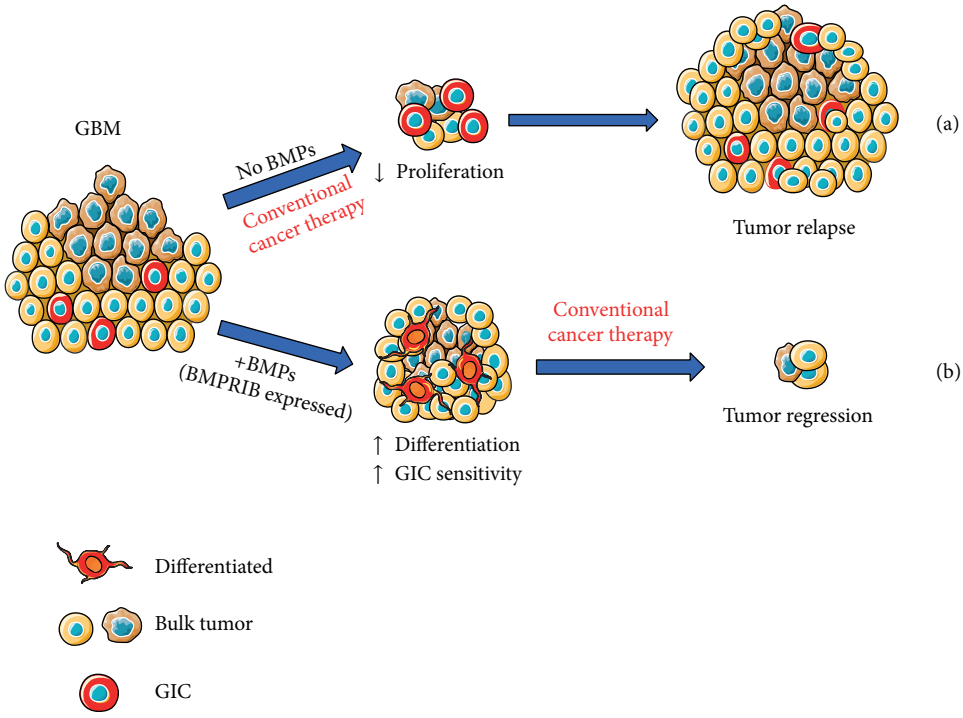

Figure 1: (a) Glioma initiating cells seem to be radioresistant and chemoresistant to conventional therapies and, eventually, this results in tumor recurrence. (b) One approach to target GICs in GBM could be to develop a specific chemotherapeutic agent (such as BMPs or newly synthesized molecules mimicking BMPs) able to induce GICs to differentiate into cells more amenable to standard therapy. The expression of BMPRIB would be key for inducing differentiation of GICs.

This efficacy was also confirmed in a higher tumor burden setting, when the virus was inoculated 7 weeks after tumor cell implantation [27].

Early this year, the group of García-Fuentes reported the design of an implantable microparticles system optimized for the controlled release of BMP7 as a bioinspired device against GICs. The delivery system was based on the formation of heparin-BMP7 microparticles, further entrapped in a biodegradable polyester matrix. The obtained microparticles efficiently encapsulated BMP7 and released it in a controlled manner with minimum burst effect for over two months while maintaining protein bioactivity. Released BMP7 showed a remarkable capacity to stop tumor formation in an *in vitro* GIC model [32] and strongly limited growth of GIC orthotopic xenografts in immunocompromised mice (González-Gómez and collaborators, unpublished).

In summary, the combination of conventional surgery, chemotherapy, and radiotherapy with stem cell-orientated therapy may provide a new promising treatment for reducing GBM recurrence and improving patient survival. Targeting GICs with BMPs may be an innovative way to achieve this goal. Given BMPs markedly inhibit the cancer stem-like cells in other neoplasms, both from the central nervous system such as oligodendrogliomas [52] or from nonneural origin such as prostate [53] or breast tumors [54], the development of BMP-based treatments may provide new opportunities for therapeutic intervention of different cancer types besides GBM.

6. Concluding Remarks

In the last 10 years, for the vast majority of cancers, tumor prognosis and response to therapy have been improved by technological advances in molecular biology. Nevertheless, astrocytic glioma patients still face a poor prognosis, with even the more advanced treatments offering very limited results. In glioblastoma, most patients undergo recurrence, possibly due to the failure to eradicate GICs. Targeting GICs has opened the door to the development of new potential clinical therapies and interventions. Given BMPs block proliferation and drive differentiation of GICs *in vitro* and in mouse models of glioma, they have been proposed as promising tumor-suppressive drugs. Delivery or expression of BMP ligands causes sustained tumor regression and greatly enhances survival in xenograft mouse models. Moreover, BMPs increase GIC responsiveness to chemotherapy through downregulation of MGMT and low BMP levels are prognostic for poor survival in human glioma. Thus, BMPs or newly synthesized molecules mimicking BMP binding to its receptors may be exploited as innovative GIC-orientated treatments for astrocytic glioma.

Conflict of Interests

The authors declare that there is no conflict of interests regarding the publication of this paper.

Authors' Contribution

Pilar González-Gómez and Nilson Praia Anselmo equally contributed to the paper.

Acknowledgments

This study was supported by grants from Ministerio de Sanidad y Consumo (MSC; Fondo de Investigación Sanitaria, PI12/101) and Comunidad de Madrid (S2010/BMD-2336) to Helena Mira. They are grateful to Marcos García-Fuentes and Pilar Sánchez for sharing unpublished results. Nilson Praia Anselmo is a recipient of a postdoctoral fellowship from "Ciência sem Fronteiras"—Brazil Scientific Mobility Program/CAPES.

References

[1] P. Kleihues, D. N. Louis, B. W. Scheithauer et al., "The WHO classification of tumors of the nervous system," *Journal of Neuropathology and Experimental Neurology*, vol. 61, no. 3, pp. 215–225, 2002.

[2] D. N. Louis, H. Ohgaki, O. D. Wiestler et al., "The 2007 WHO classification of tumours of the central nervous system," *Acta Neuropathologica*, vol. 114, no. 2, pp. 97–109, 2007.

[3] A. Jemal, R. Siegel, J. Xu, and E. Ward, "Cancer statistics, 2010," *CA Cancer Journal for Clinicians*, vol. 60, no. 5, pp. 277–300, 2010.

[4] C. E. Meacham and S. J. Morrison, "Tumour heterogeneity and cancer cell plasticity," *Nature*, vol. 501, no. 7467, pp. 328–337, 2013.

[5] C. T. Jordan, M. L. Guzman, and M. Noble, "Cancer stem cells," *The New England Journal of Medicine*, vol. 355, no. 12, pp. 1253–1261, 2006.

[6] L. E. Ailles and I. L. Weissman, "Cancer stem cells in solid tumors," *Current Opinion in Biotechnology*, vol. 18, no. 5, pp. 460–466, 2007.

[7] S. K. Singh, I. D. Clarke, T. Hide, and P. B. Dirks, "Cancer stem cells in nervous system tumors," *Oncogene*, vol. 23, no. 43, pp. 7267–7273, 2004.

[8] R. Galli, E. Binda, U. Orfanelli et al., "Isolation and characterization of tumorigenic, stem-like neural precursors from human glioblastoma," *Cancer Research*, vol. 64, no. 19, pp. 7011–7021, 2004.

[9] J. Lee, S. Kotliarova, Y. Kotliarov et al., "Tumor stem cells derived from glioblastomas cultured in bFGF and EGF more closely mirror the phenotype and genotype of primary tumors than do serum-cultured cell lines," *Cancer Cell*, vol. 9, no. 5, pp. 391–403, 2006.

[10] S. Das, M. Srikanth, and J. A. Kessler, "Cancer stem cells and glioma," *Nature Clinical Practice Neurology*, vol. 4, no. 8, pp. 427–435, 2008.

[11] S. Mazzoleni, L. S. Politi, M. Pala et al., "Epidermal growth factor receptor expression identifies functionally and molecularly distinct tumor-initiating cells in human glioblastoma multiforme and is required for gliomagenesis," *Cancer Research*, vol. 70, no. 19, pp. 7500–7513, 2010.

[12] R. Chen, M. C. Nishimura, S. M. Bumbaca et al., "A hierarchy of self-renewing tumor-initiating cell types in glioblastoma," *Cancer Cell*, vol. 17, no. 4, pp. 362–375, 2010.

[13] T. Reya, S. J. Morrison, M. F. Clarke, and I. L. Weissman, "Stem cells, cancer, and cancer stem cells," *Nature*, vol. 414, no. 6859, pp. 105–111, 2001.

[14] A. Hari Reddi, "Regulation of cartilage and bone differentiation by bone morphogenetic proteins," *Current Opinion in Cell Biology*, vol. 4, no. 5, pp. 850–855, 1992.

[15] J. M. Wozney, "Bone morphogenetic proteins," *Progress in Growth Factor Research*, vol. 1, no. 4, pp. 267–280, 1989.

[16] M. Kim and S. Choe, "BMPs and their clinical potentials," *BMB Reports*, vol. 44, no. 10, pp. 619–634, 2011.

[17] A. Kallioniemi, "Bone morphogenetic protein 4-a fascinating regulator of cancer cell behavior," *Cancer Genetics*, vol. 205, no. 6, pp. 267–277, 2012.

[18] A. Singh and R. J. Morris, "The Yin and Yang of bone morphogenetic proteins in cancer," *Cytokine and Growth Factor Reviews*, vol. 21, no. 4, pp. 299–313, 2010.

[19] S. Liu, Z. Tian, F. Yin et al., "Expression and functional roles of Smad1 and BMPR-IB in glioma development," *Cancer Investigation*, vol. 27, no. 7, pp. 734–740, 2009.

[20] Q. Wu and J. Yao, "BMP4, a new prognostic factor for glioma," *World Journal of Surgical Oncology*, vol. 11, article 264, 2013.

[21] Z. Bao, C. Zhang, W. Yan et al., "BMP4, a strong better prognosis predictor, has a subtype preference and cell development association in gliomas," *Journal of Translational Medicine*, vol. 11, article 100, 2013.

[22] L. Persano, F. Pistollato, E. Rampazzo et al., "BMP2 sensitizes glioblastoma stem-like cells to Temozolomide by affecting HIF-1alpha stability and MGMT expression," *Cell Death and Disease*, vol. 3, p. e412, 2012.

[23] S. G. M. Piccirillo, B. A. Reynolds, N. Zanetti et al., "Bone morphogenetic proteins inhibit the tumorigenic potential of human brain tumour-initiating cells," *Nature*, vol. 444, no. 7120, pp. 761–765, 2006.

[24] Z. Zhou, L. Sun, Y. Wang et al., "Bone morphogenetic protein 4 inhibits cell proliferation and induces apoptosis in glioma stem cells," *Cancer Biotherapy and Radiopharmaceuticals*, vol. 26, no. 1, pp. 77–83, 2011.

[25] B. Liu, Q. Chen, D. Tian et al., "BMP4 reverses multidrug resistance through modulation of BCL-2 and GDNF in glioblastoma," *Brain Research*, vol. 1507, pp. 115–124, 2013.

[26] M. Rahman, H. Azari, L. Deleyrolle, S. Millette, H. Zeng, and B. A. Reynolds, "Controlling tumor invasion: bevacizumab and BMP4 for glioblastoma," *Future Oncology*, vol. 9, no. 9, pp. 1389–1396, 2013.

[27] R. Duggal, U. Geissinger, Q. Zhang et al., "Vaccinia virus expressing bone morphogenetic protein-4 in novel glioblastoma orthotopic models facilitates enhanced tumor regression and long-term survival," *Journal of Translational Medicine*, vol. 11, no. 1, article 155, 2013.

[28] C. Scheufler, W. Sebald, and M. Hülsmeyer, "Crystal structure of human bone morphogenetic protein-2 at 2.7 Å resolution," *Journal of Molecular Biology*, vol. 287, no. 1, pp. 103–115, 1999.

[29] S. R. Chirasani, A. Sternjak, P. Wend et al., "Bone morphogenetic protein-7 release from endogenous neural precursor cells suppresses the tumourigenicity of stem-like glioblastoma cells," *Brain*, vol. 133, no. 7, pp. 1961–1972, 2010.

[30] A. Klose, Y. Waerzeggers, P. Monfared et al., "Imaging bone morphogenetic protein 7 induced cell cycle arrest in experimental gliomas," *Neoplasia*, vol. 13, no. 3, pp. 276–285, 2011.

[31] C. M. Tate, R. Pallini, L. Ricci-Vitiani et al., "A BMP7 variant inhibits the tumorigenic potential of glioblastoma stem-like

cells," *Cell Death and Differentiation*, vol. 19, no. 10, pp. 1644–1654, 2012.

[32] E. Reguera-Nunez, C. Roca, E. Hardy, M. de la Fuente, N. Csaba, and M. Garcia-Fuentes, "Implantable controlled release devices for BMP-7 delivery and suppression of glioblastoma initiating cells," *Biomaterials*, vol. 35, no. 9, pp. 2859–2867, 2014.

[33] D. L. Griffith, P. C. Keck, T. K. Sampath, D. C. Rueger, and W. D. Carlson, "Three-dimensional structure of recombinant human osteogenic protein 1: structural paradigm for the transforming growth factor β superfamily," *Proceedings of the National Academy of Sciences of the United States of America*, vol. 93, no. 2, pp. 878–883, 1996.

[34] H. Ohgaki and P. Kleihues, "The definition of primary and secondary glioblastoma," *Clinical Cancer Research*, vol. 19, no. 4, pp. 764–772, 2013.

[35] H. S. Phillips, S. Kharbanda, R. Chen et al., "Molecular subclasses of high-grade glioma predict prognosis, delineate a pattern of disease progression, and resemble stages in neurogenesis," *Cancer Cell*, vol. 9, no. 3, pp. 157–173, 2006.

[36] R. G. W. Verhaak, K. A. Hoadley, E. Purdom et al., "Integrated genomic analysis identifies clinically relevant subtypes of glioblastoma characterized by abnormalities in PDGFRA, IDH1, EGFR, and NF1," *Cancer Cell*, vol. 17, no. 1, pp. 98–110, 2010.

[37] W. Yan, W. Zhang, G. You et al., "Molecular classification of gliomas based on whole genome gene expression: a systematic report of 225 samples from the Chinese Glioma Cooperative Group," *Neuro-Oncology*, vol. 14, no. 12, pp. 1432–1440, 2012.

[38] J. Lee, M. J. Son, K. Woolard et al., "Epigenetic-mediated dysfunction of the bone morphogenetic protein pathway inhibits differentiation of glioblastoma-initiating cells," *Cancer Cell*, vol. 13, no. 1, pp. 69–80, 2008.

[39] C. Liu, G. Tian, Y. Tu, J. Fu, C. Lan, and N. Wu, "Expression pattern and clinical prognostic relevance of bone morphogenetic protein-2 in human gliomas," *Japanese Journal of Clinical Oncology*, vol. 39, no. 10, pp. 625–631, 2009.

[40] A. M. Bond, O. G. Bhalala, and J. A. Kessler, "The dynamic role of bone morphogenetic proteins in neural stem cell fate and maturation," *Developmental Neurobiology*, vol. 72, no. 7, pp. 1068–1084, 2012.

[41] D. M. Panchision and R. D. G. McKay, "The control of neural stem cells by morphogenic signals," *Current Opinion in Genetics and Development*, vol. 12, no. 4, pp. 478–487, 2002.

[42] H. Mira, Z. Andreu, H. Suh et al., "Signaling through BMPR-IA regulates quiescence and long-term activity of neural stem cells in the adult hippocampus," *Cell Stem Cell*, vol. 7, no. 1, pp. 78–89, 2010.

[43] Y. Sun, J. Hu, L. Zhou, S. M. Pollard, and A. Smith, "Interplay between FGF2 and BMP controls the self-renewal, dormancy and differentiation of rat neural stem cells," *Journal of Cell Science*, vol. 124, no. 11, pp. 1867–1877, 2011.

[44] J. Teh and S. Chen, "Metabotropic glutamate receptors and cancerous growth," *Wiley Interdisciplinary Reviews: Membrane Transport and Signaling*, vol. 1, no. 2, pp. 211–220, 2012.

[45] A. Arcella, G. Carpinelli, G. Battaglia et al., "Pharmacological blockade of group II metabotropic glutamate receptors reduces the growth of glioma cells in vivo," *Neuro-Oncology*, vol. 7, no. 3, pp. 236–245, 2005.

[46] C. Ciceroni, A. Arcella, P. Mosillo et al., "Type-3 metabotropic glutamate receptors negatively modulate bone morphogenetic protein receptor signaling and support the tumourigenic potential of glioma-initiating cells," *Neuropharmacology*, vol. 55, no. 4, pp. 568–576, 2008.

[47] C. Ciceroni, M. Bonelli, E. Mastrantoni et al., "Type-3 metabotropic glutamate receptors regulate chemoresistance in glioma stem cells, and their levels are inversely related to survival in patients with malignant gliomas," *Cell Death and Differentiation*, vol. 20, no. 3, pp. 396–407, 2013.

[48] A. D. Norden, G. S. Young, K. Setayesh et al., "Bevacizumab for recurrent malignant gliomas: efficacy, toxicity, and patterns of recurrence," *Neurology*, vol. 70, no. 10, pp. 779–787, 2008.

[49] O. L. Chinot, W. Wick, W. Mason et al., "Bevacizumab plus radiotherapy-temozolomide for newly diagnosed glioblastoma," *The New England Journal of Medicine*, vol. 370, no. 8, pp. 709–722, 2014.

[50] M. R. Gilbert, J. J. Dignam, T. S. Armstrong et al., "A randomized trial of bevacizumab for newly diagnosed glioblastoma," *The New England Journal of Medicine*, vol. 370, no. 8, pp. 699–708, 2014.

[51] R. K. Jain, "Normalization of tumor vasculature: an emerging concept in antiangiogenic therapy," *Science*, vol. 307, no. 5706, pp. 58–62, 2005.

[52] M. Srikanth, J. Kim, S. Das, and J. A. Kessler, "BMP signaling induces astrocytic differentiation of clinically derived oligodendroglioma propagating cells," *Molecular Cancer Research*, vol. 12, no. 2, pp. 283–294, 2014.

[53] A. Kobayashi, H. Okuda, F. Xing et al., "Bone morphogenetic protein 7 in dormancy and metastasis of prostate cancer stem-like cells in bone," *Journal of Experimental Medicine*, vol. 208, no. 13, pp. 2641–2655, 2011.

[54] J. T. Buijs, G. van der Horst, C. van den Hoogen et al., "The BMP2/7 heterodimer inhibits the human breast cancer stem cell subpopulation and bone metastases formation," *Oncogene*, vol. 31, no. 17, pp. 2164–2174, 2012.

Hindawi Publishing Corporation
BioMed Research International
Volume 2014, Article ID 827327, 9 pages
http://dx.doi.org/10.1155/2014/827327

Research Article

Tumor and Endothelial Cell Hybrids Participate in Glioblastoma Vasculature

Soufiane El Hallani,[1] Carole Colin,[2] Younas El Houfi,[1] Ahmed Idbaih,[1,3] Blandine Boisselier,[1] Yannick Marie,[1] Philippe Ravassard,[1] Marianne Labussière,[1] Karima Mokhtari,[4] Jean-Léon Thomas,[1] Jean-Yves Delattre,[1,3] Anne Eichmann,[5] and Marc Sanson[1,3]

[1] *Sorbonne Universités, UPMC, Université Paris 06, Inserm, CNRS, UM 75, U 1127, UMR 7225, ICM, 75013 Paris, France*
[2] *UMR911-CRO2, Faculté de Médecine de la Timone, Université de la Méditerranée, 13000 Marseille, France*
[3] *AP-HP, Groupe Hospitalier Pitié-Salpêtrière, Service de Neurologie Mazarin, 75013 Paris, France*
[4] *AP-HP, Groupe Hospitalier Pitié-Salpêtrière, Service de Neuropathologie Raymond Escourolle, 75013 Paris, France*
[5] *INSERM U833, Collège de France, 75005 Paris, France*

Correspondence should be addressed to Marc Sanson; marc.sanson@psl.aphp.fr

Received 11 February 2014; Accepted 2 March 2014; Published 24 April 2014

Academic Editor: Giuseppe Lombardi

Background. Recently antiangiogenic therapy with bevacizumab has shown a high but transient efficacy in glioblastoma (GBM). Indeed, GBM is one of the most angiogenic human tumors and endothelial proliferation is a hallmark of the disease. We therefore hypothesized that tumor cells may participate in endothelial proliferation of GBM. *Materials and Methods.* We used *EGFR* FISH Probe to detect *EGFR* amplification and anti-CD31, CD105, VE-cadherin, and vWF to identify endothelial cells. Endothelial and GBM cells were grown separately, labeled with GFP and DsRed lentiviruses, and then cocultured with or without contact. *Results.* In a subset of GBM tissues, we found that several tumor endothelial cells carry *EGFR* amplification, characteristic of GBM tumor cells. This observation was reproduced *in vitro*: when tumor stem cells derived from GBM were grown in the presence of human endothelial cells, a fraction of them acquired endothelial markers (CD31, CD105, VE-cadherin, and vWF). By transduction with GFP and DsRed expressing lentiviral vectors, we demonstrate that this phenomenon is due to cell fusion and not transdifferentiation. *Conclusion.* A fraction of GBM stem cells thus has the capacity to fuse with endothelial cells and the resulting hybrids may participate in tumor microvascular proliferation and in treatment resistance.

1. Introduction

Glioblastomas (GBM) are the most frequent and malignant primary brain tumors in adults with poor prognosis despite surgery and conventional radio-chemotherapy. Histologically, GBM are highly angiogenic and characterized by microvascular proliferations (previously called endothelial cell proliferations) typically consisting on multilayered tufts of mitotically active endothelial cells together with smooth muscle cells and pericytes [1]. Among targeted therapies tested to date, only antiangiogenic drugs and particularly anti-VEGF have shown efficacy with a nearly 50% of responders [2, 3]. However, this effect is always transient suggesting that GBM can acquire secondary antiangiogenic resistance. Therefore, understanding tumor endothelial cell abnormalities is important to optimize therapy. It is well established that tumor blood vessels differ from normal vessels by altered morphology, blood flow, permeability, and basement membrane deposition [4–7]. Furthermore, evidence indicates that tumor endothelial cells overexpress specific genes, proliferate rapidly, and are sensitive to growth factors and resistant to chemotherapeutic drugs [8–12]. Surprisingly, tumor endothelial cells can harbor the same chromosomal abnormality as tumor cells in B-cell lymphomas [13], multiple myeloma [14], and neuroblastoma [15], suggesting a tumor origin of at least a fraction of intratumoral endothelial cells.

Another subpopulation of tumor cells possesses characteristics associated with normal stem cells, specifically the ability to give rise to all cell types found in a particular cancer sample [16]. In brain tumors, including GBM, tumor stem cells have been shown to possess marked capacity for proliferation, self-renewal, and differentiation into all neural lineages [17]. It has also been suggested that normal mouse neural stem cells cocultured with human endothelial cells convert into endothelial cells by transdifferentiation [18].

We here investigated whether endothelial cells of tumor origin might be present in human GBM samples and whether these cells derive from GBM stem cells. Analysis of *EGFR* amplified human GBM tissues by fluorescent *in situ* hybridization (FISH) combined with immunophenotyping [15] showed rare endothelial cells exhibiting *EGFR* amplification. We then investigated the capacity of GBM stem cells (GSC) to acquire an endothelial phenotype *in vitro* and demonstrate that this property results from cell fusion and not transdifferentiation.

2. Materials and Methods

2.1. GBM Tissue Preparation. Formalin-fixed, paraffin-embedded tissue sections (5 μm) from 10 GBM tumors (World Health Organization classification of brain tumors [1]) carrying *EGFR* amplification identified by CGHa analysis [19] were deparaffinized twice with xylene. The slides were subsequently rehydrated in a series of ethanol solution (100%, 90%, and 70%), washed with phosphate-buffered saline (PBS), and treated with antigen retrieval solution (citrate buffer pH 9.0; Dako Cytomation, France) at 96°C for 20 minutes.

2.2. Fluorescent In Situ Hybridization and Immunofluorescence. Briefly, slides were blocked with PBS/3% bovine serum albumin (BSA) for 20 minutes and immunostained with mouse anti-human CD31 (1 : 20; Dako Cytomation, France) for 30 minutes at room temperature. Alexa 488-conjugated goat anti-mouse antibody (1 : 1000; Molecular Probes, Invitrogen, France) was added as secondary reagent. After immunostaining, slides were washed three times for 5 minutes each in PBS containing 0.5% Tween-20 (Sigma-Aldrich, France). Only sections of high morphologic quality were used for fluorescent *in situ* hybridization (FISH). The *EGFR* FISH Probe Mix (Dako Cytomation, France) was used according to the manufacturer's instructions. Slides were dehydrated through a series of ethanol washes (70%, 90%, and 100%), denatured in the presence of the specific probes at 82°C for 5 minutes, and incubated overnight in a humid chamber at 45°C. Posthybridization washes were performed, and the slides were mounted in antifade medium Fluoromount-G (Interchim, France) with DAPI (Sigma-Aldrich, France). Slides were analyzed using a Zeiss AxioImager.Z1 microscope.

2.3. Cell Cultures

2.3.1. Culture of Primary GBM Stem Cells and Sphere Forming Assay. GBM samples were provided by the local Department of Neurosurgery from informed and consenting patient, as approved by the local Research Ethics Boards at the Salpetriere Hospital. Histologic analyses were done by the Department of Neuropathology. Samples were washed with Hanks' balanced salt solution (Invitrogen, France), dissected, sectioned, and enzymatically dissociated with both 5 mg/mL of Trypsin (Sigma-Aldrich, France) and 200 U/mL of DNAse (Sigma-Aldrich, France) for 10 minutes at 37°C. Erythrocytes were lysed using NH_4Cl. Cells were then seeded into T75 flasks at 10000 cells/cm^2. Culture medium (neurosphere medium) consisted of DMEM/F12 (Invitrogen, France) supplemented with 20 ng/mL of epidermal growth factor (EGF), 20 ng/mL of basic fibroblast growth factor (bFGF; both from Sigma-Aldrich, France), B27 (1 : 50; Invitrogen, France), and 1% Penicillin/Streptomycin. Cultures were incubated in 5% CO_2 at 37°C. After 3 days of culture, CD133 Microbead Kit (Miltenyi Biotech, France) was used to isolate CD133$^+$ tumor cell population according to the manufacturer's instructions. Sorted cells were resuspended in neurosphere medium and maintained in 5% CO_2/95% O_2 atmosphere at 37°C. Formed primary spheres were harvested, dissociated into single cells, and plated at the density of 5000 cells/cm^2 in neurosphere medium. Cultures were fed by changing half of the medium every 3 days. Subsphere-forming assay (also called passage) was repeated every 10 days.

2.3.2. Human Endothelial Cell Culture. Purified human umbilical vein endothelial cells (HUVEC) and human umbilical artery endothelial cells (HUAEC) were obtained from Promocell. Immortalized human cerebral microvascular endothelial cells (hCMEC) were obtained from Dr. Pierre Olivier Couraud (Institut Cochin, France). Endothelial cells were cultured with endothelial cell growth medium EGM-2 (Lonza, France) that contains vascular endothelial growth factor (VEGF), basic fibroblast growth factor (bFGF), epidermal growth factor (EGF), insulin growth factor I (IGF-I), hydrocortisone, ascorbic acid, and 2% fetal bovine serum.

2.4. Differentiation Assay of Tumor Spheres. Primary GBM spheres were plated onto sterile multiwell glass slide coated with poly-L-ornithine (Sigma-Aldrich, France) in neurosphere medium lacking EGF and bFGF but supplemented with 10% fetal bovine serum. Cells were fixed after 7 days of differentiation culture with 4% paraformaldehyde for 15 minutes, blocked with PBS/3% BSA for 20 minutes, and immunostained for 1 hour with primary antibodies against nestin (1 : 200; mouse monoclonal IgG1; Santa Cruz Biotechnology, Germany), GFAP (1 : 400; rabbit polyclonal; Dako Cytomation, France), and neuronal class III β-tubulin (Tuj1; 1 : 500; mouse monoclonal IgG2a; Covance, France). After washes, appropriate secondary antibodies were incubated for 1 hour (1 : 1000; Alexa 594 goat anti-mouse IgG1, Alexa 488 goat anti-rabbit and Alexa 594 goat anti-mouse IgG2a from Molecular Probes, Invitrogen, France). DAPI (Sigma-Aldrich, France) was used for nuclei staining. Slides were mounted in antifade medium Fluoromount-G (Interchim, France) and examined under a Zeiss AxioImager.Z1 microscope.

2.5. Endothelial and GBM Cells Cocultures

2.5.1. Noncontact Coculture. Cocultures were prepared on Transwell inserts with 0.4 μm pore size and 6.5 mm diameter (Corning Incorporated, France) placed in 24 well plates. Briefly, GFP-GSC (p3) were seeded at 2×10^4 cells per well in the bottom wells of Transwells, and human endothelial cells were seeded at a ratio of 1 : 1 in the membrane insert wells. Cells were cultured with EGM-2 medium for 5 days. Cell layer fractions were analyzed using Nikon Eclipse TE2000U fluorescence inverted microscope.

2.5.2. Direct Contact Coculture. Dissociated human endothelial cells (5×10^5) and GFP-GSC (5×10^5) were mixed in EGM-2 medium and seeded into T75 flask. After 3 days of culture, cells were dissociated, plated onto sterile multiwell glass slides (1×10^4 on an 8-well slide), and allowed to adhere for 24 hours prior to staining.

2.6. Endothelial Markers Immunofluorescence. After 3–5 days, coculture medium was washed away for 10 minutes with PBS before fixation with 4% paraformaldehyde for 15 minutes. Fixed cells were blocked with PBS/3% BSA for 20 minutes and permeabilized for intracytoplasmic antigen with PBS/0.1% Triton X-100. The following primary antibodies were incubated in blocking solution at room temperature for 1 hour: CD31 (1 : 50; mouse monoclonal IgG1; Dako Cytomation, France), CD105 (1 : 5; mouse monoclonal IgG1; Dako Cytomation, France), VE-cadherin (1 : 50; mouse monoclonal IgG1; eBioscience, France), and vWF (1 : 50; mouse monoclonal IgG1; Dako Cytomation, France). Following 3 washes, Alexa 594 goat anti-mouse IgG (1 : 1000; Molecular Probes, Invitrogen, France) was incubated in blocking solution at room temperature for 1 hour as secondary antibody. Nuclei were stained with DAPI (Sigma-Aldrich, France). Slides were mounted in antifade medium Fluoromount-G (Interchim, France) and examined under a Zeiss AxioImager.Z1 microscope. Fluorescence images were captured using AxioCam MRm camera and analyzed with AxioVision Rel. 4.6 software (Carl Zeiss).

2.7. Lentiviral Infection. GFP and DsRed lentivirus vector construction and virus production were performed by Dr. Philippe Ravassard (Pierre and Marie Curie University) as previously described [20]. Dissociated GSC were infected with GFP-expressing retroviral vector and HUVEC were infected with DsRed-expressing retroviral vector. Labeled cells were selected using a fluorescence-activated cell sorter (FACS Aria, BD Biosciences). The efficiency of transduction was over 80%.

2.8. Cell Sorting. Freshly dissociated cells from GSC-GFP and HUVEC-DsRed cocultures were resuspended in PBS/0.5%BSA/2 mM EDTA solution. Labeled cells were sorted using a fluorescence-activated cell sorter (FACS Aria, BD Biosciences) on the basis of single-cell viability and the presence of double-positive GFP and DsRed fluorescence.

2.9. Reverse Transcription-PCR. Total RNA was extracted from GSC and hCMEC using RNable (Eurobio, France) and verified by electrophoresis on Agilent 2100 Bioanalyzer (Agilent Technologies, France). cDNA was synthesized with 200 units of M-MLV Reverse Transcriptase (Invitrogen, France) in 15 μL of 1x first strand buffer (Promega, France), 2 mmol/L deoxynucleotide triphosphates in the presence of 40 units RNase inhibitor RNasin (Promega), 0.5 μg random primers (Promega), and 1 μg total RNA. Semiquantitative PCR amplifications were done with the following primer sequences: CD31 forward 5′-TCCGGATCTATGACTCAGGG-3′ and reverse 5′-ACAGTTGACCCTCACGATCC-3′; VE-cadherin forward 5′-TCCTCTGCATCCTCACTATCACA-3′ and reverse 5′-GTAAGTGACCAACTGCTCGTGAA-3′; ALAS forward 5′-TGCAGTCCTCAGGGCAGTCT-3′ and reverse 5′-TGGCCCCAACTTCCATCAT-3′ as control. The PCR conditions were as follows: 5 minutes at 94°C for denaturation, followed by 30 seconds at 94°C, 1 min at 60°C, and 1 min 30 sec at 72°C for 35 cycles and 7 min at 72°C for final elongation. The RT-PCR products were electrophoretically analyzed in 1% agarose and visualized by ethidium bromide staining.

3. Results

3.1. Several Intratumoral Endothelial Cells Harbor EGFR Amplification. We analyzed paraffin sections from 10 GBM with *EGFR* amplification, retrieved from our CGHa database [19], using CD31 monoclonal antibody to identify endothelial cells and FISH detection of *EGFR* amplification to identify tumor cells. As shown in Figure 1(a), *EGFR* amplification was detected as double minutes by red hybridization signals in a large proportion of cells present in GBM tissues. CD31 monoclonal antibody stained endothelial cells but not tumor cells (Figure 1(b)). Only 6 out of 10 GBM sections presented dense microvascular network with high morphologic quality after CD31 immunofluorescence and were then subjected to *EGFR* FISH. Endothelial cells carrying *EGFR* amplification, as shown in Figures 1(c) and 1(d), were identified in 3 out of these 6 GBM tumors. This event was episodic as we were able to count less than a hundred of CD31-*EGFR* FISH costained cells per section. Thus, we identified a minority of tumor endothelial cells that could derive from primary GBM cells.

3.2. Glioblastoma Stem Cells Acquire an Endothelial Phenotype When Cocultured with Human Endothelial Cells. We established 3 GBM stem cell primary cultures (GSC-1, GSC-2, and GSC-3) that demonstrated growth into tumor spheres (Figure 2(a)). They were generated from solid primary adult GBMs carrying *EGFR* amplification and showed conservative genomic profile in culture (Figure 2(b)). Undifferentiated tumor spheres immunostained for nestin (a characteristic neural stem cell marker) and revealed multilineage potential (expression of GFAP for astrocytes and TUJ-1 for neurons) in the differentiation assay as shown in Figure 2(d). We next explored the ability of GSC to transdifferentiate into endothelial cells. None of them expressed or stained with CD31 and

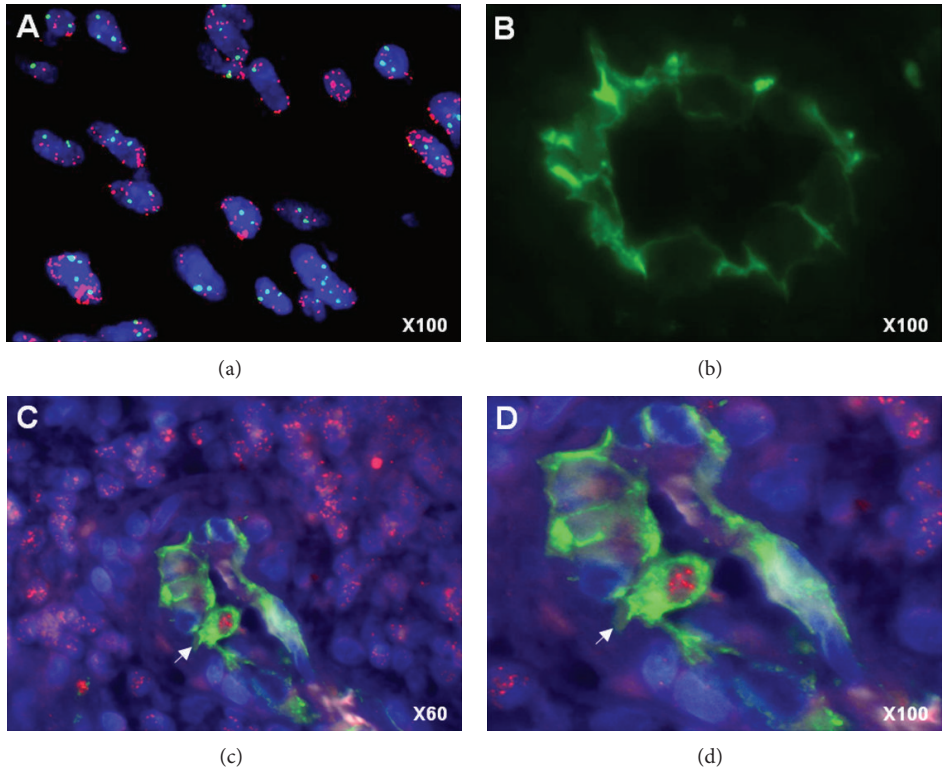

Figure 1: Glioblastoma-derived endothelial cells. (a) Nuclei are stained with DAPI (blue), FISH *EGFR* probe (red) label tumor cells carrying *EGFR* amplification as double minutes (display multiple red signals). (b) Endothelial cells are detected by anti-CD31 immunofluorescence staining. ((c), (d)) A CD31+ (green) endothelial cell (arrow) carrying *EGFR* amplification (multiple red signals) is visible in a GBM microvessel.

VE-cadherin endothelial markers even after growth in EGM-2 medium, known to promote endothelial differentiation [21] (Figure 2(c)).

To test the hypothesis that GSC might need a more specific microenvironment for endothelial conversion, we cocultured GSC-GFP with different human endothelial cells (HUVEC, HUAEC, and hCMEC) allowing cell-cell contact. In this condition, some GSC-GFP exhibited cobblestone morphology and expressed specific endothelial markers including CD31, CD105, VE-cadherin, and vWF (Figure 3(a)). The endothelial-like GSC-GFP were found consistently, but their percentage was variable (0.2% to 1%) depending on the GSC and the endothelial cell types used in direct coculture (Figure 3(b)). However, this conversion was not observed in noncontact coculture, suggesting the implication of cell fusion or cell contact factors.

3.3. Some Glioblastoma Stem Cells Acquire the Endothelial Phenotype through Cell Fusion. The fact that most endothelial-like tumor cells were multinucleated suggested that GSC may acquire endothelial phenotype through cell fusion, rather than cell transdifferentiation. To test this hypothesis, we used DsRed protein-expressing HUVEC to detect cell fusion in fluorescent microscopy. When GSC-GFP were cocultured with HUVEC-DsRed, binucleated cells coexpressing both GFP and DsRed were observed (Figure 4(a), (A)–(C)). GFP+/DsRed+ fused cells maintained CD31 expression (Figure 4(a), (D)), meaning that the endothelial phenotype was dominant. We isolated the GFP+/DsRed+ cells by cell sorting and cultured them in EGM-2 medium to monitor their behavior over time. Most of these cells with heterocaryons were quiescent and died after 5 to 7 days of culture. A small fraction (less than 1%) gave rise to viable mononuclear hybrids expressing the parental GFP and DsRed, as shown in Figure 4(b).

4. Discussion

As early as 1948, several observations suggested that cancer cells are located in the walls of tumor blood vessels and participate in their assembly [22, 23]. This is known as "mosaic vessels" where tumor cells form a part of the vessel surface, while the remaining part is covered by endothelium [24]. But in this case, tumor cells in apparent contact with the lumen do not show an endothelial phenotype. We report here that human GBM contain some tumor endothelial cells carrying the same cytogenetic abnormality as tumor cells. This phenomenon was reported previously in B-cell lymphomas [13], multiple myeloma [14], and neuroblastoma [15]. Since a common precursor can give rise to hematopoietic lineage and endothelial cells in hematopoietic tumors, a common progenitor targeted by neoplastic transformation and sharing specific genetic abnormalities can differentiate into tumor cells or endothelial cells [13, 14]. This hypothesis is not applicable to solid tumors of nonhematopoietic origin. Alternative explanations include tumor microenvironment

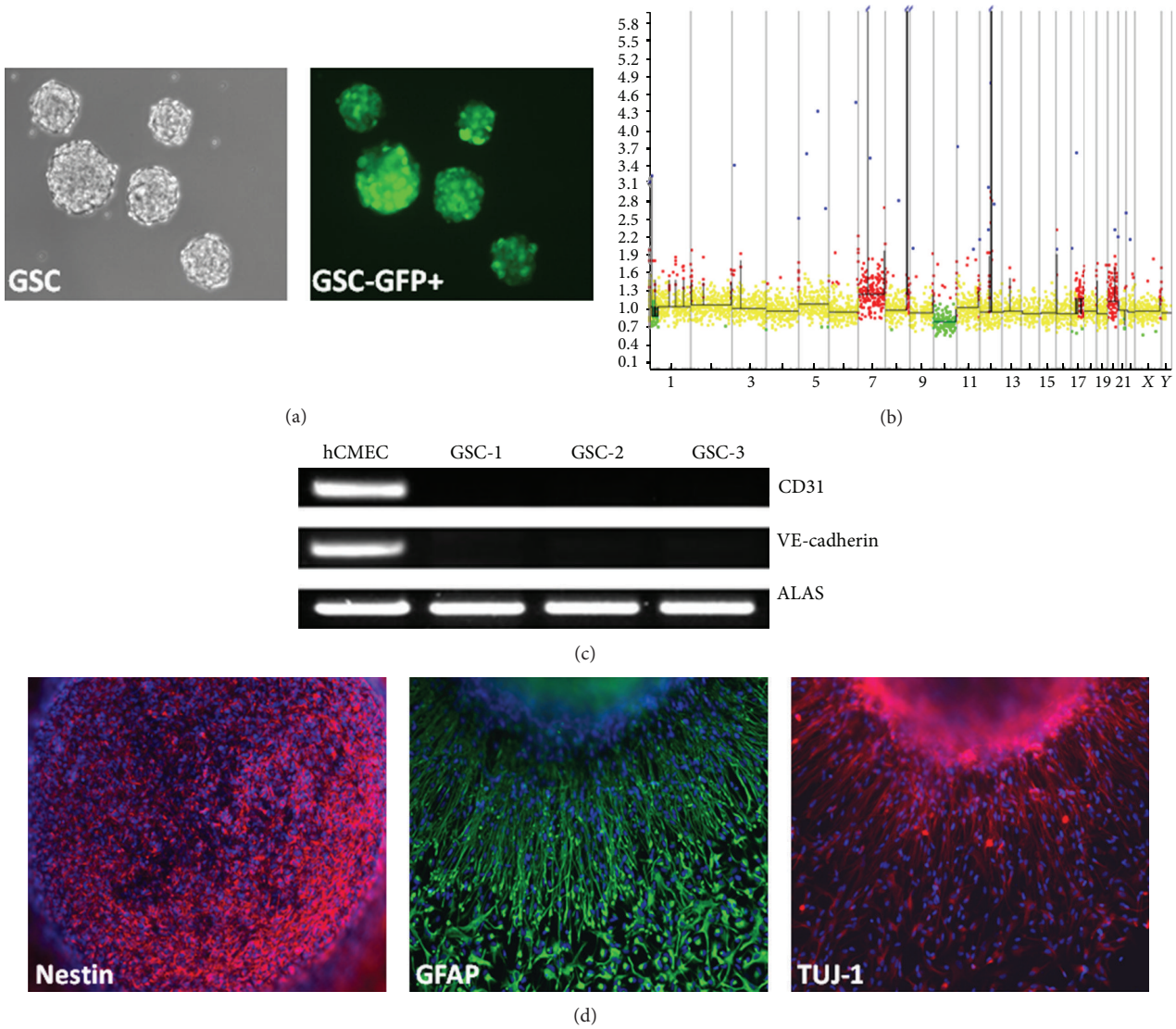

Figure 2: Glioblastoma stem cell characterization. (a) Phase contrast and fluorescent microscopy of GSC-1-GFP+ growing into tumor spheres in neurosphere medium (magnification ×10). (b) Comparative genomic hybridization array (CGHa) of GSC-1 demonstrating tumor genomic alterations. Each BAC (bacterial artificial chromosome) spotted on the comparative genomic hybridization array is represented by a dot. BACs are ordered on the *x*-axis according to their position in the genome. For each chromosome, the telomere of the short arm is on the left and the telomere of the long arm is on the right. The *y*-axis corresponds to fluorescence ratio. Yellow, green, and red indicate, respectively, genomic copy number normal, loss, and gain. Genetic alteration includes complete chromosome 10 loss (green) and gain of chromosome 7 with *EGFR* amplification (arrow). (c) RT-PCR analysis showing specific expression of endothelial markers CD31 and VE-cadherin by hCMEC and not by GSC-1, GSC-2, and GSC-3 after differentiation in EGM-2 medium. ALAS is used as control. (d) Immunostaining of tumor sphere cells for neural stem cell marker (nestin) at the beginning of the differentiation assay, then astrocytic (GFAP) and neuronal (TUJ-1) markers by the differentiated cells around a tumor sphere at day 7 (magnification ×10).

[25, 26], tumor cell transdifferentiation, and cell fusion [27]. Our data strongly suggest that GBM stem cell acquires endothelial phenotype through cell fusion and participates in microvascular structures.

This is consistent with a recent study in which human glioma lines marked with DsRed protein were grafted in eGFP-expressing NOD/Scid mouse to study tumor-host interactions [28]. Using fluorescence-activated cell sorting (FACS), this model is allowed to completely separate host cells from tumor cells and to detect double-positive cells, possibly arising from cell fusion events. Furthermore, CD31 expression was found in 0.3% of separated tumor cells when phenotyped [28]. In normal brain, neural stem cells exist in vascular niches where endothelial cells provide direct cell contacts and secreted factors that regulate neural stem cell function [29, 30]. Similarly, GBM stem cells are maintained within vascular niches that mimic the neural stem cell niche [31]. Nestin+/CD133+ cells within sections of human GBM

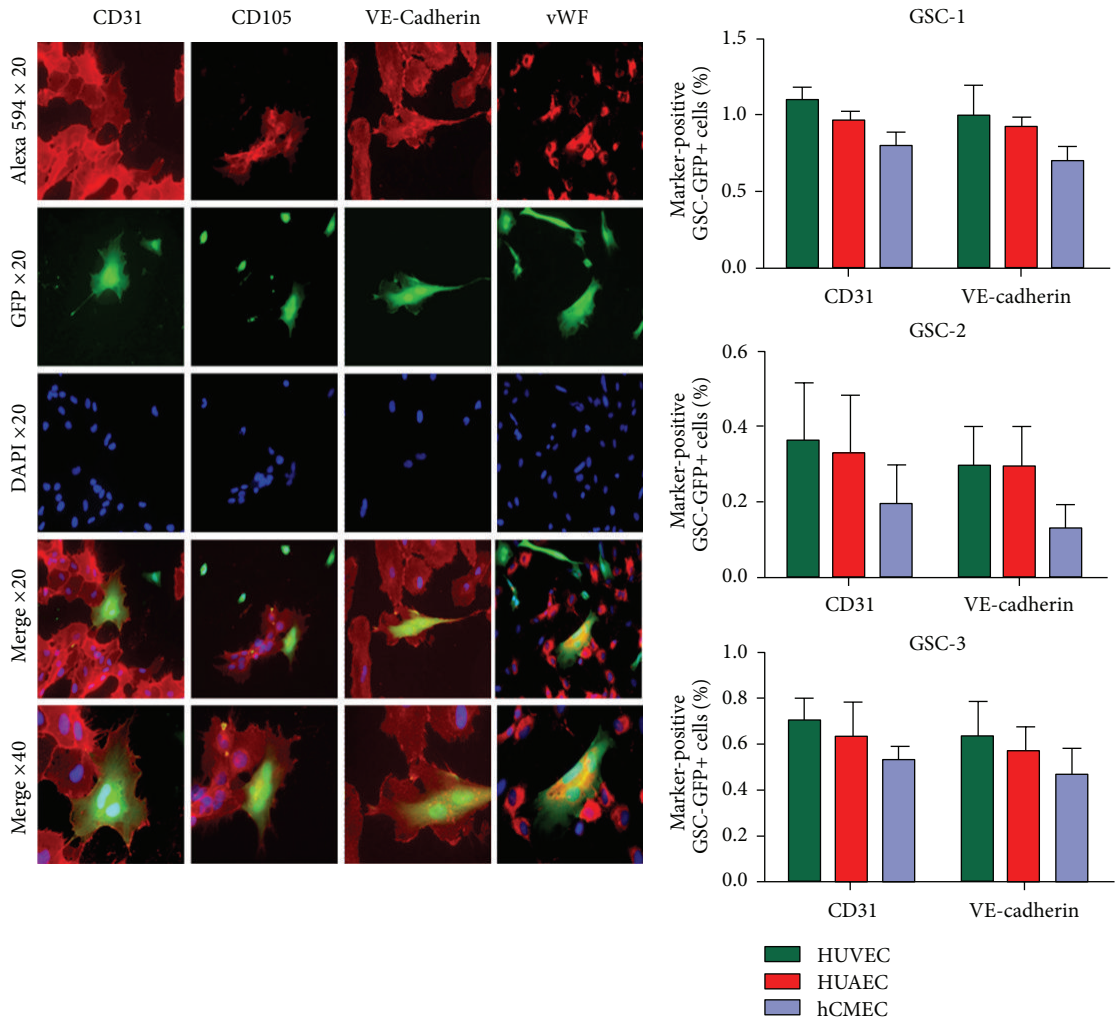

FIGURE 3: A subset of glioblastoma stem cells acquires an endothelial phenotype. (a) When GSC-GFP were cocultured with human endothelial cells, several multinucleated and cobblestone GSC-GFP expressing CD31, CD105, VE-cadherin, and vWF were observed (b). The percentage of GSC-GFP expressing CD31 and VE-cadherin obtained in coculture with HUVEC, HUAEC, and hCMEC is indicated for GSC-1, GSC-2, and GSC-3.

are located in close proximity to tumor capillaries [31]. This organization can favor cell fusion by facilitating cell contact between GBM stem cells and endothelial cells.

Cell fusion has been debated in adult stem cells plasticity. Several reports revealed the ability for stem cells to change fate through cell fusion rather than cell transdifferentiation. New hybrids resulting from nuclear fusion can generate mononuclear differentiated progeny that exhibit both parental phenotypes [18, 32–35]. These findings raise the possibility that cell fusion has undiscovered functions which can promote disease, especially cancer. The idea that cell fusion contributes to cancer progression was introduced almost 100 years ago with a proposal that malignancy is a consequence of hybridization between leukocytes and somatic cells [36]. Sixty years later, this idea was expanded by proposing that hybridization of tumor cells with lymphocytes results in metastatic cells [37] and that cell fusion promotes the phenotypic and genotypic diversity of tumors [38]. The best defended theory is cancer cell fusion with macrophages or other migratory bone marrow-derived cells which provides a unifying explanation for metastasis [39]. Although host cell-cancer cell fusion has been demonstrated and well documented in animals [40], there is as yet far less information on human cancer. A few human cases have recently been reported [41–45], but it is unclear whether the scarcity of reports on cell fusion in human tumors is due to rarity of this event or to a difficulty to detect it.

In addition to cell fusion, we cannot exclude that transdifferentiation of GBM stem cells into endothelial cells may exist. Conversion from GBM to endothelial phenotype was not observed in noncontact coculture, suggesting either cell fusion or cell-cell contact mediated transdifferentiation. Recently two recent papers showed that transdifferentiation of GBM stem cells into endothelial cells does exist in GBM (p7). Notch pathway is involved in this mechanism [46–48].

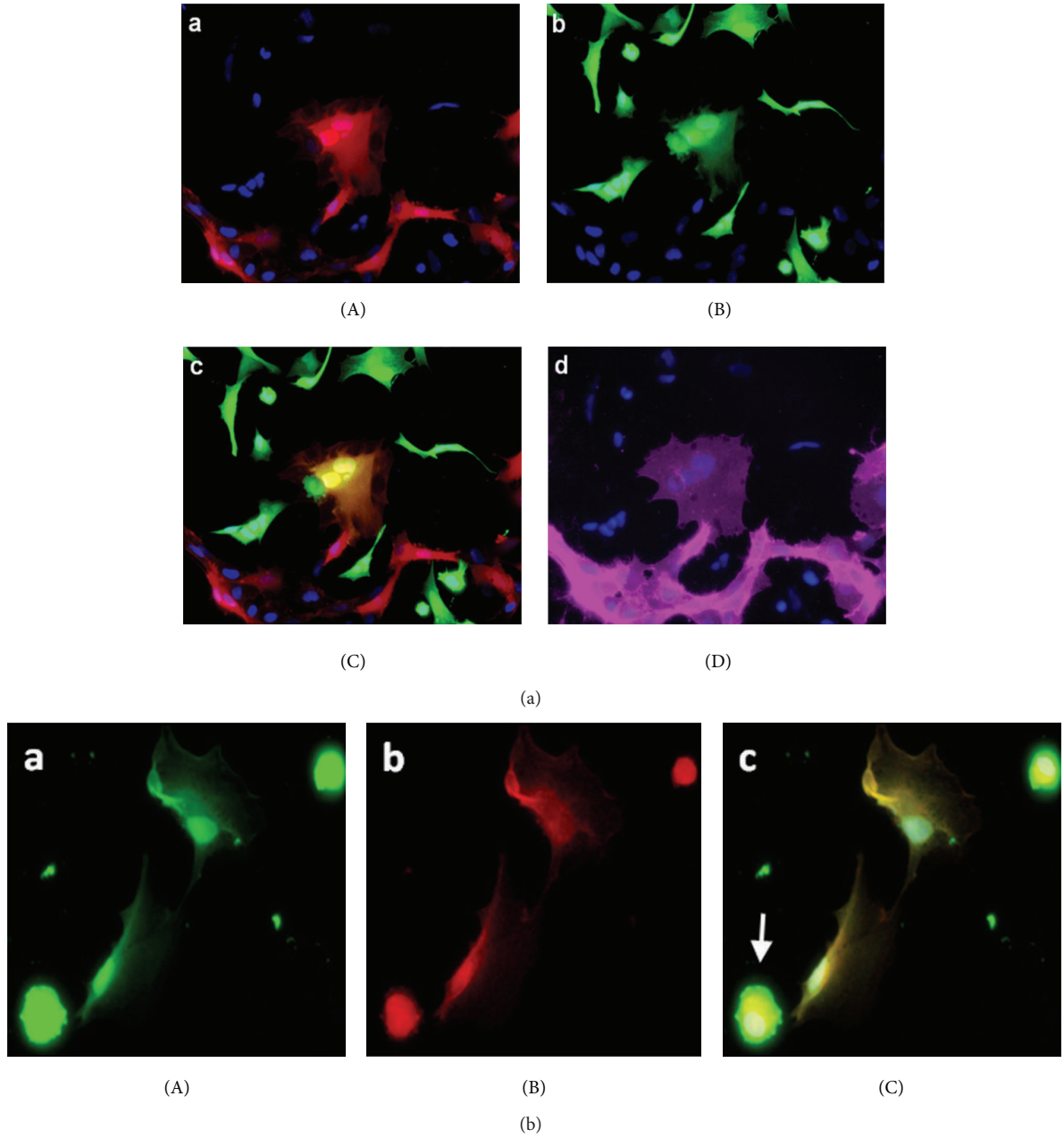

Figure 4: Glioblastoma stem cell fusion with endothelial cells. (a) When GSC-GFP were cocultured with HUVEC-DsRed, we observed binucleated cell expressing both DsRed (A) and GFP (B) (merged in (C)) corresponding to hybrid cell and exhibiting endothelial phenotype as shown by CD31 immunostaining (D). (b) After hybrid cell selection by cell sorting, mononuclear hybrids expressing parental GFP (A) and DsRed (B) were observed (merged in (C)). Apoptotic body of died fused cell (arrow).

Considering that cell fusion can be linked to several fundamental features of cancer, more investigations are needed to clarify this emergent concept of "hidden enemy" in cancer pathology. In addition, the presence of these hybrid cells in GBM endothelium supports new therapeutic approaches, such as intravascular targeted strategy directed against the EGFRVIII mutant, a specific antigen expressed by 20–30% of GBM [49].

Conflict of Interests

The authors declare that there is no conflict of interests regarding the publication of this paper.

Acknowledgments

This work is supported by a Grant from the Institut National du Cancer (PL 046) and the Institut de France (Fondation

Energie). S. El Hallani and C. Colin were supported by the Ligue Nationale Contre le Cancer.

References

[1] D. N. Louis, H. Ohgaki, O. D. Wiestler et al., "The 2007 WHO classification of tumours of the central nervous system," *Acta Neuropathologica*, vol. 114, no. 2, pp. 97–109, 2007.

[2] J. J. Vredenburgh, A. Desjardins, J. E. Herndon II et al., "Phase II trial of bevacizumab and irinotecan in recurrent malignant glioma," *Clinical Cancer Research*, vol. 13, no. 4, pp. 1253–1259, 2007.

[3] T. N. Kreisl, L. Kim, K. Moore et al., "Phase II trial of single-agent bevacizumab followed by bevacizumab plus irinotecan at tumor progression in recurrent glioblastoma," *Journal of Clinical Oncology*, vol. 27, no. 5, pp. 740–745, 2009.

[4] D. M. McDonald and P. L. Choyke, "Imaging of angiogenesis: from microscope to clinic," *Nature Medicine*, vol. 9, no. 6, pp. 713–725, 2003.

[5] F. Mollica, R. K. Jain, and P. A. Netti, "A model for temporal heterogeneities of tumor blood flow," *Microvascular Research*, vol. 65, no. 1, pp. 56–60, 2003.

[6] D. M. McDonald and P. Baluk, "Significance of blood vessel leakiness in cancer," *Cancer Research*, vol. 62, no. 18, pp. 5381–5385, 2002.

[7] P. Baluk, S. Morikawa, A. Haskell, M. Mancuso, and D. M. McDonald, "Abnormalities of basement membrane on blood vessels and endothelial sprouts in tumors," *The American Journal of Pathology*, vol. 163, no. 5, pp. 1801–1815, 2003.

[8] B. St. Croix, C. Rago, V. Velculescu et al., "Genes expressed in human tumor endothelium," *Science*, vol. 289, no. 5482, pp. 1197–1202, 2000.

[9] B. Bussolati, I. Deambrosis, S. Russo, M. C. Deregibus, and G. Camussi, "Altered angiogenesis and survival in human tumor-derived endothelial cells," *The FASEB Journal*, vol. 17, no. 9, pp. 1159–1161, 2003.

[10] K. Hida and M. Klagsbrun, "A new perspective on tumor endothelial cells: unexpected chromosome and centrosome abnormalities," *Cancer Research*, vol. 65, no. 7, pp. 2507–2510, 2005.

[11] C. Grange, B. Bussolati, S. Bruno, V. Fonsato, A. Sapino, and G. Camussi, "Isolation and characterization of human breast tumor-derived endothelial cells," *Oncology Reports*, vol. 15, no. 2, pp. 381–386, 2006.

[12] K. Hida, Y. Hida, D. N. Amin et al., "Tumor-associated endothelial cells with cytogenetic abnormalities," *Cancer Research*, vol. 64, no. 22, pp. 8249–8255, 2004.

[13] B. Streubel, A. Chott, D. Huber et al., "Lymphoma-specific genetic aberrations in microvascular endothelial cells in B-cell lymphomas," *The New England Journal of Medicine*, vol. 351, no. 3, pp. 250–259, 2004.

[14] G. M. Rigolin, C. Fraulini, M. Ciccone et al., "Neoplastic circulating endothelial cells in multiple myeloma with 13q14 deletion," *Blood*, vol. 107, no. 6, pp. 2531–2535, 2006.

[15] A. Pezzolo, F. Parodi, M. V. Corrias, R. Cinti, C. Gambini, and V. Pistoia, "Tumor origin of endothelial cells in human neuroblastoma," *Journal of Clinical Oncology*, vol. 25, no. 4, pp. 376–383, 2007.

[16] D. Bonnet and J. E. Dick, "Human acute myeloid leukemia is organized as a hierarchy that originates from a primitive hematopoietic cell," *Nature Medicine*, vol. 3, no. 7, pp. 730–737, 1997.

[17] S. K. Singh, I. D. Clarke, M. Terasaki et al., "Identification of a cancer stem cell in human brain tumors," *Cancer Research*, vol. 63, no. 18, pp. 5821–5828, 2003.

[18] N. Terada, T. Hamazaki, M. Oka et al., "Bone marrow cells adopt the phenotype of other cells by spontaneous cell fusion," *Nature*, vol. 416, no. 6880, pp. 542–545, 2002.

[19] A. Idbaih, Y. Marie, C. Lucchesi et al., "BAC array CGH distinguishes mutually exclusive alterations that define clinicogenetic subtypes of gliomas," *International Journal of Cancer*, vol. 122, no. 8, pp. 1778–1786, 2008.

[20] H. A. Russ, Y. Bar, P. Ravassard, and S. Efrat, "In vitro proliferation of cells derived from adult human β-cells revealed by cell-lineage tracing," *Diabetes*, vol. 57, no. 6, pp. 1575–1583, 2008.

[21] S. Heydarkhan-Hagvall, K. Schenke-Layland, J. Q. Yang et al., "Human adipose stem cells: a potential cell source for cardiovascular tissue engineering," *Cells Tissues Organs*, vol. 187, no. 4, pp. 263–274, 2008.

[22] R. A. Willis, *Pathology of Tumour*, Butterworth Heinemann, Oxford, UK, 1948.

[23] F. Hammersen, B. Endrich, and K. Messmer, "The fine structure of tumor blood vessels. I. Participation of non-endothelial cells in tumor angiogenesis," *International Journal of Microcirculation, Clinical and Experimental*, vol. 4, no. 1, pp. 31–43, 1985.

[24] Y. S. Chang, E. di Tomaso, D. M. McDonald, R. Jones, R. K. Jain, and L. L. Munn, "Mosaic blood vessels in tumors: frequency of cancer cells in contact with flowing blood," *Proceedings of the National Academy of Sciences of the United States of America*, vol. 97, no. 26, pp. 14608–14613, 2000.

[25] B. Vogelstein and K. W. Kinzler, "Cancer genes and the pathways they control," *Nature Medicine*, vol. 10, no. 8, pp. 789–799, 2004.

[26] N. Ferrara and R. S. Kerbel, "Angiogenesis as a therapeutic target," *Nature*, vol. 438, no. 7070, pp. 967–974, 2005.

[27] K. Mortensen, J. Lichtenberg, P. D. Thomsen, and L.-I. Larsson, "Spontaneous fusion between cancer cells and endothelial cells," *Cellular and Molecular Life Sciences*, vol. 61, no. 16, pp. 2125–2131, 2004.

[28] S. P. Niclou, C. Danzeisen, H. P. Eikesdal et al., "A novel eGFP-expressing immunodeficient mouse model to study tumor-host interactions," *The FASEB Journal*, vol. 22, no. 9, pp. 3120–3128, 2008.

[29] T. D. Palmer, A. R. Willhoite, and F. H. Gage, "Vascular niche for adult hippocampal neurogenesis," *Journal of Comparative Neurology*, vol. 425, no. 4, pp. 479–494, 2000.

[30] Q. Shen, S. K. Goderie, L. Jin et al., "Endothelial cells stimulate self-renewal and expand neurogenesis of neural stem cells," *Science*, vol. 304, no. 5675, pp. 1338–1340, 2004.

[31] C. Calabrese, H. Poppleton, M. Kocak et al., "A perivascular niche for brain tumor stem cells," *Cancer Cell*, vol. 11, no. 1, pp. 69–82, 2007.

[32] Q.-L. Ying, J. Nichols, E. P. Evans, and A. G. Smith, "Changing potency by spontaneous fusion," *Nature*, vol. 416, no. 6880, pp. 545–548, 2002.

[33] J. L. Spees, S. D. Olson, J. Ylostalo et al., "Differentiation, cell fusion, and nuclear fusion during ex vivo repair of epithelium by human adult stem cells from bone marrow stroma," *Proceedings of the National Academy of Sciences of the United States of America*, vol. 100, no. 5, pp. 2397–2402, 2003.

[34] G. Vassilopoulos, P.-R. Wang, and D. W. Russell, "Transplanted bone marrow regenerates liver by cell fusion," *Nature*, vol. 422, no. 6934, pp. 901–904, 2003.

[35] X. Wang, H. Willenbring, Y. Akkari et al., "Cell fusion is the principal source of bone-marrow-derived hepatocytes," *Nature*, vol. 422, no. 6934, pp. 897–901, 2003.

[36] O. Aichel, *Vorträge und Aufsätze über Entvickelungsmechanik der Organismen*, chapter XIII, Wilhelm Engelmann, Leipzig, Germany, 1911.

[37] L. B. Mekler, "Hybridization of transformed cells with lymphocytes as 1 of the probable causes of the progression leading to the development of metastatic malignant cells," *Vestnik Akademii Meditsinskikh Nauk SSSR*, vol. 26, no. 8, pp. 80–89, 1971.

[38] T. F. C. S. Warner, "Cell hybridization: an explanation for the phenotypic diversity of certain tumours," *Medical Hypotheses*, vol. 1, no. 1, pp. 51–57, 1975.

[39] J. M. Pawelek and A. K. Chakraborty, "Fusion of tumour cells with bone marrow-derived cells: a unifying explanation for metastasis," *Nature Reviews Cancer*, vol. 8, no. 5, pp. 377–386, 2008.

[40] D. Duelli and Y. Lazebnik, "Cell fusion: a hidden enemy?" *Cancer Cell*, vol. 3, no. 5, pp. 445–448, 2003.

[41] T. L. Andersen, P. Boissy, T. E. Sondergaard et al., "Osteoclast nuclei of myeloma patients show chromosome translocations specific for the myeloma cell clone: a new type of cancer-host partnership?" *The Journal of Pathology*, vol. 211, no. 1, pp. 10–17, 2007.

[42] A. Chakraborty, R. Lazova, S. Davies et al., "Donor DNA in a renal cell carcinoma metastasis from a bone marrow transplant recipient," *Bone Marrow Transplantation*, vol. 34, no. 2, pp. 183–186, 2004.

[43] Y. Yilmaz, R. Lazova, M. Qumsiyeh, D. Cooper, and J. Pawelek, "Donor Y chromosome in renal carcinoma cells of a female BMT recipient: visualization of putative BMT—tumor hybrids by FISH," *Bone Marrow Transplantation*, vol. 35, no. 10, pp. 1021–1024, 2005.

[44] C. R. Cogle, N. D. Theise, D. Fu et al., "Bone marrow contributes to epithelial cancers in mice and humans as developmental mimicry," *Stem Cells*, vol. 25, no. 8, pp. 1881–1887, 2007.

[45] I. Avital, A. L. Moreira, D. S. Klimstra et al., "Donor-derived human bone marrow cells contribute to solid organ cancers developing after bone marrow transplantation," *Stem Cells*, vol. 25, no. 11, pp. 2903–2909, 2007.

[46] L. Ricci-Vitiani, R. Pallini, M. Biffoni et al., "Tumour vascularization via endothelial differentiation of glioblastoma stem-like cells," *Nature*, vol. 468, no. 7325, pp. 824–828, 2010.

[47] R. Wang, K. Chadalavada, J. Wilshire et al., "Glioblastoma stem-like cells give rise to tumour endothelium," *Nature*, vol. 468, no. 7325, pp. 829–835, 2010.

[48] Y. Soda, T. Marumoto, D. Friedmann-Morvinski et al., "Transdifferentiation of glioblastoma cells into vascular endothelial cells," *Proceedings of the National Academy of Sciences of the United States of America*, vol. 108, no. 11, pp. 4274–4280, 2011.

[49] H. K. Gan, A. H. Kaye, and R. B. Luwor, "The EGFRvIII variant in glioblastoma multiforme," *Journal of Clinical Neuroscience*, vol. 16, no. 6, pp. 748–754, 2009.

Hindawi Publishing Corporation
BioMed Research International
Volume 2014, Article ID 232561, 8 pages
http://dx.doi.org/10.1155/2014/232561

Clinical Study

5-Aminolevulinic Acid Fluorescence in High Grade Glioma Surgery: Surgical Outcome, Intraoperative Findings, and Fluorescence Patterns

Alessandro Della Puppa,[1] Pietro Ciccarino,[1] Giuseppe Lombardi,[2] Giuseppe Rolma,[3] Diego Cecchin,[4] and Marta Rossetto[1]

[1] *Department of Neurosurgery, Padua University Hospital, Azienda Ospedaliera di Padova, Via Giustiniani 2, 35128 Padova, Italy*
[2] *Department of Oncology, IOV IRCCS Oncology Institute of Padua, Via Gattamelata 64, 35128 Padova, Italy*
[3] *Neuroradiology Unit, Padua University Hospital, Via Giustiniani 2, Padua, 35128 Padova, Italy*
[4] *Department of Medicine (DIMED), Nuclear Medicine Service, University of Padua, Via Giustiniani 2, 35128 Padova, Italy*

Correspondence should be addressed to Marta Rossetto; marta_rossetto@libero.it

Received 11 February 2014; Accepted 10 March 2014; Published 8 April 2014

Academic Editor: Anna Luisa Di Stefano

Background. 5-Aminolevulinic acid (5-ALA) fluorescence is a validated technique for resection of high grade gliomas (HGG); the aim of this study was to evaluate the surgical outcome and the intraoperative findings in a consecutive series of patients. *Methods*. Clinical and surgical data from patients affected by HGG who underwent surgery guided by 5-ALA fluorescence at our Department between June 2011 and February 2014 were retrospectively evaluated. Surgical outcome was evaluated by assessing the resection rate as gross total resection (GTR) > 98% and GTR > 90%. We finally stratified data for recurrent surgery, tumor location, tumor size, and tumor grade (IV versus III grade sec. WHO). *Results*. 94 patients were finally enrolled. Overall GTR > 98% and GTR > 90% was achieved in 93% and 100% of patients. Extent of resection (GTR > 98%) was dependent on tumor location, tumor grade ($P < 0.05$), and tumor size ($P < 0.05$). In 43% of patients the boundaries of fluorescent tissue exceeded those of tumoral tissue detected by neuronavigation, more frequently in larger (57%) ($P < 0.01$) and recurrent (60%) tumors. *Conclusions*. 5-ALA fluorescence in HGG surgery enables a GTR in 100% of cases even if selection of patients remains a main bias. Recurrent surgery, and location, size, and tumor grade can predict both the surgical outcome and the intraoperative findings.

1. Introduction

High grade gliomas are extremely aggressive lesions and represent the most common primary malignant brain tumors with an annual incidence of 5.26/100.000/year. Despite several efforts on surgical techniques, oncological therapies, and molecular understandings prognosis is poor. Among factors affecting patients' outcome, extent of surgical removal and functional preservation have been proved to have a great impact; therefore, continuous refinements of surgical approaches and techniques are investigated [1–3].

The extent of tumor resection (EOR) is proved to be an important prognostic factor in HGG. Therefore, several neurosurgeons tried to quantify the EOR through a threshold of resection correlated with a significant improvement in overall survival. One of the most comprehensive series set this threshold at 95–100% rate of resection [4] with a median survival of 13 months compared with 8.8 months in patients with a EOR < 98%. However, Sanai and colleagues clearly demonstrated that in selected newly diagnosed HGG patient OS begins to benefit from an EOR ≥ 78% and that this trend of improvement increases at highest levels of resection [5].

The role of surgery on recurrent HGG is still debated. However, in recurrent GBMs, some authors showed a more favorable response to chemotherapy in patients harboring a residual disease <10 cm^3 [6]. Moreover, a great association between survival and recurrence with EOR of 70% and residual volume (RV) of 5 cm^3 is proved to occur as recently demonstrated in a large series of Johns Hopkins' group [7].

5-Aminolevulinic acid (5-ALA) is a natural precursor of haemoglobin that produces synthesis and accumulation of fluorescent porphyrins, particularly PPIX. The concentration of PPIX is elevated in several tumoral tissues such as HGG, and in central nervous system its concentration is significantly higher in malignant tissue than in normal brain. PPIX fluorescence can be visualized through a modified surgical microscope able to shift from a white light to a violet-blue illumination using a dielectric 440 nm short-pass filter into the illumination path. Intraoperatively, under white light, no fluorescence is visible while shifting at violet-blue illumination tumor tissue fluorescing and three main patterns can be distinguished: necrotic area that usually displays no or only inhomogeneous red fluorescence, solid viable tumor showing bright fluorescence intensity, and the transitional area of infiltrating and invasive brain tissue appearing as "vague" fluorescence. From a pathological point of view, these three different fluorescence patterns have been studied and correlated with tissue specimens. In solid tumor and invasive areas, 5-ALA showed a positive predictive value of 100% and 97%, respectively, while in normal tissue a negative predictive value of 67% [8] was found.

In 2006, Stummer and colleagues published the first phase III trial on resection and survival in 5-ALA-assisted glioma surgery. Their randomized controlled multicentric study evidenced that a total removal of the tumor was achieved in 65% of patients assigned 5-ALA compared with 36% in patients who underwent traditional surgery [9]. Actually, level 2b evidence shows that 5-ALA-assisted surgery is more effective than conventional surgery in increasing EOR and prolonging overall survival in GBM [10].

2. Materials and Methods

2.1. Patient Population. We screened for surgery with 5-ALA all patients consulting our unit whose MRI scans were suggestive of HGG, from June 2011 to February 2014. Resectability was decided over T1-weighted gadolinium Magnetic Resonance Imaging (T1-GdMRI). Inclusion criteria for enrolment were MRI suggestive for high grade glioma (HGG) both newly diagnosed and recurrent ones, gross total surgical removal (GTR) (i.e., >90%) deemed possible at preoperative assessment, and plan for surgery guided by 5-ALA fluorescence with the assistance of MRI neuronavigation (T1Gd). Tumor location was analyzed on contrast-enhanced T1 sequences and the proximity to eloquent structures was assessed with diffusion tensor and functional Magnetic Resonance Imaging (MRI) images. According to previous authors [4, 13, 14] were regarded as eloquent areas: primary motor and sensory cortex, the basal ganglia, thalamus, hypothalamus, cerebral peduncles, the brainstem, the dentate nucleus, the presumed language areas (identified by fMRI), the primary visual cortex, and essential white matter tracts linked to these eloquent regions (identified by DTI). Patients were divided into "patients with tumor in eloquent areas" when tumor was into or close (less than 10 mm) to eloquent structures and "patients with tumor in noneloquent areas" when tumor was more far than 10 mm from eloquent areas. Tumor location and extent of resection were defined by an expert neuroradiologist based on pre- and postoperative Magnetic Resonance Imaging (MRI). Informed consent was obtained from all patients. Tumor grade was histologically confirmed in all cases.

2.2. Surgical Strategy. Patients were administered orally 20 mg/kg 5-aminolevulinic acid 2–4 h before surgery, as previously described [15]. All operations were performed with a Zeiss Pentero microscope equipped with a fluorescent 400 nm UV light and filters. All patients were operated on in a MRI neuronavigational setting. Diffusion tensor and functional Magnetic Resonance Imaging (MRI) were performed to visualize functional cortical areas and cerebral fiber tracts, and subsequently loaded in the neuronavigational system according to tumor location. Microsurgical removal was started using standard white xenon light and switched to the violet-blue excitation light whenever tumor boundaries were visually indistinct from healthy brain tissue. At the end of resection, the cavity was systematically checked in the violet-blue light mode for any residual tumor. In the cases in which resection was stopped and residual fluorescent tissue was still present in the boundaries, the fluorescence intensity was recorded (as bright or vague fluorescence) [15]. In all cases, at the end of resection neuronavigational record of surgical boundaries was carried out. With regard to the functional area involved, intraoperative monitoring was performed either in asleep or in awake surgery, depending on both patient and tumor features. A standard intraoperative surgical and neurophysiological protocol was followed for patients with tumor in eloquent areas. Such protocol entailed MRI neuronavigation and continuous electroencephalography (EEG), electrocorticography (ECoG), and multichannel electromyography recordings. Monitoring included tracking of Motor Evoked Potentials (MEPs), sensory evoked potentials (SEPs), and cortical and subcortical stimulation as previously reported [16]. Two criteria were followed to stop resection: first, the lack of tumoral tissue at white light and of fluorescent tissue at final blue light control. The second one was the localization of either a functional area or a cortical tract during fluorescent tissue resection. Pre- and postoperative MRI formal reports were reevaluated by a neuroradiologist. In order to compare 5-ALA fluorescence and neuronavigation data with regard to identification of surgical boundaries, pre- and postoperative GdT1 MRI images, and intraoperative neuronavigation data at the end of resection, were finally compared by an expert neuroradiologist.

2.3. Research Variables. Our study focused on defining the extent of resection and intraoperative fluorescence patterns in patients affected by HGG who underwent surgery guided by 5-ALA fluorescence and assisted by MRI neuronavigation and neurophysiological monitoring. The assessment of the extent of resection was carried out by MRI studies with a 1.5 T GE scanner. According to previous authors [4, 17, 18] extent of resection was reported as gross total resection more than 98% (GTR > 98%), and gross total Resection more than 90% (GTR > 90%). Subtotal resection was a resection less than

90% with a residual volume more than 10%. All MRI studies included Fluid Attenuated Inversion Recovery, T2-weighted and T1-weighted, before and after administration of gadolinium (Gd) contrast medium (gadopentetate dimeglumine). A volumetric Gd T1-weighted MRI study was finally performed. Control MRI was performed within 72 h from surgery, in order to evaluate degree of removal. The extent of resection of enhancing tissue was carefully measured by an expert neuroradiologist, comparing volumetric postoperative magnetic resonance imaging (MRI) with volumetric preoperative MRI.

Intraoperative fluorescence data were registered and retrospectively evaluated on video records. In particular, the different fluorescent nuances and the pattern of fluorescence were assessed according to previous reports [8, 19].

The extent of resection of enhancing tissue was carefully measured by an expert neuroradiologist, comparing volumetric postoperative magnetic resonance imaging (MRI) with volumetric preoperative MRI.

In order to compare 5-ALA fluorescence and neuronavigation data with regard to identification of surgical boundaries, pre- and postoperative GdT1 MRI images and intraoperative neuronavigation data at the end of resection were finally compared by an expert neuroradiologist.

Our study finally stratified the data for specific subgroups of patients. With this purpose, recurrent surgery, tumor location (eloquent versus noneloquent), tumor size (< versus > or = 9 cm^3), and tumor grade (IV versus III WHO grade) [20] were analyzed. We calculated the median tumoral volume through a 3D volumetric measurement of preoperative MR imaging studies by the modified ellipsoid volume equation as follows: $(A \times B \times C)/2$, where A, B, and C represent the 3 largest orthogonal diameters of the lesion.

2.4. Statistical Analysis. Statistical analysis to compare the categorical variables was performed via χ^2 test in two-way tables. If any value was <10 Fisher's exact test was used (2-sided). A P value <0.05 was considered significant.

3. Results

Ninety-four patients (53 males and 41 females) were enrolled (Table 1). The median age was 58 years (range 27–79 years). 61 patients were affected by newly diagnosed gliomas, while 33 patients had second surgery for recurrent glioma.

Histopathological results showed 81 patients harbored glioblastomas (WHO Grade IV) and 13 grade III gliomas (astrocytoma, oligoastrocytoma, and oligodendroglioma WHO Grade III). 43 patients presented a tumor growing in an "eloquent area" whilst 51 patients did not. Surgery was assisted by neurophysiological monitoring in all cases of eloquent area tumors (43/43) and in 45/51 (88%) of noneloquent area tumors.

3.1. Extent of Resection. Extent of resection data is summarized in Table 2. Patients were divided into two groups according to extent of resection. Gross total removal > 90% was achieved in all (94/94) patients enrolled in the study. Gross total removal >98% was achieved in 88 patients (93%).

Table 1: Clinical and surgical characteristics of patients.

Parameter	No. (%)
Number of patients	94
Male/female	53/41
Mean age	58
Newly diagnosed HGG	61
Recurrent HGG	33
Tumor grade	
GBM	81
Grade III glioma	13
Astrocytoma	7
Oligoastrocytoma	3
Oligodendroglioma	3
Tumor location	
Eloquent area	43
Noneloquent area	51
Monitoring assisted surgery	
Eloquent area tumors	43 (100%)
Noneloquent area tumors	45 (88%)

In particular, GTR > 98% was achieved in 39/43 (90%) of patients with tumor located in eloquent areas and in 49/51 (96%) of patients with tumor located in noneloquent areas ($P = 0.407$) (Figure 1), in 57/61 (93%) and in 31/33 (94%) of patients affected by newly diagnosed and recurrent glioma, in 78/81 (96%) and in 10/13 (79%) of patients affected by a grade IV and grade III glioma ($P = 0.018$), in 45/51 (88%) and in 43/43 (100%) of patients affected by a larger (≥9 cm^3) and smaller (<9 cm^3) tumor, respectively ($P = 0.029$).

As far as tumors located in eloquent areas are concerned, in 39 out of 43 patients the resection was stopped because a functional area or cortical tract was identified or because MEP amplitudes were reduced in an area where fluorescent tumor cells were still visible (Figure 2). In all these patients, bright fluorescent tissue was detected at final control.

3.2. Fluorescent Data. All tumours presented fluorescent under blue light. Bright fluorescence was detected in all patients, whilst vague fluorescence was reported in only 81/94 (86%) of cases.

The 3-layer model of fluorescence was reported in 63% of cases (60/94): in 54/61 (88%) and in 6/33 (18%) of patients affected by newly diagnosed and recurrent glioma ($P < 0.001$), in 60/81 (74%) and in 0/13 (0%) of patients affected by a grade IV and grade III glioma ($P < 0.001$), and in 32/51 (62%) and in 28/43 (65%) of patients affected by a larger (≥9 cm^3) and smaller (<9 cm^3) tumor, respectively.

3.3. Tumour Boundaries. The tumor boundaries detected by neuronavigation differed by fluorescence data in 43% of cases (41/94). In all 41 patients fluorescent tissue was detected over boundaries identified by neuronavigation. Conversely, neuronavigation never showed tumor tissue in not fluorescent areas. The divergence between neuronavigation and 5-ALA fluorescence was reported in 21/61 (34%) and in 20/33 (60%)

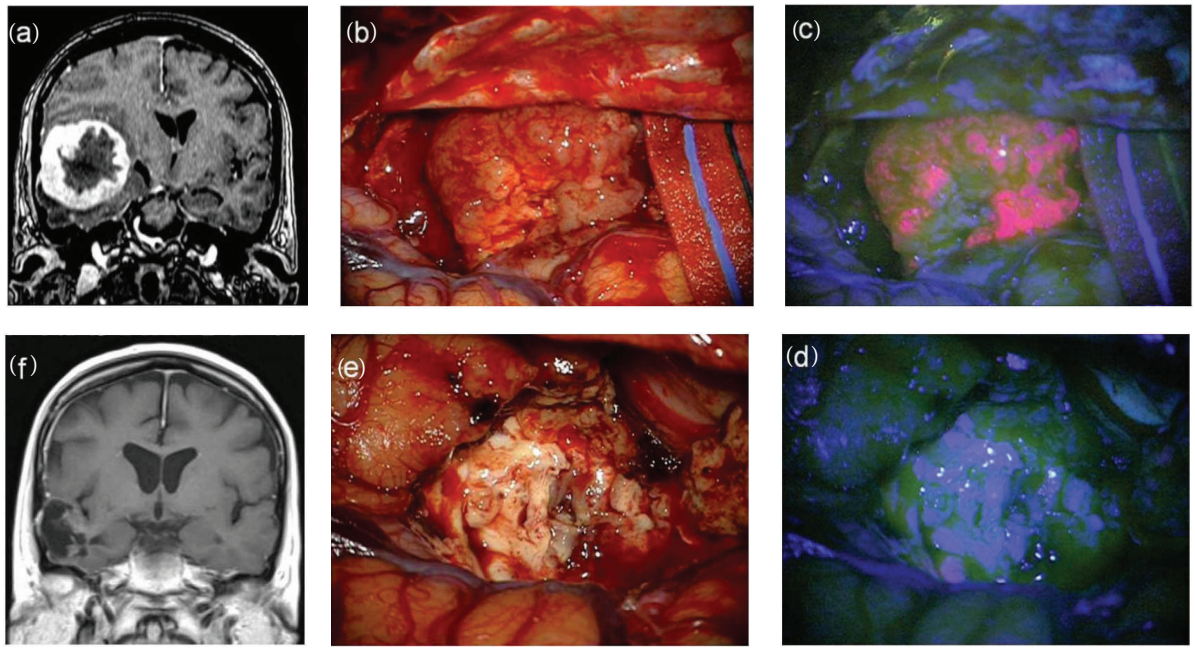

Figure 1: F 63/Y, preoperative MRI scan with gadolinium showing a large temporal high grade glioma (a). Intraoperative view: tumor resection under white (b) and blue (c) light till the complete removal of lesion. Final view at blue (d) and white light (e). Postoperative MRI scan with gadolinium (f) showing the complete resection of tumor. Histological report: glioblastoma (astrocytoma grade IV sec WHO).

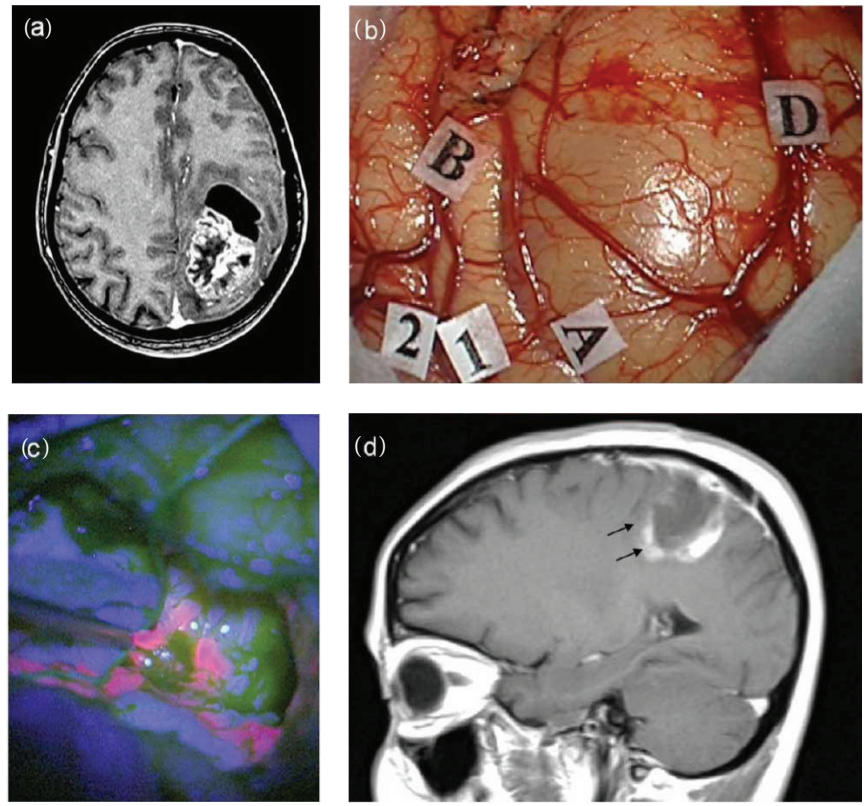

Figure 2: F 47/Y, preoperative MRI scan with gadolinium showing a large frontoparietal glioma (a). Intraoperative view: (b) identification by MRI-navigation of tumor boundaries on the cortical surface (markers A; B; D) and identification by mapping of surrounding motor area (1, 2). Resection under blue-light (c) showing a bright fluorescent tumor. The postoperative MRI scan (d) shows a residual tumor (black arrows). Histological report: glioblastoma (astrocytoma grade IV sec WHO).

Table 2: Resection rates reported in recent publications basing on tumors localization.

Authors, year	Rate of resection		
	All cerebral localizations	Noneloquent areas	Eloquent areas
Stummer et al., 2006 [9]	65%°	69%°	61%°
Feigl et al., 2010 [11]	—	—	64%*
Díez Valle et al., 2011 [12]	100%*	—	—
Schucht et al., 2012 [13]	89%°	97%°	74%°
Present series	93%*	96%*	90%*

°Contrast resection enhanced tumor (CRET); *gross total removal >98%; —: not reported.

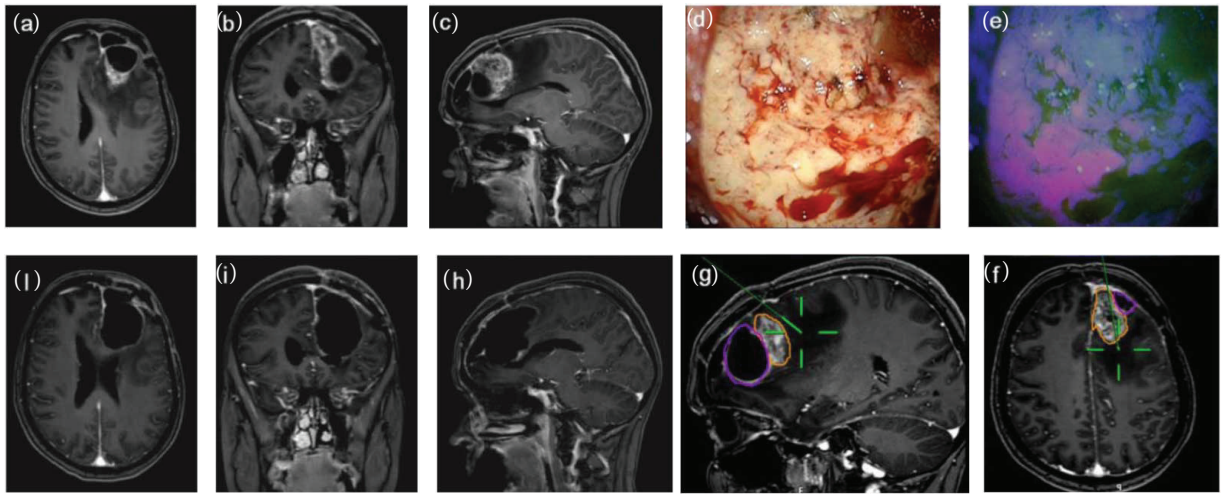

Figure 3: F/43Y, preoperative MRI scan with gadolinium showing a recurrent frontal glioblastoma (a–c). Intraoperative view: tumor resection under white (d) and blue (e) light. Intraoperative boundaries of surgical cavity at MRI navigation after resection under blue light (f-g). Postoperative MRI scan with gadolinium (h–j) showing the complete tumor resection and the postsurgical cavity roughly larger than tumor size at preoperative imaging. Histological report: recurrent glioblastoma (astrocytoma grade IV sec WHO).

of patients affected by newly diagnosed and recurrent glioma ($P = 0.845$), in 34/81 (42%) and in 7/13 (53%) of patients affected by a grade IV and grade III glioma ($P = 0.549$), and in 29/51 (57%) and in 12/43 (28%) of patients affected by a larger (>9 cm^3) and smaller (<9 cm^3) tumor, respectively ($P < 0.01$) (Figure 3).

4. Discussion

4.1. Our Present Relevant Results. GTR > 90% was achieved in 100% of patients whilst GTR > 98% was achieved in 93% of cases. Even if GTR > 98% was greater between patients affected by tumors in noneloquent areas (96 versus 90%), the difference was not statistically significant. Based on our results extent of resection rate was significantly higher in IV grade gliomas ($P = 0.029$) and in smaller tumors ($P = 0.018$). Concerning divergence between neuronavigation and 5-ALA fluorescence, we found a significant difference just regarding tumor volume, in particular in lesion >9 cm^3 ($P < 0.01$) while WHO grade and recurrent surgery were not statistically significant. Finally, the 3-layer pattern of fluorescence was more frequently preserved in newly diagnosed tumors compared to recurrence ($P < 0.001$) and in IV grade than in III grade gliomas ($P < 0.001$).

4.2. Comparison of Our Relevant Results to Those of Other Studies. GTR > 98% rate in our series was achieved in 93% of cases considering patients harboring lesions in both eloquent and noneloquent areas. These data have been found by several other works that focused on the utility of 5-ALA in gliomas surgery [12, 13]. However, as shown in Table 2, resection rate data are strictly dependent on the main bias of the proportion of patients with HGG in eloquent and noneloquent area in each study. In fact, as accurately reported by Schucht and coworkers [13], overall resection rate (contrast resection enhanced tumor—CRET) in their population was 89%: in noneloquent tumors CRET rate was 97% while it clearly decreased up to 74% in eloquent areas gliomas. These data however should be read according to the largeness of each study. In fact Stummer and colleagues reported a 65% of GTR, but it should be considered that this GTR rate arises from the largest and unique phase III trial and it reflects the surgical achievements of several Institutions with different expertise [9]. On the other hand, it seems that the increasing rate of GTR reported by these studies may arise from a growing experience in modern techniques of intraoperative mapping/monitoring and fluorescence-guided surgery. As a matter of fact, functional preservation and maintaining quality of life are undoubtedly a mandatory goal in glioma

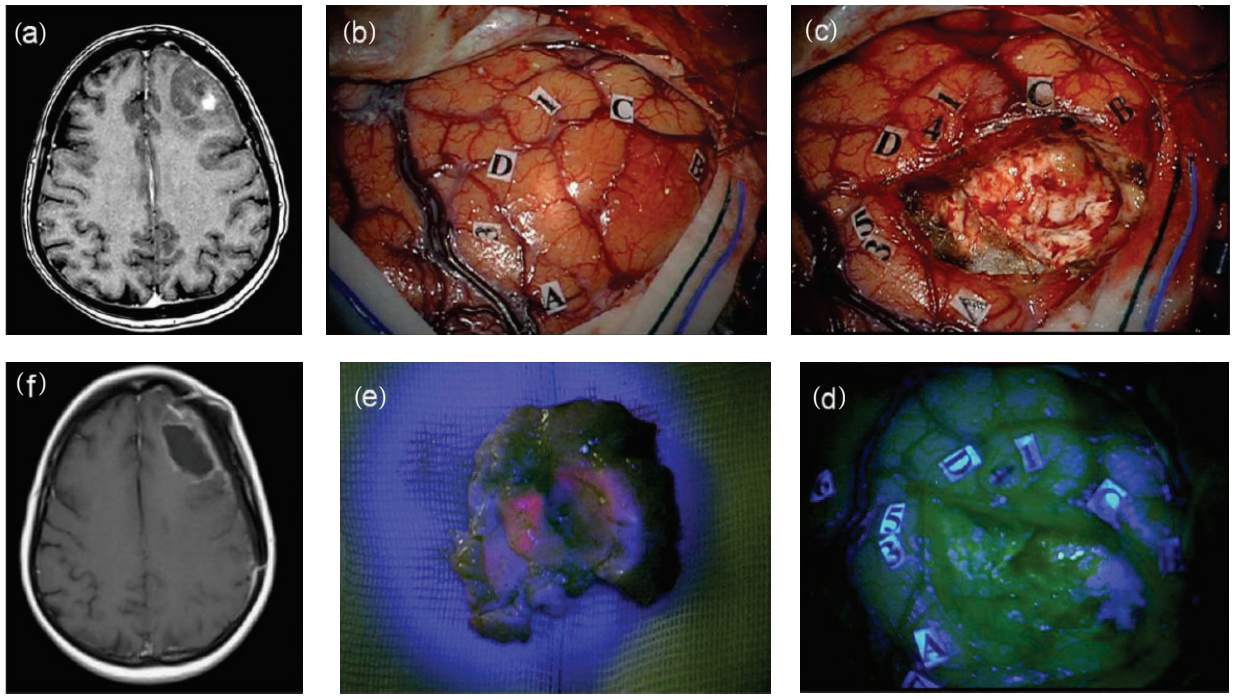

Figure 4: F 47/Y, preoperative MRI scan with gadolinium showing a left frontal high grade glioma (a). Intraoperative view: (b) identification by MRI-navigation of tumor boundaries on the cortical surface (markers A, B, C, D) and identification by mapping in awake surgery of surrounding language areas (1–5). (c) Final inspection of the surgical cavity under blue-light (d) showing no fluorescent residual tumor. The tumor at blue-light inspection showed a fluorescent inner part corresponding to enhancing component at preoperative MRI (a). The postoperative MRI scan (f) confirms the complete resection of tumor (f). Histological report: anaplastic astrocytoma (astrocytoma grade III sec WHO).

surgery since patients harboring HGG have a limited life expectancy. However, function protection can limit EOR in critical area gliomas. Stummer and colleagues found that, in 5-ALA assisted surgery, residual tumor volumes on postoperative MRI were greater in patients with glioma in eloquent regions compared with patients harboring tumor in noneloquent regions. In their study proximity to eloquent areas was the only independent factor on residual tumor [15]. Therefore, surgery assisted by both 5-ALA and neurophysiological monitoring represents an increasing interested field. In 2010 Feigl and coworkers performed this multimodal approach (5-ALA associated with motor evoked potentials and cortical and subcortical stimulation) in 18 patients with HGG in critical areas obtaining a GTR in 64% of cases while in 24% of cases surgical removal was stopped according to neurophysiological data and impairment was recorded in about 11% of cases [11]. Recently, we published our series of 31 patients with HGG in eloquent areas treated with this multimodal approach. We achieved a GTR (>98%) in 93% of cases and we stopped surgery in 26% to avoid neurological deficits. Finally, a postoperative impairment was found in 3% at 3-month follow-up [16]. Other authors, even if considering gliomas both in eloquent and in noneloquent areas, focused on 5-ALA and neurophysiological assisted surgery providing satisfactory and safe results [12, 13] compared to other multimodal approaches such as intraoperative MRI and neurophysiological monitoring [21].

4.3. MR Contrast Enhanced Tumor and 5-ALA Fluorescence. Analyzing our results we found a significant divergence between 5-ALA fluorescence and MR contrast enhanced tumor according to neuronavigation data. In particular considering lesions >9 cm^3 we discovered that 5-ALA fluorescing tissue expanded significantly over tumor volume scheduled by contrast enhanced tumor at MRI ($P = 0.01$) (Figure 3). As well known [22] during surgery volumetric deformations occur and brain morphology changes through a dynamic process called brain shift. This phenomenon determines a continuous modification of cerebral structures and therefore a progressive inaccuracy of neuronavigation data resulting in no longer trusted during surgical intervention. This finding has a particular relevance since neuronavigation data are based on uploaded contrast enhanced tumor images. As reported by a recent study focused on this topic 5-ALA-guided surgery extends up to 6 mm beyond the MRI contrast enhanced tumor [23]. A more extended tumor resection undoubtedly risks function preservation especially in critical areas. Therefore, neurophysiological monitoring represents a synergistic tool maximizing resection and minimizing neurological deficits.

4.4. Indications for Future Research. In our experience we found a definitely more constant 3-layer pattern of fluorescence in newly diagnosed IV grade than in III grade

(Figure 4) and recurrent gliomas, as a peculiar and characteristic pattern of fluorescence of these tumors. According to previous studies on GBM in fact, focusing on pathological morphology and spatial distribution in tumor bulk, a three-layer concentric model was found due to a different microenvironmental regulation [24]. Furthermore, we found a resection rate of grade III lower than grade IV gliomas. Literature lacks studies focusing on Grade III gliomas resection guided by 5-ALA fluorescence and our study was not designed to do that. However, recent findings documented a possible use of 5-ALA in detecting anaplastic foci within LGG with no evidence of preoperative contrast enhancement [25]. Widhalm and colleagues studied 17 patients with grad II and III gliomas without focal contrast enhancement and they found that focal 5-ALA fluorescence was a significant factor differentiating grade 2 and grade 3 gliomas. A main issue and surgical trick emerging by our data was the lower rate of resection in larger tumors. Probably, the collapse of the surgical cave during resection does not allow maintaining the blue light perpendicular illumination of tumor representing the ideal situation for identification of pathological tissue.

5. Conclusions

5-ALA fluorescence in HGG surgery can achieve a GTR in 100% of cases even if selection of patients remains a main bias. Indeed, only patients in whom gross total surgical removal was deemed possible at preoperative assessment were enrolled in the study. Recurrent surgery, tumor location, tumor size, and tumor grade are variables that in our experience can predict both the surgical outcome and the intraoperative findings. Our data must be confirmed by further studies.

Conflict of Interests

The authors declare that there is no conflict of interests regarding the publication of this paper.

References

[1] N. Sanai and M. S. Berger, "Glioma extent of resection and its impact on patient outcome," *Neurosurgery*, vol. 62, no. 4, pp. 753–764, 2008.

[2] D. A. Hardesty and N. Sanai, "The value of glioma extent of resection in the modern neurosurgical era," *Frontiers in Neurology*, vol. 3, article 140, 2012.

[3] M. J. McGirt, D. Mukherjee, K. L. Chaichana, K. D. Than, J. D. Weingart, and A. Quinones-Hinojosa, "Association of surgically acquired motor and language deficits on overall survival after resection of glioblastoma multiforme," *Neurosurgery*, vol. 65, no. 3, pp. 463–469, 2009.

[4] M. Lacroix, D. Abi-Said, D. R. Fourney et al., "A multivariate analysis of 416 patients with glioblastoma multiforme: prognosis, extent of resection, and survival," *Journal of Neurosurgery*, vol. 95, no. 2, pp. 190–198, 2001.

[5] N. Sanai, M. Polley, M. W. McDermott, A. T. Parsa, and M. S. Berger, "An extent of resection threshold for newly diagnosed glioblastomas: clinical article," *Journal of Neurosurgery*, vol. 115, no. 1, pp. 3–8, 2011.

[6] G. E. Keles, K. R. Lamborn, S. M. Chang, M. D. Prados, and M. S. Berger, "Volume of residual disease as a predictor of outcome in adult patients with recurrent supratentorial glioblastomas multiforme who are undergoing chemotherapy," *Journal of Neurosurgery*, vol. 100, no. 1, pp. 41–46, 2004.

[7] K. L. Chaichana, I. Jusue-Torres, R. Navarro-Ramirez et al., "Establishing percent resection and residual volume thresholds affecting survival and recurrence for patients with newly diagnosed intracranial glioblastoma," *Neuro-Oncology*, no. 1, pp. 113–122, 2014.

[8] M. A. Idoate, R. Díez Valle, J. Echeveste, and S. Tejada, "Pathological characterization of the glioblastoma border as shown during surgery using 5-aminolevulinic acid-induced fluorescence," *Neuropathology*, vol. 31, no. 6, pp. 575–582, 2011.

[9] W. Stummer, U. Pichlmeier, T. Meinel, O. D. Wiestler, F. Zanella, and H. Reulen, "Fluorescence-guided surgery with 5-aminolevulinic acid for resection of malignant glioma: a randomised controlled multicentre phase III trial," *The Lancet Oncology*, vol. 7, no. 5, pp. 392–401, 2006.

[10] W. Stummer, H. Reulen, T. Meinel et al., "Extent of resection and survival in glioblastoma multiforme: identification of and adjustment for bias," *Neurosurgery*, vol. 62, no. 3, pp. 564–576, 2008.

[11] G. C. Feigl, R. Ritz, M. Moraes et al., "Resection of malignant brain tumors in eloquent cortical areas: a new multimodal approach combining 5-aminolevulinic acid and intraoperative monitoring," *Journal of Neurosurgery*, vol. 113, no. 2, pp. 352–357, 2010.

[12] R. Díez Valle, S. Tejada Solis, M. A. Idoate Gastearena, R. García de Eulate, P. Domínguez Echávarri, and J. Aristu Mendiroz, "Surgery guided by 5-aminolevulinic fluorescence in glioblastoma: volumetric analysis of extent of resection in single-center experience," *Journal of Neuro-Oncology*, vol. 102, no. 1, pp. 105–113, 2011.

[13] P. Schucht, J. Beck, J. Abu-Isa et al., "Gross total resection rates in contemporary glioblastoma surgery: results of an institutional protocol combining 5-ALA intraoperative fluorescence imaging and brain mapping," *Neurosurgery*, vol. 71, no. 5, pp. 927–935, 2012.

[14] R. Sawaya, M. Hammoud, D. Schoppa et al., "Neurosurgical outcomes in a modern series of 400 craniotomies for treatment of parenchymal tumors," *Neurosurgery*, vol. 42, no. 5, pp. 1044–1055, 1998.

[15] W. Stummer, A. Novotny, H. Stepp, C. Goetz, K. Bise, and H. J. Reulen, "Fluorescence-guided resection of glioblastoma multiforme by using 5-aminolevulinic acid-induced porphyrins: a prospective study in 52 consecutive patients," *Journal of Neurosurgery*, vol. 93, no. 6, pp. 1003–1013, 2000.

[16] A. della Puppa, S. de Pellegrin, E. d'Avella et al., "5-aminolevulinic acid (5-ALA) fluorescence guided surgery of high-grade gliomas in eloquent areas assisted by functional mapping. Our experience and review of the literature," *Acta Neurochirurgica*, vol. 155, no. 6, pp. 965–972, 2013.

[17] N. Butowski, K. R. Lamborn, M. S. Berger, M. D. Prados, and S. M. Chang, "Historical controls for phase II surgically based trials requiring gross total resection of glioblastoma multiforme," *Journal of Neuro-Oncology*, vol. 85, no. 1, pp. 87–94, 2007.

[18] M. A. Vogelbaum, S. Jost, M. K. Aghi et al., "Application of novel response/progression measures for surgically delivered therapies for gliomas: Response Assessment in Neuro-Oncology (RANO) working group," *Neurosurgery*, vol. 70, no. 1, pp. 234–243, 2012.

[19] E. Rampazzo, A. della Puppa, C. Frasson et al., "Phenotypic and functional characterization of Glioblastoma cancer stem cells identified through 5-aminolevulinic acid-assisted surgery," *Journal of Neuro-Oncology*, vol. 116, no. 3, pp. 505–513, 2014.

[20] D. N. Louis, H. Ohgaki, O. D. Wiestler et al., "The 2007 WHO classification of tumours of the central nervous system," *Acta Neuropathologica*, vol. 114, no. 2, pp. 97–109, 2007.

[21] C. Senft, M. Forster, A. Bink et al., "Optimizing the extent of resection in eloquently located gliomas by combining intraoperative MRI guidance with intraoperative neurophysiological monitoring," *Journal of Neuro-Oncology*, vol. 109, no. 1, pp. 81–90, 2012.

[22] A. Nabavi, P. M. Black, D. T. Gering et al., "Serial intraoperative magnetic resonance imaging of brain shift," *Neurosurgery*, vol. 48, no. 4, pp. 787–797, 2001.

[23] P. Schucht, S. Knittel, J. Slotboom et al., "5-ALA complete resections go beyond MR contrast enhancement: shift corrected volumetric analysis of the extent of resection in surgery for glioblastoma," *Acta Neurochirurgica*, vol. 156, no. 2, pp. 305–312, 2014.

[24] L. Persano, E. Rampazzo, A. della Puppa, F. Pistollato, and G. Basso, "The three-layer concentric model of glioblastoma: cancer stem cells, microenvironmental regulation, and therapeutic implications," *TheScientificWorldJournal*, vol. 11, pp. 1829–1841, 2011.

[25] G. Widhalm, S. Wolfsberger, G. Minchev et al., "5-aminolevulinic acid is a promising marker for detection of anaplastic foci in diffusely infiltrating gliomas with nonsignificant contrast enhancement," *Cancer*, vol. 116, no. 6, pp. 1545–1552, 2010.

Hindawi Publishing Corporation
BioMed Research International
Volume 2014, Article ID 154350, 5 pages
http://dx.doi.org/10.1155/2014/154350

Clinical Study

Facing Contrast-Enhancing Gliomas: Perfusion MRI in Grade III and Grade IV Gliomas according to Tumor Area

Anna Luisa Di Stefano,[1,2] Niels Bergsland,[3] Giulia Berzero,[1,4] Lisa Farina,[5] Elisa Rognone,[5] Matteo Gastaldi,[6] Domenico Aquino,[7] Alessandro Frati,[8] Francesco Tomasello,[9] Mauro Ceroni,[2,6] Enrico Marchioni,[1] and Stefano Bastianello[2,5]

[1] *Neuro-Oncology Unit, C. Mondino National Neurological Institute, 27100 Pavia, Italy*
[2] *Department of Brain and Behavioral Sciences, University of Pavia, 27100 Pavia, Italy*
[3] *Magnetic Resonance Laboratory, IRCCS Don Gnocchi Foundation, 20148 Milan, Italy*
[4] *Neuroscience Consortium, University of Pavia, Monza Policlinico and Pavia Mondino, 27100 Pavia, Italy*
[5] *Neuroradiological Department, C. Mondino National Neurological Institute, 27100 Pavia, Italy*
[6] *General Neurology Unit, C. Mondino National Neurological Institute, 27100 Pavia, Italy*
[7] *Department of Neuroradiology, IRCCS Foundation Neurological Institute C. Besta, 20133 Milan, Italy*
[8] *Department of Neurosurgery, IRCCS Neuromed, Pozzilli (IS), University of Rome La Sapienza, 00185 Rome, Italy*
[9] *Department of Neurosurgery, University of Messina, 98122 Messina, Italy*

Correspondence should be addressed to Anna Luisa Di Stefano; annaluisadistefano@gmail.com

Received 14 February 2014; Accepted 6 March 2014; Published 3 April 2014

Academic Editor: Lombardi Giuseppe

Tumoral neoangiogenesis characterizes high grade gliomas. Relative Cerebral Blood Volume (rCBV), calculated with Dynamic Susceptibility Contrast (DSC) Perfusion-Weighted Imaging (PWI), allows for the estimation of vascular density over the tumor bed. The aim of the study was to characterize putative tumoral neoangiogenesis via the study of maximal rCBV with a Region of Interest (ROI) approach in three tumor areas—the contrast-enhancing area, the nonenhancing tumor, and the high perfusion area on CBV map—in patients affected by contrast-enhancing glioma (grades III and IV). Twenty-one patients were included: 15 were affected by grade IV and 6 by grade III glioma. Maximal rCBV values for each patient were averaged according to glioma grade. Although rCBV from contrast-enhancement and from nonenhancing tumor areas was higher in grade IV glioma than in grade III (5.58 and 2.68; 3.01 and 2.2, resp.), the differences were not significant. Instead, rCBV recorded in the high perfusion area on CBV map, independently of tumor compartment, was significantly higher in grade IV glioma than in grade III (7.51 versus 3.78, $P = 0.036$). In conclusion, neoangiogenesis encompasses different tumor compartments and CBV maps appear capable of best characterizing the degree of neovascularization. Facing contrast-enhancing brain tumors, areas of high perfusion on CBV maps should be considered as the reference areas to be targeted for glioma grading.

1. Introduction

Gliomas are the most common brain primary neoplasms and are classified based on histologic parameters including atypia, vascular endothelial proliferation, necrosis, and mitosis [1, 2]. A common histopathological characteristic for both grade III and grade IV glioma is vascular endothelial proliferation,which is known to correspond to blood brain barrier disruption and tumoral neoangiogenesis [3, 4] as evidenced by contrast-enhancement observed using conventional Magnetic Resonance Imaging (MRI).Although neuroradiological necrosis is a hallmark of glioblastoma (GBM; grade IV glioma), it is not a constant finding. Therefore it can be difficult to distinguish between grade III and grade IV gliomas using conventional MRI.

Dynamic Susceptibility Contrast (DSC) Perfusion-Weighted Imaging (PWI) measures concentration of a paramagnetic contrast material in the organ, providing reliable information

on blood flow and vascularization. Among other perfusion parameters such as Cerebral Blood Flow (CBF) and Mean Transit Time (MTT), Cerebral Blood Volume (CBV) was shown to best correlate with tumoral neoangiogenesis and subsequently glioma grading. In particular, Relative Cerebral Blood Volume (rCBV), reflecting increased capillary density, was shown to be significantly higher in high grade gliomas (grade III and grade IV gliomas) than low grade gliomas (grade II glioma) and with higher values in grade IV [5].

Although rCBV increase is recognized as a surrogate marker of malignancy [6–8], differentiation between grade III and grade IV glioma is not consistently reproducible [8–11].

Furthermore, rCBV increases in glioblastoma multiforme (GBM) peritumoral area [10] and the peculiar pattern of rCBV increase surrounding glioblastoma contrast-enhancing tumor bed [12, 13] raises the question of where measuring rCBV values may best distinguish between grade III and grade IV gliomas.

In this study we investigated rCBV differences in patients with grade III and grade IV glioma using a Region of Interest- (ROI-) based method in three different tumor areas: the contrast-enhancing area, the nonenhancing tumor, and the high perfusion area on CBV map.

The aim of the study was to determine which tumor compartments showed rCBV differences related to glioma grade.

2. Materials and Methods

We examined perfusion MRI from 21 patients affected by histologically proven high grade gliomas: fifteen patients were affected by grade IV glioma and 6 patients by grade III glioma.

Twelve patients underwent a DSC perfusion examination before surgery and 9 with residual tumor were examined after surgery after a median of 6.8 months. All patients undergoing perfusion after surgery had residual tumor and were not in progression at the time of DSC perfusion examination. All patients in this study were affected by primary disease and in particular grade IV glioma patients were all affected by primary GBM.

Demographical characteristics of patients are detailed in Table 1. Glioma grading was assessed by an experienced neuropathologist according to WHO criteria 2007 [2]. The study was approved by the local Institutional Review Board and all patients provided informed consent.

All participants were scanned using a 1.5T Philips Intera Gyroscan (Philips Medical System, Best, The Netherlands) with a maximum slew rate of 150 $Tm^{-1}\,s^{-1}$ and a maximum gradient amplitude of 30 mT/m. All scans were performed using an 8-channel SENSE (sensitivity encoding parallel imaging) head coil.

The scanning protocol included the following.

An axial 2D spin-echo (SE) T2-weighted Fluid Attenuated Inversion Recovery (FLAIR) image: echo time (TE)/repetition time (TR)/inversion time (TI) = 140/11000/2800 ms, flip angle (FA) = 90°, echo train length (ETL) = 50, acquisition matrix = 256 × 188, FOV = 250 mm^2 (for an in-plane resolution of 0.9 mm × 1.3 mm), slice thickness = 5 mm, gap = 1 mm, number of excitations (NEX) =2, and number of slices = 24.

Table 1: Patients' clinical data and tumor diagnosis.

WHO glioma grade	Number of patients	Age (years) (median, range)	Sex ratio (male/female)
III	6	49 (24–66)	6.0
IV	15	63 (23–80)	1.5

An axial 2D SE T1-weighted image: TE/TR = 15/649.5 ms, FA = 90°, ETL = 1, acquisition matrix = 260 × 209, FOV = 250 mm^2 (in-plane resolution of 0.9 mm × 1.2 mm), slice thickness = 5 mm, gap = 1 mm, NEX = 2, and number of slices = 24.

An axial 3D perfusion weighted gradient echo (GRE) sequence (Principles of Echo Shifting with a Train of Observations, PRESTO) for Dynamic Susceptibility Contrast MRI: TE/TR = 8/16.72 ms (effective T2 = 23.71 ms), FA = 7°, ETL = 7, acquisition matrix = 64 × 64, FOV = 220 mm^2 (in-plane resolution of 3.44 mm × 3.44 mm), slice thickness = 3 mm, NEX = 1, and number of slices = 30 with 40 temporal localizations. This sequence was acquired with a standard dose of 0.2 mmol/Kg body weight of gadopentetate dimeglumine (Gd-DTPA) contrast agent (Gadovist) which was injected at a rate of 4 mL/s, followed by a 20 mL continuous saline flush. Using a 0.05 mmol/Kg dose, presaturation of the baseline signal prior to the PWI acquisition was done to reduce T1-effects as well as potential contrast leakage effects due to blood brain barrier disruption.

An axial 3D T1-weighted fast field echo (FFE) sequence after the PWI: TE/TR = 4.6/25 ms, FA = 30°, ETL = 1, acquisition matrix = 256 × 256, FOV = 250 mm^2 (in-plane resolution of 0.98 mm × 0.98 mm), slice thickness = 1.6 mm, gap = 0, NEX = 1, and number of slices = 170.

Postprocessing was performed using Olea Medical PerfScape software (version 2.0). The DSC acquisition was corrected for patient motion using the built-in feature of PerfScape. The T1 SE, FLAIR, and T1 3D FFE images were then coregistered and resampled into the space of the DSC MRI. It is well known that disruption of the blood brain barrier, as is common in high grade tumors, can lead to inaccurate measures of CBV [14]. As such, the correction for leakage effects option in PerfScape was employed.

Relative CBV (rCBV) was calculated from three separate ROIs that were placed in three different compartments: the area of contrast-enhancement, the nonenhancing tumor, and high perfusion area seen on the CBV color overlay maps. In the contrast-enhancement area, necrosis was excluded from CBV measure. The nonenhancing surrounding tumor ROIs corresponded to areas of T2/FLAIR hyperintensity outside contrast-enhancement. We ensured that T2/FLAIR ROIs were not placed in areas of contrast-enhancement as all images were coregistered. Placement of ROIs on the CBV map was performed in high perfusion areas independently of the contrast-enhancement and T2/FLAIR ROI locations.

Morphology and size of the ROIs were constant (elliptical-40 mm^2 area) and the maximum value was recorded for each compartment according to Law et al. [15].

Table 2: Mean rCBV values according to histological grading. Relative Cerebral Blood Volume (rCBV) was measured with the ROI-based approach in three distinct areas: the high perfusion area on CBV map ("CBV map" in the table), the contrast-enhanced area ("CE" in the table), and the nonenhancing tumor ("Non-CE" in the table). Only rCBV values measured in the high perfusion area in CBV map showed significant difference between grade III and grade IV gliomas.

WHO glioma grade	rCBV; mean (SD)					
	CBV map	*P*	CE	*P*	Non-CE	*P*
Glioma grade III	3.78 (1.70)	**0.036**	3.01 (1.02)	0.27	2.20 (1.73)	0.71
Glioma grade IV	7.51 (3.84)		5.58 (5.48)		2.68 (2.93)	

All values were normalized to a corresponding ROI placed in contralateral normal brain parenchyma. All ROIs were placed by two operators (A.D, N.B.) via consensus. Maximal rCBV values for each patient were averaged according to glioma grade.

Differences between grades and tumor areas were tested using *t*-test. ANOVA was used in order to compare rCBV values in different subgroups of patients. Contingency analysis was performed by Fisher's exact test. In all analyses we considered a *P* value of 0.05 (two-sided) as being statistically significant.

3. Results

Twelve patients underwent a DSC perfusion examination before surgery (3 patients affected by grade III glioma and 9 patients affected by grade IV glioma) and 9 patients with residual tumor were examined after surgery after a median of 6.8 months (3 patients affected by grade III glioma and 6 by grade IV glioma). Distribution of patients according to the timing of perfusion MRI (presurgery versus postsurgery) was not significantly different between grade III glioma and grade IV ($P = 0.67$).

In the grade III glioma subgroup, 2 patients were affected by anaplastic oligodendroglioma and 4 patients by anaplastic astrocytoma; in the grade IV glioma subgroup all patients were affected by glioblastoma.

Mean rCBV values from patients are detailed in Table 2. In the grade III glioma subgroup, mean rCBV was higher in the contrast-enhanced area than nonenhancing tumor (3.01 and 2.20, resp., $P = 0.11$); rCBV recorded in CBV map, independently of tumor compartment as seen on conventional MRI, was 3.78.

In glioma grade IV, mean rCBV was higher in contrast-enhanced area than nonenhancing tumor (5.58 and 2.68, resp., $P = 0.04$); the mean rCBV recorded in the CBV map was 7.51.

Between glioma grade III and glioma grade IV, no significant differences in rCBV were observed in the contrast-enhancement area and in the nonenhancing tumor ($P = 0.27$ and 0.71, resp.). Inversely, mean rCBV was significantly higher in grade IV gliomas than in grade III ($P = 0.036$) in the high perfusion area of CBV map independently of tumor compartment, as seen on conventional MRI (Figure 1).

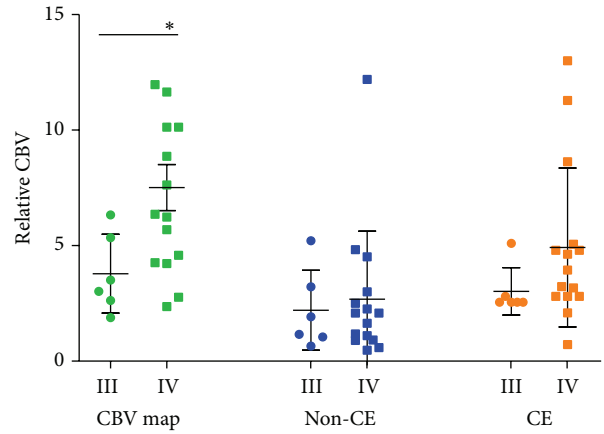

Figure 1: Scatter-plot diagram representing rCBV values according to grade and tumor area. Circles represent grade III, squares grade IV. Green color represents rCBV values measured in CBV map; blue color represents rCBV values measured in the nonenhancing tumor (Non-CE); orange color represents rCBV values measured in enhancing area (CE). Lines correspond to mean value and error bars to standard error of the mean. Only rCBV values measured in the high perfusion area in CBV map showed significant difference between grade III and grade IV gliomas.

4. Discussion

Neovascular proliferation is a hallmark of malignant gliomas and PWI is useful in glioma grading through detection of vascular density and of the grade of tumor-associated neovascularization [7, 16].

The measure of rCBV is commonly used in order to predict glioma grade or to differentiate radionecrosis from tumor recurrence in a diagnostic setting. Several reports on rCBV increases in peritumoral area of glioblastoma [10, 13] have suggested that there is a mismatch between the extension of effective vascular proliferation and area of contrast-enhancement.

In this work we mapped rCBV maximal increase in two different compartments of glioma grade III and glioma grade IV—the contrast-enhancing area and nonenhancing tumor with a ROI-based method. rCBV was also recorded in high perfusion area of CBV map independently of corresponding tumor area on conventional MRI.

Values of rCBV recorded in this work are consistent with the other reports in the literature [6]. As expected we found a significantly higher rCBV in contrast-enhanced area than in nonenhancing tumor in the grade IV glioma subgroup.

Concerning rCBV differences according to the tumor grade, we did not find significant differences of rCBV values recorded in contrast-enhancing area or nonenhancing tumor between grades III and IV.

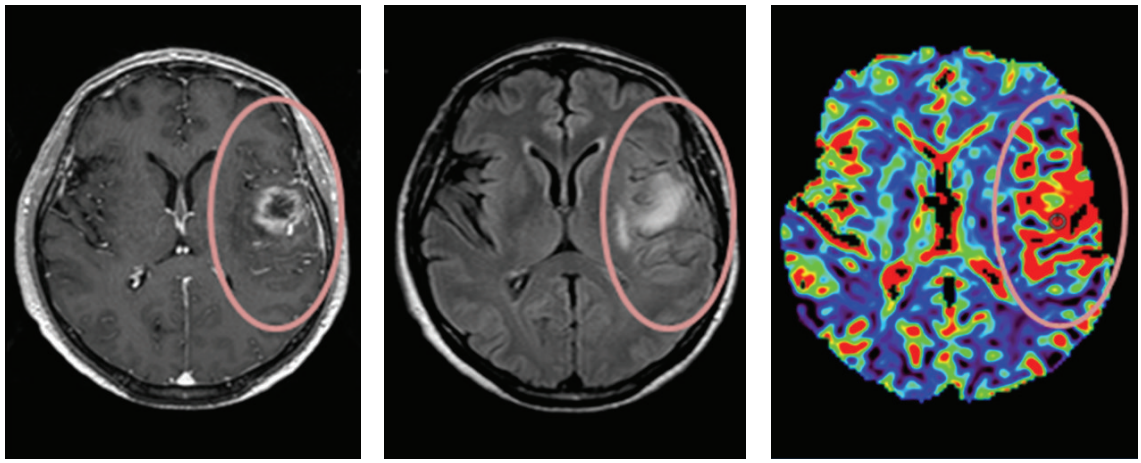

(a) (b) (c)

Figure 2: Axial coregistered contrast-enhanced axial T1-weighted image (a), FLAIR image (b), and CBV map (c) from a patient affected by glioma grade IV. In the CBV map (c) warmer colors indicate higher CBV values suggesting higher perfusion and neovascularization. Comparison of CBV map (c) and contrast-enhanced axial T1-weighted image highlights a mismatch area (surrounded by the circle) corresponding to the extension of the high perfusion area outside the contrast-enhancement: this indicates a more extensive neovascularization than that shown by conventional MRI (a, b).

Only measures of rCBV in the high perfusion area on the CBV map showed a significant difference between grade III glioma and grade IV, with higher values in grade IV.

Taken together, these results support the idea that neoangiogenesis heterogeneously encompasses both contrast-enhancing and nonenhancing tumor areas. The contrast-enhancing areas appear to reflect a higher degree of neoangiogenesis, although the difference with respect to nonenhancing areas was significant only in grade IV glioma subgroup.

Interestingly, we did not find significant differences in maximal rCBV in neither of these two areas when comparing grades III and IV. This suggests that basing rCBV measurements on signal characteristics of conventional MRI may not be sufficient to distinguish between grade III and grade IV gliomas.

Glioblastoma has been shown to present with a more heterogeneous neovascularization than grade III glioma [12]. In particular glioblastoma present, more so than with lower grades, areas with low perfusion due to necrosis, area of focal rCBV increase, and also increased rCBV values in peritumoral normal-appearing parenchyma [14, 17].

In particular, a special pattern of rCBV increase in peritumoral area can occur in a "stripe like" fashion which has been termed a "striate sign." This feature has been described as mostly represented in glioblastoma rather than lower grade gliomas and in particular with respect to grade III glioma [12, 13]. The same authors showed that this specific pattern of rCBV in peritumoral area was significantly associated with normalized choline increase and with the subsequent appearance of contrast-enhancement in the same area [12, 13]. A similar example of mismatch between high perfusion area from CBV map and contrast-enhancement observed in our patients is shown in Figure 2. Histopathologically, these patterns of rCBV may reflect diffuse migration of glioma cells along vascular channels of the white matter tracts spreading beyond the visible tumor border [18].

Taken together, these results support the hypothesis that only the rCBV map represents extensively the neovascular phenomena, its extension into apparently normal surrounding parenchyma, and its quantitative difference among glioma grades.

Limits of the study are the small sample size and potential sampling differences from the ROI-dependent method of measure which may increase interobserver variability. Nevertheless the latter is the most used in clinical routine. Additionally, all ROIs were placed in consensus by two authors. The fact that some patients were scanned before surgery and other patients afterwards presents an additional confound. However, we did not find any significant differences between the pre-/posttreatment groups (results not shown). Nevertheless, we cannot rule out the possibility that surgical intervention in some patients may have influenced the results.

In conclusion, maximal rCBV values measured directly on the CBV map seem to best characterize the extensive neoangiogenesis phenomena of high grade gliomas and quantitative difference of microvascular density between grade III and grade IV glioma. Such measurements should be considered as the reference map for glioma grading and potentially for serial measures of rCBV modification during antiangiogenic treatment.

Conflict of Interests

The authors declare that there is no conflict of interests regarding the publication of this paper.

Acknowledgments

The study was supported by a Grant of the National Ministry of University and Research, PRIN 2008 "2008979 M8 K_003." The authors are grateful to OLEA Medical for providing OLEA PerfScape Software for postprocessing perfusion analysis. Dr. Di Stefano is supported by an investigator Fellowship from Collegio Ghislieri, Pavia, Italy.

References

[1] D. N. Louis, H. Ohgaki, O. D. Wiestler et al., "The 2007 WHO classification of tumours of the central nervous system," *Acta Neuropathologica*, vol. 114, no. 2, pp. 97–109, 2007.

[2] D. N. Louis, H. Ohgaki, O. D. Wiestler, and W. K. Cavenee, *WHO Classification of Tumours of the Central Nervous System*, IARC, Lyon , France, 2007.

[3] R. Felix, W. Schorner, and M. Laniado, "Brain tumors: MR imaging with gadolinium-DTPA," *Radiology*, vol. 156, no. 3, pp. 681–688, 1985.

[4] B. L. Dean, B. P. Drayer, C. R. Bird et al., "Gliomas: classification with MR imaging," *Radiology*, vol. 174, no. 2, pp. 411–415, 1990.

[5] J. R. Petrella and J. M. Provenzale, "MR perfusion imaging of the brain: techniques and applications," *American Journal of Roentgenology*, vol. 175, no. 1, pp. 207–219, 2000.

[6] T. Sugahara, Y. Korogi, M. Kochi et al., "Correlation of MR imaging-determined cerebral blood volume maps with histologic and angiographic determination of vascularity of gliomas," *American Journal of Roentgenology*, vol. 171, no. 6, pp. 1479–1486, 1998.

[7] H. J. Aronen, F. S. Pardo, D. N. Kennedy et al., "High microvascular blood volume is associated with high glucose uptake and tumor angiogenesis in human gliomas," *Clinical Cancer Research*, vol. 6, no. 6, pp. 2189–2200, 2000.

[8] E. A. Knopp, S. Cha, G. Johnson et al., "Glial neoplasms: dynamic contrast-enhanced T2*-weighted MR imaging," *Radiology*, vol. 211, no. 3, pp. 791–798, 1999.

[9] N. Fayed, J. Dávila, J. Medrano, and S. Olmos, "Malignancy assessment of brain tumours with magnetic resonance spectroscopy and dynamic susceptibility contrast MRI," *European Journal of Radiology*, vol. 67, no. 3, pp. 427–433, 2008.

[10] S. Cha, E. A. Knopp, G. Johnson, S. G. Wetzel, A. W. Litt, and D. Zagzag, "Intracranial mass lesions: dynamic contrast-enhanced susceptibility-weighted echo-planar perfusion MR imaging," *Radiology*, vol. 223, no. 1, pp. 11–29, 2002.

[11] R. Sanz-Requena, A. Revert-Ventura, L. Martí-Bonmatí, Á. Alberich-Bayarri, and G. García-Martí, "Quantitative MR perfusion parameters related to survival time in high-grade gliomas," *European Radiology* , vol. 23, no. 12, pp. 3456–3465, 2013.

[12] S. Blasel, K. Franz, M. Mittelbronn et al., "The striate sign: peritumoural perfusion pattern of infiltrative primary and recurrent gliomas," *Neurosurgical Review*, vol. 33, no. 2, pp. 193–203, 2010.

[13] S. Blasel, K. Franz, H. Ackermann, S. Weidauer, F. Zanella, and E. Hattingen, "Stripe-like increase of rCBV beyond the visible border of glioblastomas: site of tumor infiltration growing after neurosurgery," *Journal of Neuro-Oncology*, vol. 103, no. 3, pp. 575–584, 2011.

[14] J. L. Boxerman, K. M. Schmainda, and R. M. Weisskoff, "Relative cerebral blood volume maps corrected for contrast agent extravasation significantly correlate with glioma tumor grade, whereas uncorrected maps do not," *American Journal of Neuroradiology*, vol. 27, no. 4, pp. 859–867, 2006.

[15] M. Law, R. J. Young, J. S. Babb et al., "Gliomas: predicting time to progression or survival with cerebral blood volume measurements at dynamic susceptibility-weighted contrast-enhanced perfusion MR imaging," *Radiology*, vol. 247, no. 2, pp. 490–498, 2008.

[16] B. R. Rosen, J. W. Belliveau, J. M. Vevea, and T. J. Brady, "Perfusion imaging with NMR contrast agents," *Magnetic Resonance in Medicine*, vol. 14, no. 2, pp. 249–265, 1990.

[17] I. C. Chiang, Y. T. Kuo, C. Y. Lu et al., "Distinction betweenhigh-grade gliomas and solitary metastases using peritumoral 3-T magnetic resonance spectroscopy, diffusion, and perfusion imagings," *Neuroradiology*, vol. 46, no. 8, pp. 619–627, 2004.

[18] P. J. Kelly, C. Daumas-Duport, and D. B. Kispert, "Imaging-based stereotaxic serial biopsies in untreated intracranial glial neoplasms," *Journal of Neurosurgery*, vol. 66, no. 6, pp. 865–874, 1987.